EVALUATING CROP PHYSIOLOGICAL AND STAND AGE-RELATED CONTROLS OVER SOIL CARBON AND NITROGEN DYNAMICS IN PERENNIAL AND ANNUAL GRAINS

A Dissertation
SUBMITTED TO THE FACULTY OF THE
UNIVERSITY OF MINNESOTA
BY

Stella Louise Woeltjen

IN PARTIAL FULFILLMENT OF THE REQUIREMENTS
FOR THE DEGREE OF DOCTOR OF PHILOSOPHY

Dr. Jessica Gutknecht and Dr. Jacob Jungers

2023

© Stella Louise Woeltjen 2023

Acknowledgements

I thank my advisors, Dr. Jessica Gutknecht and Dr. Jacob Jungers. Their passion for sustainable agriculture, devotion to student mentorship, and never-ending patience were critical to my ability to complete this work, and I thank them both for the many hours they dedicated to my graduate work and my development as an effective agroecosystem researcher. I would also like to thank my committee members, Dr. Anna Cates and Dr. Sarah Hobbie, for the insights they offered into this work. Their kind, constructive feedback on my writing immensely improved the quality of my work and enhanced my capacity to effectively design and defend my research.

I am also appreciative of the technicians and students from the Soils and Ecosystem Ecology for Climate Resilient Systems and Sustainable Cropping Systems labs who assisted in completing the field sample collection and sample processing for these studies. Without them, this research would not have been possible.

Finally, I thank all the mentors, family and friends who supported me as I completed my graduate work. I want to give special thanks to my husband, Jacob Woeltjen, for supporting me throughout my graduate school journey and always being willing to listen to me talk about soil. I also thank my parents, Keith Pey and Sheila Pey, for inspiring their children to be curious about the world around them and always encouraging me to go where my passions led me.

Dedication

This thesis is dedicated to the soils in agricultural systems.

Abstract

Little is known about how the cycling of carbon (C) and fertilizer nitrogen (N) between crop tissues and soil pools is expressed in perennial grains such as intermediate wheatgrass (IWG, *Thinopyrum intermedium* (Host) Barkworth and Dewey), and whether these processes change within a growing season and across IWG stand age. To evaluate these ideas, we established three studies to quantify 1) root growth and decomposition, 2) C uptake and partitioning to crop-microbial-soil pools, and 3) N sources and N conservation in first-year IWG (IWG-1), second-year IWG (IWG-2), third-year IWG (IWG-3) and annual wheat (Wheat).

These studies illuminated age-related changes in IWG root growth and decomposition, and C uptake and partitioning. In the 0 – 15 cm depth interval, IWG-1 new root growth was 1.7 times greater than that of IWG-2, and IWG-1 (14 – 17%) retained significantly more new C in roots than IWG-2 (6%) at the time of peak new C recovery. Conversely, IWG-2 root decomposition and utilization of new C by saprotrophic fungi was significantly greater than that of IWG-1, with the proportion of new soil microbial biomass C recovered from saprotrophic fungi increasing from 30% to 40% between IWG-1 and IWG-2. Together, these results indicated IWG transitioned from a system dominated by belowground C inputs and new root growth to one dominated by the loss of belowground C via root decomposition and heterotrophic decomposition across the first two years following establishment, in line with a system transitioning from an acquisitive to conservative growth strategy.

The transition to a system dominated by the decomposition of belowground root inputs suggests IWG may develop a greater capacity for recycling N from root tissues to inorganic soil N pools, thereby lessening the need for external fertilizer N inputs. However, the proportion of tissue N sourced from fertilizer increased between the first and third IWG production year, suggesting reliance on fertilizer N increases with stand age. Optimizing IWG N management recommendations to adequately meet IWG N demands will be critical to reducing reliance on external fertilizer inputs and ensuring IWG remains a profitable and sustainable alternative to annual grains in agricultural landscapes.

Table of Contents

List of Tables

List of Figures

Preface

When compared to annual grain cropping systems, the establishment of perennial grass crops in agricultural landscapes is expected to positively impact the economic and social sustainability of agricultural communities, along with improving regional environmental health. Perennial cropping systems are associated with management practices and crop physiological attributes that improve environmental quality through efficient resource use and nutrient uptake and utilization. In particular, the dense root networks, high carbon (C) uptake and belowground C partitioning, and efficient uptake and conservation of fertilizer-applied nitrogen (N) serve to increase soil C storage, reduce reliance on fertilizer N inputs and diminish agricultural-derived N losses. These attributes all serve to improve the provisioning of ecosystem services by agricultural systems.

Intermediate wheatgrass (IWG, *Thinopyrum intermedium* (Host) Barkworth and Dewey), a cool-season grass domesticated for grain and forage production, is currently gaining attention as a perennial alternative to annual grain crops. The extensive root systems, high C uptake and belowground C partitioning, and well-developed N conservation strategies make perennial crops like IWG well-suited to improve soil C storage, minimize N losses and reduce reliance on external fertilizer N inputs. However, little is known about how these attributes are expressed in IWG systems, and whether these processes change within a growing season and as IWG stands age. As IWG stands often remain in production for 3 - 5 years, this gap in knowledge significantly challenges the understanding of how IWG will contribute to soil C storage and crop-soil N retention as stands age. To evaluate these ideas, we established three studies to address stand age-

related effects on IWG 1) root growth and decomposition, 2) C uptake and partitioning to crop-soil-microbial pools, and 3) N availability, primary N sources and utilization of N conservation mechanisms.

Chapter 1 describes a study that utilized sequential core and ingrowth core techniques to quantify standing root stocks, root growth and root decomposition in IWG and spring wheat (*Triticum aestivum* L.). Along with verifying previous findings that IWG produces and maintains larger root stocks than annual crops, we found that the second-year IWG systems generally maintained larger standing root stocks over the growing season than either the first-year IWG or wheat. In evaluating the processes of root growth and decomposition that maintain standing root stocks, a clear shift in root dynamics was observed between the first and second IWG production year. Within just two years of establishment, IWG shifted from a system dominated by root growth to one characterized by root decomposition and limited new root growth.

Chapter 2 builds on research that was driven by the findings in Chapter 1. In Chapter 2, the fate of photosynthate C was directly traced through crop tissue and soil pools, including aboveground tissues, roots, soil and rhizosphere soil microbial biomass in IWG and wheat using ^{13}C tracer methods. We saw clear differences in C uptake and partitioning between wheat and IWG, and evidence of stand age-related changes in C uptake and partitioning. In wheat, C was transferred from aboveground tissues to soil C pools and soil microbial biomass, suggesting new C inputs readily contribute to soil C storage in these systems. However, as almost all the Wheat root biomass decomposes within the same growing season in which it was produced (as seen in Chapter 1), root-

derived C inputs may be largely respired within the same growing season in which they were generated, yielding limited longer-term contributions of wheat root inputs to soil C storage. Conversely, the first-year IWG stored a larger proportion of new C in roots relative to wheat. The storage of new C in roots and the associated mycorrhizal networks that colonize them may extend the spatial and temporal extent over which IWG contributes to soil C storage, with first-year IWG root-derived C potentially contributing to soil C pools even after crop termination. By the second production year, new C inputs were largely retained in aboveground biomass or exported from the system via soil CO_2 efflux. Coupled with the increasing proportion of new microbial C recovered from saprotrophic fungi, these results support findings from Chapter 1 that suggest C cycling in IWG is dominated by C decomposition processes in the second production year.

We found further evidence of significant changes in IWG resource and nutrient use with stand age in a study described in Chapter 3. In this study, we applied ^{15}N-fertilizer tracer methods to directly track the fate of fertilizer-derived N through aboveground tissues, roots, and soil pools, allowing us to evaluate N availability, N translocation and conservation, primary N sources used to support tissue growth and maintenance, and fertilizer-derived N uptake and removal. Aboveground tissue N content and soil NO_3-N declined with stand age, supporting previous findings that IWG stands are N limited during the first several production years. However, although perennial grasses often respond to N limitation by increasing the amount and proportion of internally translocated N, we saw evidence of the contrary. The amount of N translocated belowground between maturity and senescence declined significantly with stand age,

suggesting an alternative mechanism underlies the decline in tissue N content and soil available NO_3-N. IWG retained low proportions of applied fertilizer in aboveground tissues and root tissues across all stand ages, relying primarily on non-fertilizer-derived sources of N to meet the demands of tissue growth and maintenance, although the increase in fertilizer N recovery from aboveground tissues suggests an increased reliance on fertilizer N as IWG stands age. The low assimilation of applied fertilizer N highlights the need for additional research regarding optimal N fertilizer management in aging IWG stands.

Together, these studies illuminate important changes in resource use and nutrient availability that develop over the 1 – 3 years following IWG establishment. Within just two years of establishment, we saw clear evidence that IWG shifts from a system dominated by root growth and belowground C allocation, to one characterized by root decomposition and exportation of new C inputs from the crop-soil system via soil respiration. While the enhanced decomposition in the second-year IWG suggests a greater capacity to transform root-derived C into more stable soil C compounds and recycle root-derived N into soil pools, the increase in decomposition may also signal changes in the nutrient status of IWG systems that could be detrimental to the ability of IWG to contribute to soil C accrual and long-term grain production. The low proportion of aboveground N sourced from fertilizer implies the majority of IWG N is sourced from non-fertilizer sources, such as the decomposition of IWG crop tissues and the mineralization of native organic N, which may in turn promote organic matter priming and limited soil C accrual. These ideas were corroborated by results from Chapter 2,

where high losses of new C to respiration and reduced belowground C inputs were observed in the second-year IWG. As such, optimizing IWG N management recommendations to more adequately meet the N demands of IWG will be critical to maximizing IWG contributions to soil C storage, reducing reliance on external fertilizer inputs and ensuring IWG remains a sustainable alternative to annual grains in agricultural landscapes.

Figure P.1 Conceptual figure highlighting key results from thesis.

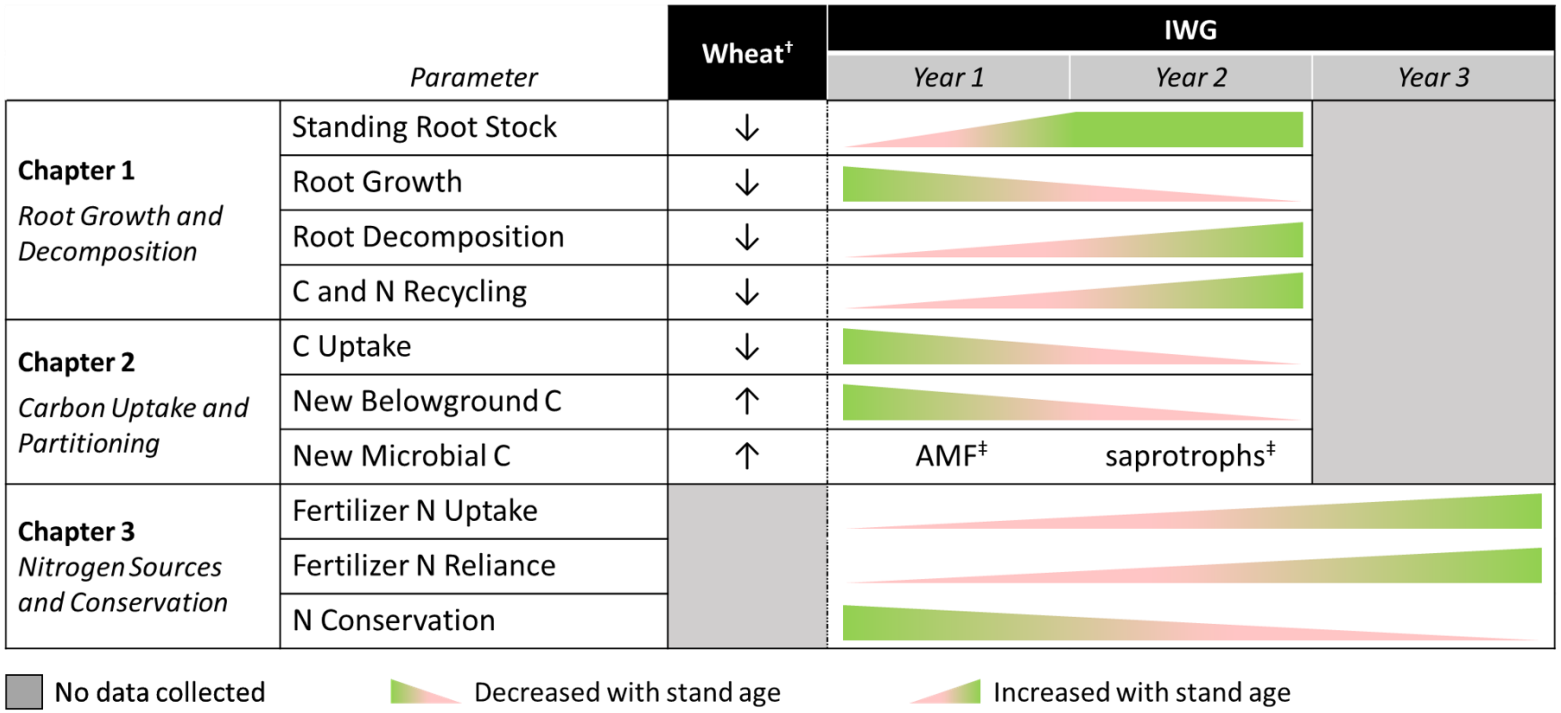

† Direction of arrow indicates values are relatively lower or higher compared to IWG

‡ Indicates whether more new microbial C was stored in AMF or Saprotrophs when compared that of other cropping systems (Wheat, IWG-1 or IWG-2)

Chapter 1 : Effect of Stand Age and Growth Period on Root Growth and Decomposition in Perennial and Annual Grains

Synopsis

Perennial crops such as intermediate wheatgrass (IWG; *Thinopyrum intermedium* (Host) Barkworth and Dewey) produce and maintain larger standing root stocks than annual small grain crops. However, previous studies largely report standing root stock measurements collected at a single point in the growing season and do not separate processes of root growth from root decomposition, which presents a significant gap in our understanding of how roots can contribute to soil organic carbon (C) accrual or other soil properties through time. To fill this knowledge gap, we established a root growth study in 1-year-old IWG (IWG-1), 2-year-old IWG (IWG-2) and annual spring wheat (Wheat; *Triticum aestivum* L.). A combination of sequential coring and root ingrowth core methods were used to measure standing root stock, new root production, root decomposition and turnover of root C and root N between perennial and annual grains and across IWG stand ages. As expected, the standing root stock was 3.2 – 6.5 and 6.3 – 9.9 times higher in IWG-1 and IWG-2 than Wheat, respectively, with these differences attributable to significantly higher early-season root production rates and longer perennial grain crop growing seasons. Although both IWG-1 and IWG-2 exhibited greater new root production and root decomposition than Wheat, clear stand age-related changes in root growth and decomposition were observed. Total root production and root production rates were up to 1.7 and 2.6 times greater in IWG-1 than IWG-2, demonstrating a decline in

new root production as IWG stands age. Conversely, root decomposition almost doubled from 1.39 kg m^{-3} to 2.43 kg m^{-3} between IWG-1 and IWG-2 in the 0 – 15 cm depth interval, marking a shift between the first and second IWG production years from a system dominated by root growth to one dominated by root decomposition. Since root C inputs associated with active root production are more readily stabilized than root inputs derived from the decomposition of root tissues, these findings suggest that the contribution of root-derived C to stabilized soil C pools and associated soil parameters may decline as IWG stands age. However, additional research is needed to directly link these root dynamics to changes in soil C cycling.

Introduction

Perennial grain crops have the potential to improve the social, economic, and environmental health of agricultural systems by diversifying crops on the landscape, agricultural products, and agronomic practices used for crop production (Robertson et al., 2017; Crews et al., 2018). In terms of environmental health, the agronomic practices characteristic of perennial cropping systems and physiological traits inherent to perennial crops impart a suite of ecological benefits on agricultural landscapes. When compared to annual crops, the reduced tillage and diminished fertilizer inputs of perennial cropping systems reduces soil nitrate leaching (Jungers et al., 2019; Reilly et al., 2022), enhances nutrient uptake (Sprunger et al., 2018), and promotes the formation of stable soil aggregates (Tiemann and Grandy, 2015; Rakkar et al., 2023). Physiological differences in carbon (C) uptake and partitioning between perennial and annual grains (Woeltjen, 2023,

Chapter 2) such as greater photosynthetic activity (Jaikumar et al., 2013; Jaikumar et al., 2016), higher belowground C allocation to roots (Sainju et al., 2017), and extensive root production in perennial grains also contribute to the development of more robust soil microbial communities (Liang et al., 2012; Tiemann and Grandy, 2015; McKenna et al., 2020; Audu et al., 2022) and increase the potential sequestration of atmospheric CO_2 in belowground C pools of perennial cropping systems. The potential to increase belowground root and soil C in perennial cropping systems is largely dependent on these latter physiological traits: belowground C allocation and production of extensive root networks. Especially in perennial cropping systems characterized by yearly aboveground biomass removal, root C inputs, either via exudation during active root growth or decomposition of root tissues, represent the primary pathways through which C enters soil (Villarino et al., 2021).

Perennial crops that consistently allocate C belowground and generate large root stocks are expected to have an advantage for increasing soil C pools when compared with annuals. Intermediate wheatgrass (IWG; *Thinopyrum intermedium*, (Host) Barkworth and Dewey), a cool-season perennial grass domesticated for grain and forage production, is emerging as a perennial alternative to annual small grains. Like other perennial grass crops, IWG allocates a large amount of dry matter and C belowground to support the development of deep, dense root networks (Sainju et al., 2017; Sprunger et al., 2018; Bergquist et al., 2022). Coarse and fine root biomass in IWG can be up to 4.8 and 2.6 times greater than in wheat, and total C storage in IWG roots was 6 to 15 times greater in IWG than wheat, indicating that root C contents are also considerably higher in IWG than

wheat (Sprunger et al., 2018a; Sprunger et al. 2018b). Even compared to other perennial grass crops, such as smooth bromegrass and switchgrass, IWG was shown to produce significantly larger standing root stocks to a depth of 1.2 m (Sainju et al., 2017). Despite ample evidence of greater standing root stocks in IWG than other annual crops and perennial grasses, the effect of larger root stocks on soil parameters, including soil C dynamics, remains unclear.

The lack of clarity regarding the relationship between root stocks and soil C and N cycling is due in part to methodological constraints related to temporal variability. Most studies have compared perennial and annual grain crop rooting patterns by measuring standing root stocks at a single time point in the growing season (e.g., Sprunger et al., 2018). However, standing root stocks fluctuate widely across the growing season, and standing root stock measurements collected at a single point in time fail to capture this seasonal variability. For example, IWG root production is expected to be maximal in the early part of the growing season but subsides as IWG approaches physiological maturity (Pugliese et al., 2019). The removal of aboveground biomass at physiological maturity further shifts root growth patterns, with perennial systems often experiencing an increase in root growth following defoliation (Wang et al., 2018; Wei et al., 2019). Furthermore, no studies have evaluated changes in annual root dynamics in IWG as stands age, despite evidence that C uptake and partitioning change dramatically between the first two production years in perennial grass crops (Jaikumar et al., 2013; Woeltjen, 2023, Chapter 2). The lack of temporal studies (regarding both within growing seasons and across stand ages) represents a significant gap in our understanding of how

IWG will affect soil properties such as soil C accrual over its production period when compared to annual grains.

Beyond the lack of temporal studies, few studies isolated the root growth and decomposition processes that drive changes in standing root stocks. The processes of root growth and root decomposition differentially affect soil C storage potential. During active root growth, tissues exude low molecular weight compounds that are rapidly and preferentially stabilized into soil organic matter pools (Villarino et al., 2021). Conversely, root tissues are decomposed more slowly, and the decomposition products could be stored in less stable soil C pools (Villarino et al., 2021). Standing root stock measurements alone are unable to disentangle root growth and decomposition processes, leaving a gap in our understanding of how changes in standing root stocks between perennial and annual grains, or within aging perennial grain stands, will affect soil C and N cycling. Methods that isolate root growth, such as the use of root ingrowth cores to quantify gross root production, should be used in conjunction with standing stock measurements to gain a broader picture of the root growth and decomposition processes occurring in perennial and annual grain systems,

To address these gaps in research, we measured standing root stocks, root growth, root decomposition and root-derived C and N turnover in perennial (IWG) and annual grain cropping systems using paired sequential core and root ingrowth core methods. The annual grain system was represented by spring wheat (*Triticum aestivum* L.), a common small grain grown in the Upper Midwest, USA. We used two IWG stands, one in its first year of production (IWG-1) and one in its second year of production (IWG-2), allowing

us to isolate stand age-related effects on IWG root dynamics while comparing root dynamics between perennial and annual grains. To address uncertainties in seasonal root dynamics, we sampled roots at five times throughout the growing season aligning with five key physiological growth stages: spring vegetative growth, elongation, maturity, post-harvest early regrowth and post-harvest late regrowth. We expected standing root stocks, root growth and root decomposition to be greater in both IWG systems than wheat due to the difference in life strategy. Between the two IWG systems, we expected standing root stocks, root growth and root decomposition to be greater in the older IWG-2 stand than IWG-1 due to the difference in stand age and expected continued root growth over time. Across the growing season, we expected root stocks and root growth in all systems to increase during the early part of the growing season (i.e., between vegetative growth and stem elongation), and for root growth to subside around physiological maturity. In IWG systems, we expected to see an increase in root production during fall regrowth, after grain and biomass were harvested at physiological maturity, followed by a decline in root stocks and root growth as stands undergo senescence.

Materials and Methods

Study Location and Site Description

This study was established at the Rosemount Research and Outreach Center located in southeast Minnesota (44˚42′ N, 93˚05′ W) during the 2020 and 2021 growing seasons. Temperature and precipitation varied across experiment years (fig. 1.1), with

2021 being categorized as a moderate to severe drought year. Soils are deep, well-drained silt loams classified as Typic Hapludolls (NRCS, 2023).

We utilized a modified staggered-start approach with repeated measures to isolate the effect of life strategy (i.e., annual vs. perennial cropping system treatments) and intermediate wheatgrass (IWG; *Thinopyrum intermedium*, (Host) Barkworth and Dewey) stand age on root growth dynamics at various points throughout the growing season. Each experiment year, a 1-year-old intermediate wheatgrass (IWG-1) and a 2-year-old intermediate wheatgrass (IWG-2) stand were selected to represent the perennial grain cropping systems. The annual grain system was spring wheat (Wheat; *Triticum aestivum* L.), and Wheat was planted in a different field each experiment year. Each experiment year, three different fields (each field containing one cropping system per field) were included, so all three cropping systems were represented in both experiment years (table 1.1). All fields in this study were within a 1.45 km radius and were verified to have similar site conditions, including soil texture and hillslope position. In each field, four replicate blocks were delineated.

The agronomic management details for each cropping system can be found in table 1.1. Both IWG-1 and IWG-2 were harvested for grain annually when approaching physiological maturity (see Heineck et al., 2022, table 1.1). After grain harvest, remaining IWG straw was mowed to a height of 10 cm and removed from the field. Similarly, spring wheat was harvested for grain annually at physiological maturity (table 1.1), at which point all aboveground biomass was cut to 10 cm and removed from the field.

Sequential Cores

Sequential coring methods were used to estimate the standing root stock every six weeks to align with five key crop growth stages (figure 1.2, table 1.2). The growth stages can be described as follows, along with their associated range of Zadok's growth stage scores: vegetative growth (20-29), stem elongation (30-37), physiological maturity (87-91), early vegetative regrowth (20-24) and late vegetative regrowth (25-29; Zadoks et al., 1974. Since wheat was harvested at maturity and the field was subsequently planted to a new crop, sequential cores were not collected from wheat after the maturity sampling. At each sampling, a 5 cm diameter auger was placed adjacent to the crop crown at a 45-degree angle to the soil surface (Steingrobe et al., 2001; supplemental figure 1.1). The auger was then pounded into the soil to extract a 21 cm long core of soil to a vertical depth of 15 cm. Soil cores were placed in bags and stored on ice in a cooler during sampling, then transported to a laboratory where they were kept at 4 C until further processing. In total, four replicate cores were collected from each cropping system at each of the five samplings. Shortly after extraction, roots were separated from soil using hydropneumatic elutriation (Smucker et al., 1982). Briefly, the process uses compressed air and water to flush soil free from roots over a 410-micron mesh screen. Following elutriation, roots were dried at 60 C then further cleaned by hand to remove remaining organic debris and sand particles prior to weighing.

Ingrowth Cores

Total root production across the growing season and root production rates between each crop growth stage were quantified using root ingrowth cores (fig. 1.2; Neill 1992; Steingrobe et al., 2001; Chen et al., 2016). In brief, immediately following sequential core extraction (table 1.2), a 5 cm x 21 cm cylinder root ingrowth core constructed from galvanized steel mesh (3.5 mm) was inserted into the cored hole. In the field, root ingrowth cores were then packed to field bulk density with a root-free soil mixture composed of soil collected from the experimental area within each cropping system field. Soil for the root-free soil mixture was always collected within 1 week of ingrowth core installation to ensure the nutrient concentrations of root-free soil mixtures closely approximated those of the surrounding area (Steingrobe et al., 2001). After collection from the field, the soil was brought to the laboratory where it was passed through a 2 mm sieve to remove root fragments. Since sieving disrupted native soil aggregation, fine sand was added to the root-free soil at a ratio of 1:3 sand:soil (Sprunger et al., 2017). The root-free soil mixture was then pre-weighed to achieve the mass of soil mixture needed to achieve field bulk density within ingrowth cores (Steingrobe et al., 2001).

Root ingrowth cores incubated *in situ* for approximately 6 weeks, long enough to allow roots to recolonize the ingrowth core but short enough to ensure little to no decomposition occurred during the ingrowth period (Steingrobe et al., 2001; Chen et al., 2016). Therefore, the root biomass captured in each ingrowth core was a measurement of total root production. At the end of the 6-week ingrowth period, a sharp spade was driven

along the edges of the ingrowth cores to sever roots protruding from the ingrowth core. The spade was then used to remove the cores from the surrounding soil (supplemental figure 1.1). Any remaining roots protruding from the edges of the core were clipped at the ingrowth core edge using scissors. The soil from ingrowth cores was transferred to a plastic bag and stored in a cooler during field sampling. In the laboratory, ingrowth cores were kept at 4 C until further processing, and roots were separated from soil using the methods described for sequential cores.

Root Parameters and Calculations

The sampling schematic and basis for calculations is shown in Figure 1.2. Because soil cores were taken at a 45-degree angle to the soil surface (representing both vertical and horizontal distance), all root biomass values are reported as root mass per soil volume to a 15 cm depth.

The standing root stock at each sampling event was determined as the total mass of roots extracted in sequential cores. The root production rate was calculated from the mass of roots collected from ingrowth cores, as follows:

$$Root\ production\ rate\ (kg\ m^{-3}\ day^{-1}) = \frac{IG}{IP}$$

where for a given growth period IG was the mass of roots (kg m^{-3}) collected from the ingrowth core and IP was the ingrowth core incubation period (in days), or the number of days cores were allowed to incubate *in situ*. Since we assume minimal decomposition occurred during the ingrowth core incubation period, the root mass collected from the ingrowth core represented the total mass of roots produced during the incubation period,

or the total root production. We present the total root production across the growing season, which was calculated as:

$$Total\ root\ production\ (kg\ m^{-3}) = IG_{vegetative\ to\ elongation} + IG_{elongation\ to\ maturity} + IG_{maturity\ to\ late\ regrowth} + IG_{late\ to\ early\ regrowth}$$

where IG was the root mass (kg m^{-3}) collected from the ingrowth core during each respective growth period.

The mass of roots decomposed over the growing season was determined using the change in standing root stock and total root production across the growing season (Komainda et al., 2018). The change in standing root stock across the growing season was calculated as the difference in standing root stock between the vegetative sampling event ($SRS_{vegetative}$) and final sequential core extraction (SRS_{final}) for each cropping system:

$$\Delta SRS_{growing\ season}\ (kg\ m^{-3}) = SRS_{final} - SRS_{vegetative}$$

Since Wheat was harvested at maturity, after which the field was prepared for planting of the subsequent crop and was unable to be further sampled, SRS_{final} was the standing root stock at the maturity sampling event. In IWG-1 and IWG-2, the crops continued growing after grain harvest, and SRS_{final} was therefore the standing root stock at the late regrowth sampling event. As the change in standing root stock over the growing season is determined by the difference between new root production and root decomposition, root decomposition was estimated as the difference between the change

in standing root stock across the growing season (i.e., net root production; kg m^{-3}) and total root production (kg m^{-3}), similar to calculations used by Komainda et al. (2018):

$$Root\ decomposition\ (kg\ m^{-3}) = \Delta SRS_{growing\ season}\ - total\ root\ production$$

Root C and N turnover in the upper 15 cm of the soil profile was then estimated as follows:

$$Root\ turnover\ (kg\ m^{-3}) = root\ decomposition * C\ or\ N\ concentration$$

where the C or N concentration were the average root C and N concentration collected from an adjacent experiment (Woeltjen, 2023, Chapter 2). The methods of root C and N determination are described in Woeltjen (2023, Chapter 2), but in brief, roots from each cropping system were extracted to a depth of 15 cm, dried at 60 C for 48 h and ground using a ball mill. Root samples were then prepared for elemental analysis via dry combustion using an elemental analyzer coupled to a continuous-flow Isoprime 100 isotope ratio mass spectrometer (Elementar Pyrocube, Elementar Americas, Inc.) to determine root C and N concentration.

Statistical Analysis

All statistical analysis was performed using R (R Core Team, 2022). The effect of cropping system, crop growth stage and experiment year (and their interactions) on

standing stock and root production rate was evaluated using linear mixed effects models. Using the *lme* function from the nlme package (Pinheiro et al., 2000), random intercept models were created with a random effects structure of growth stage nested within block replicate. Standing stock values were square-root transformed prior to statistical analysis to meet the distribution assumptions of mixed effects models. The effect of cropping system and experiment year (and their interaction) on the total root production, root decomposition, root C turnover and root N turnover over the study period was evaluated using two-way ANOVA with the *lm* function from the stats package (R Core Team, 2022). When main effects or interactions were significant ($p < 0.05$), a Tukey's-adjusted least-squares means comparison was performed using *emmeans* from the emmeans package (Lenth, 2023). Compact letter displays were generated from the estimated means using the *cld* function from the multcomp package (Hothorn et al., 2008). Prior to post-hoc testing, all models were verified to meet model assumptions. All significant differences were evaluated when $p < 0.05$.

Results

Standing Root Stock

Standing root stock varied significantly by cropping system, growth period, experiment year, and all possible two-way interactions between variables (table 1.3). The effect of cropping system on standing root stock varied by crop growth stage (table 1.3, fig. 1.3a). At the vegetative growth stage, standing root stock from IWG-1 (0.53 kg m^{-3}) was like that of wheat (0.39 kg m^{-3}), though both were nearly 3 and 4 times lower,

respectively, than the standing root stock of the IWG-2. However, by elongation IWG-1 experienced a significant increase in standing root stock, growing by nearly 71% between the vegetative and elongation growth stages. Following elongation, the standing root stock in IWG-1 remained greater than wheat and smaller than IWG-2. Following crop maturity and harvest, no significant differences in standing root stocks were detected between IWG-1 and IWG-2. Between early and late vegetative regrowth stages, standing root stock declined by 37% and 55% in IWG-1 and IWG-2, respectively.

A two-way interaction between growth stage and experiment year was observed (table 1.3). Standing root stock was 0.73, 0.73 and 0.58 times lower in 2020 than 2021 at the elongation, early regrowth and late regrowth. No significant differences in standing root stock between 2020 and 2021 were detected at the vegetative or maturity stages.

Within experiment year, there was a significant effect of cropping system (table 1.3). In both 2020 and 2021, standing root stock was greatest in IWG-1 followed by IWG-2 and then wheat (fig. 1.3b). Differences in standing root stock were also detected between IWG-1 and IWG-2, with standing root stock in 2020 and 2021 almost 21% and 36% greater, respectively, in IWG-2 than IWG-1, marking a significant increase in standing root stock between the first- and second years of IWG production. Averaged over both 1) growth stage and 2) cropping system, standing root stocks were smaller in 2020 (0.784 kg m^{-3}) compared to 2021 (0.984 kg m^{-3}).

Root Production Rate and Total Root Production

Root production rates were significantly affected by cropping system, experiment year and all two-way interactions between cropping system, growth period and experiment year (table 1.3). When averaged across crop growth periods, significant differences in new root production rates between cropping systems were evident (fig. 1.4a). IWG-1 and IWG-2 initially maintained a new root production rate nearly 45-65% greater than that of wheat between vegetative growth and elongation. However, between elongation and maturity, root production rates in IWG-1 and IWG2 decreased precipitously to 1.84 g m^{-3} $day^{-1}$and 1.36 g m^{-3} day^{-1}, respectively, compared to 2.14 g m^{-3} day^{-1} in wheat during this same time. Following maturity and aboveground biomass removal at grain harvest, new root production rate increased in both IWG systems, returning to early-season levels for a short period before declining again between the early regrowth and late regrowth period. IWG-1 maintained a 25 - 50% higher new root production rate than IWG-2 through the last two samplings during late-season regrowth.

When averaged across experiment years, the new root production rate in IWG-1 was nearly 21% lower in 2020 than 2021, lowered from 3.54 g m^{-3} day^{-1} to 2.768 g m^{-3} day^{-1}, respectively (fig. 1.4b). Despite this decline, both IWG systems on average still maintained significantly higher new root production rates than wheat during the early part of the growing season. In 2020, a significantly higher new root production rate was observed in IWG-1 compared to IWG-2, though this trend was not observed again in 2021 (fig. 1.4b).

Root Production and Root Decomposition

Total root production varied significantly across cropping system (table 1.4). Total root production over the study period was significantly greater in both IWG systems compared to wheat, and root production was nearly twice as high in IWG-1 (2.06 kg m^{-3}) than IWG-2 (1.20 kg m^{-3}). Total root production averaged over cropping systems was similar across years, and there was no significant effect of the cropping system x experiment year interaction on total root production (table 1.4)

Root decomposition was significantly affected by cropping system (table 1.4). Averaged across cropping system, root decomposition was 9.3 times greater in IWG-2 than Wheat. Trends suggest root decomposition in IWG-1 was lower than IWG-2 and greater than wheat, though differences were not significant ($P > 0.05$). Root decomposition was not affected by experiment year or the cropping system x experiment year interaction ($P > 0.05$).

Turnover of Root C and N

Root C and N turnover differed significantly by cropping system (table 1.4). On average a significantly greater mass of C was decomposed from roots in IWG-2 compared to wheat, but the mass of decomposed root C in IWG-1 did not differ significantly from IWG-2 or Wheat. IWG systems returned a significantly greater mass of N to soil via root turnover than wheat, with root N turnover in IWG-1 and IWG-2 on average 3.4 and 3.8 times greater than in wheat. No significant differences in root N turnover were detected between IWG-1 and IWG-2. Neither root C nor root N turnover

were significantly affected by experiment year, or the cropping system x experiment year interaction ($P > 0.05$).

Grain Yields

There was a significant interactive effect of cropping system and experimental year on grain yields, where grain yields differed significantly by experimental year for the Wheat cropping system only (table 1.5). Within both the 2020 and 2021 experiment years, grain yields were significantly lower in IWG-1 and IWG-2 than Wheat, though no significant difference was detected between IWG-1 and IWG-2 in either year. No significant differences were detected in the grain yield of IWG-1 or IWG-2 between experiment years, though grain yield was significantly lower in 2021 than 2020 for Wheat.

Discussion

Standing Root Stocks and New Root Production in Annual and Perennial Grains

Standing root stocks were 3 to 6 and 6 to 10 times greater in IWG-1 and IWG-2 compared with spring wheat when averaged across growth period, in line with studies showing IWG root stocks were 4 to 25 times greater in IWG than soybean, maize and winter wheat in the upper 10 – 15 cm of soil (Sprunger et al., 2019; Reilly et al., 2022; Rakkar et al., 2023). The larger standing root stocks in IWG were associated with generally greater new root production rates (except between elongation and maturity)

compared with Wheat, with Wheat on average maintaining new root production rates around 2 g m^{-3} day^{-1} in both 2020 and 2021. The new root production rates reported for IWG-1 and IWG-2, respectively ranging from 5 g m^{-3} day^{-1} and 15 g m^{-3} day^{-1} in 2020 to 9 g m^{-3} day^{-1} and 8 g m^{-3} day^{-1} in 2021, were consistent with switchgrass monocultures (12 g m^{-3} day-1), miscanthus monocultures (8 g m^{-3} day^{-1}) and restored prairie (15 g m^{-3} day^{-1}) in their third production year (Sprunger et al., 2017). Together, these results further illustrate the capacity of IWG to build larger root stocks than annual grains and suggest higher root production rates sustained over longer perennial crop growing seasons drive the difference in standing root stocks between perennial and annual grain crops.

Root decomposition, root C turnover and root N turnover were consistently greater in IWG systems than Wheat. These results are in line with others showing systems with greater root production are associated with greater root turnover (Luo et al., 2021), but contradict studies showing systems with greater root biomass have slower root decomposition rates (Fornara et al., 2009). The discrepancy may relate to the quality of root tissues and relative ease with which root tissues are decomposed. In IWG, as with many grasses, root tissues are readily decomposed and therefore larger root biomass stocks would be expected to contribute to greater amounts of root biomass decomposed. The discrepancy underscores the need for additional mechanistic studies evaluating root turnover dynamics in perennial and annual crops.

The implications of enhanced root growth and decomposition for soil C in perennial cropping systems, such as IWG, remain unclear. In field studies, root growth and decomposition, and the subsequent inputs of root C into soil, have both been shown

to have positive, negative or no correlation with soil C levels, and this effect can vary across crop types (Guo et al., 2007; Cai et al., 2019; Morales Ruiz et al., 2020). On one hand, greater root biomass may enhance soil aggregation and stability, while allocating a larger amount of C input belowground to support the development of robust microbial communities and stable soil C (Buckeridge et al., 2020; Dijkstra et al., 2021). Evidence of enhanced aggregate stability and more diverse microbial communities has been seen in IWG, with studies showing aggregate stability and the size of some microbial functional groups was larger under IWG than Wheat in the presence of larger IWG root stocks (McKenna et al., 2020; Rakkar et al., 2023). Together with our results, these studies suggest the enhanced root growth observed in IWG systems may be beneficial for building soil quality and soil C.

The benefits of enhanced root production and decomposition, however, may be offset by root growth-related processes that accelerate C loss from the belowground system. For example, organic matter priming, or the decomposition of native organic matter induced by root growth, may offset any potential soil C gains introduced by increased root C inputs. Ye and Hall (2019) concluded that, despite the significantly greater root biomass generated by perennial biofuel grasses, the extensive root networks spurred organic matter priming and ultimately limited soil C accrual in perennial grass bioenergy systems as new root C inputs were offset by the respiratory losses of native soil C. Though the extent of organic matter priming in IWG remains unclear, others showed the amount of recently assimilated C lost to respiration increased dramatically between the first and second IWG production year, suggesting the root C inputs are not

readily stabilized into soil pools (Woeltjen, 2023, Chapter 2). Further, emerging theories suggest roots can have a destabilizing effect on soil aggregation and C pools through the direct destruction of soil aggregates in some cropping systems, although experimental evidence remains limited to support this theory (Naveed et al., 2017; Dijkstra et al., 2021). The discrepancies in the benefits and drawbacks associated with greater root growth and decomposition further challenge the ability to predict the effect of enhanced root growth and decomposition on longer-term soil C storage and soil quality in IWG systems, underscoring the need for additional research to directly link changes in root growth and decomposition to the formation of stable soil C.

Stand Age-Related Effects on Root Growth in Perennial Grains

Studies evaluating changes in root dynamics as herbaceous perennial crops age are limited and often confounded by experimental and environmental factors. In studies of standing root stocks within the same experimental plots across multiple study years, root stocks grew by 74 - 192% between the first and second production years in perennial forage and bioenergy systems (Bolinder et al., 2002; Acharya et al., 2012). In a study conducted in Wisconsin, IWG belowground biomass (of which 83 - 88% was accounted for by roots) rose substantially between the first and second IWG production years, though the authors noted these results should be interpreted with caution due to the confounding of IWG stand age with experiment year (Sakiroglu et al., 2020). Our study was one of the first to isolate the effect of stand age and avoid confounding effects of production year on IWG root dynamics by using a modified staggered-start experimental

approach. We observed standing root stocks increased by as much as 36% between the first and second IWG production years, verifying observations that perennial crops rapidly accumulate root biomass in surface soils in the first years of production (Pugliese et al., 2019).

The evaluation of root growth and decomposition in the first- and second-year IWG systems showed a clear shift from a system dominated by root growth to one dominated by root decomposition. Similar trends were seen by Woeltjen (2023, Chapter 2), where the allocation of new C to belowground pools declined significantly between the first and second IWG production year. This transition from a system dominated by root growth to one dominated by root decomposition is in line with a shift in economic growth strategies. During the establishment year, young perennial plants often employ an acquisitive growth strategy, rapidly acquiring resources and investing them into the development of extensive belowground root networks to further enhance the capacity to acquire nutrients and resources. Between the first and second production year, the crop growth strategy transitions to a more conservative state, where the crop invests in tissue maintenance and stress protection rather than the production of new tissues. The shift from acquisitive to conservative growth between the first and second production year has been seen in miscanthus (Tejera et al., 2021) and herbaceous perennials in the *Brassicaceae* family (Pastor-Pastor et al. 2015). Jaikumar et al. (2016) further found evidence that older IWG invests more heavily into mechanisms that protect against environmental stressors, such as cold temperatures. Together with this previous research,

our study presents additional evidence that IWG shifts from an acquisitive to conservative growth strategy early in the IWG production period.

The transition from an acquisitive (dominated by root growth) to conservative to (dominated by root decomposition) system has important implications for soil C and N cycling. The transition from growth-dominated to decomposition-dominated will alter the chemical quality of root inputs entering the soil and the subsequent likelihood of root-derived C stabilization and root-derived N availability. Active root growth is commonly associated with the input of C via root exudation, releasing relatively labile, low molecular-weight organic substances into the soil (Cotrufo et al., 2013). These exudates are expected to be readily utilized by microbial communities and more efficiently transformed into stable mineral-associated organic matter (Cotrufo et al., 2013; Villarino et al., 2021). Conversely, the decomposition of root tissues more efficiently forms particulate organic matter, a less stable form of soil C (Villarino et al., 2021). Therefore, in the second-year IWG stand, although more root-derived C is added to the soil through decomposition of root tissues than in IWG-1, the C derived from root decomposition may be poorly stabilized, leading to increases in respiratory C losses (Woeltjen, 2023, Chapter 2) and yielding limited advantages for soil C accrual.

Temporal Dynamics and Year-to-Year Variability in Root Parameters

Across the growing season, temporal fluctuation in IWG standing root stock and root production rates were evident and were possibly associated with environmental factors such as precipitation, nutrient availability, and physiological factors controlling C

allocation (see Woeltjen, 2023, Chapter 2) and dry matter production. Sainju et al. (2017) showed IWG total root biomass was significantly negatively correlated with soil water content, and the peak in root production rates between vegetative growth and elongation aligned with the early season peak in precipitation and subsequent increase in soil moisture availability. Soil moisture availability drives root growth and development across a variety of systems, including IWG, pastures, and prairies (Von Haden and Dornbusch 2014; Sainju et al., 2017; Luo et al., 2021). Lower rainfall coupled with increased C allocation to support aboveground reproductive growth explains the reduction in root production rates we observed between elongation and maturity. Following the harvest of grain at maturity, root production rates increased to levels like those observed between the vegetative and elongation growth stages. Others observed surges in root growth following the cutting and removal of aboveground biomass at grain harvest in IWG and other perennial systems (Wang et al., 2018; Pugliese et al., 2019; Wei et al., 2019), and this acceleration in root growth is likely driven in part by changes in soil moisture availability and inherent resource conservation strategies. Luo et al. (2021) showed that mowing of perennial pastures reduced water loss via evapotranspiration, which in turn enhanced soil water content to support a post-mowing peak in root development. In IWG, evapotranspiration rates similarly fell during the post-harvest vegetative regrowth periods (de Oliveira et al., 2018), suggesting that grain harvest in IWG may impart a similar increase to soil water availability and subsequent root growth. During this period, perennial crops also translocate resources and nutrients belowground to store for use in subsequent growing seasons, which aligns with a period

of active root growth as perennial plants allocate internal resources and nutrients belowground (Jach-Smith and Jackson, 2015). Similar to standing root stock, the final decline in root production rates between the early and late regrowth stages aligns with plant senescence.

Interestingly, IWG systems were more susceptible to year-to-year variability than Wheat, which had similar standing root stock and new root production in both 2020 and 2021. These results highlight the variability and unpredictability of root growth dynamics in IWG systems from year to year and align with other studies that documented significant year-to-year variation in root parameters. For example, Clément et al. (2022) noted average IWG root length in the early growing season at 0.5 m, 1 m and 1.25 m depths differed from 10 to 25 cm, 3 to 10 cm and 1 to 7 cm between the 2018 and 2019 experiment years, respectively. Others similarly found year-to-year variation in root biomass and associated processes in IWG (Sainju et al., 2017, Reilly et al., 2022). The greater variability in root growth parameters observed in IWG-1 compared with Wheat may be attributable to differences in genetic diversity within populations among the IWG and spring wheat crops. While spring wheat has undergone centuries of breeding to select for cultivars that consistently perform across a variety of environments, IWG has been bred for grain production for just over 30 years. Further, the differences in precipitation across experiment years likely in part drove the year-to-year variability observed in this study (Sainju et al., 2017), with the 2021 experiment year being categorized as a moderate to severe drought. Regardless of the processes driving the variability in IWG root growth and decomposition, the inconsistency in root production dynamics between

years challenges the predictability of root dynamics in IWG systems and the ability to predict how IWG root systems will influence soil C and N cycling when planted on a larger scale.

Conclusions

We found significant differences in root growth between perennial grains (IWG-1 and IWG-2) and annual grains (Wheat) and between the first- and second-year IWG stands. Regardless of stand age, IWG systems were characterized by larger standing root stocks, greater root production and increased root decomposition when compared to wheat. While the enhanced root dynamics in perennials compared to annuals may increase contributions to soil C storage, it remains unclear how the increased root growth and decomposition will affect longer-term soil C storage. Standing root stocks, root production and decomposition were also shown to differ by stand age, with IWG shifting from a system dominated by root growth to one dominated by root decomposition as stands age, and potentially transitioning the system from one that readily stabilizes root C inputs to one that stores root-derived C in less stable pools. Further, we found root dynamics in IWG systems to be more variable than wheat, challenging the predictability and ability of these systems to consistently provision ecosystem services associated with enhanced root growth. Together, these results offer crucial context to discussions of the functions roots play in perennial grain crop stands, which can offer insight to other perennial grass cropping systems.

Table 1.1 Agronomic management details for each cropping system.

		IWG-1	IWG-2	Wheat
2020	Field ID	R34	V17	R90
	Planting date	September 2019	September 2018	April 2020
	Seeding rate	13 kg live seed ha^{-1}	13 kg live seed ha^{-1}	2.7 million seeds ha^{-1}
	Row spacing	38 cm	41 cm	15 cm
	N fertilization date	April 2020	April 2019, April 2020	April 2020
	N fertilization rate	80 kg N ha^{-1}	80 kg N ha^{-1}	80 kg N ha^{-1}
	N fertilizer type	Urea	Urea	Urea
	Harvest date	August 3	August 3	July 24
2021	Field ID	R90	R34	R7-21
	Planting date	September 2020	September 2019	April 2021
	Seeding rate	13 kg live seed ha^{-1}	13 kg live seed ha^{-1}	2.7 million seeds ha^{-1}
	Row spacing	32 cm	38 cm	15 cm
	N fertilization date	April 2021	April 2020, April 2021	April 2020
	N fertilization rate	80 kg N ha^{-1}	80 kg N ha^{-1}	80 kg N ha^{-1}
	N fertilizer type	Urea	Urea	Urea
	Harvest date	July 28	July 28	July 28

Table 1.2 Extraction dates of standing root stock cores (SRS), and installation dates, extraction dates and ingrowth period of root ingrowth cores (RIC) for 2020 and 2021.

	2020			2021		
	Installation date	Extraction date	Ingrowth period (days)	Installation date	Extraction date	Ingrowth period (days)
SRS	–	05/11/2020	–	–	6/3/2021	–
	–	06/23/2020	–	–	7/16/2021	–
	–	08/07/2020	–	–	8/19/2021	–
	–	09/18/2020	–	–	10/12/2021	–
	–	10/20/2020	–	–	11/23/2021	–
RIC	05/11/2020	06/23/2020	43	6/3/2021	7/16/2021	43
	06/23/2020	08/07/2020	45	7/16/2021	8/19/2021	34
	08/07/2020	09/18/2020	42	8/19/2021	10/12/2021	54
	09/18/2020	10/20/2020	32	10/12/2021	11/23/2021	42

Table 1.3 Analysis of variance and probability of significance for standing root stock and root production rate. P-values < 0.05 are bolded.

	Standing root stock	Root production rate
Cropping system (CS)	**< 0.0001**	**< 0.0001**
Growth period (G)	**< 0.0001**	0.3335
Experiment year (Y)	**< 0.0001**	**0.0030**
CSxG	**< 0.0001**	**0.0013**
CSxY	**0.0082**	**< 0.0001**
GxY	**0.0025**	**0.0001**
CSxGxY	0.2424	0.1029

Table 1.4 Analysis of variance, probability of significance and mean of root parameters in the upper 0 – 15 cm: total root production, root decomposition, root C turnover, and root N turnover. Within a root parameter, means not sharing any lowercase letters are significantly different ($p < 0.05$) between cropping system or experiment year.

		Total root production	Root decomposition	Root C turnover	Root N turnover
ANOVA	Cropping system (CS)	**<0.0001**	**0.0010**	**0.0008**	**0.0090**
	Experiment year (Y)	0.5106	0.2562	0. 2190	0.2178
	CSxY	0.0502	0.2563	0.2937	0.0599
		$kg\ m^{-3}$	$kg\ m^{-3}$	$g\ m^{-3}$	$g\ m^{-3}$
Cropping system	IWG-1	2.06 a	1.39 ab	561 ab	12 a
	IWG-2	1.20 b	2.43 a	990 a	14 a
	Wheat	0.38 c	0.26 b	126 b	4 b
Year	2020	1.16	1.59	640	11.16
	2021	1.27	1.13	455	8.59

Table 1.5 IWG grain yields (kg ha^{-1}) harvested at physiological maturity. Means not sharing any lowercase letters are significantly different ($p < 0.05$) between cropping systems within an experiment year. Means not sharing any uppercase letters are significantly different ($p < 0.05$) between experiment years within a cropping system.

	IWG-1	IWG-2	Wheat
2020	942 Ab	369 Ab	6083 Aa
2021	1162 Ab	676 Ab	3307 Ba

Figure 1.1 Precipitation (inches) and mean daily temperature (degrees F) at study site over experimental years (2020 and 2021).

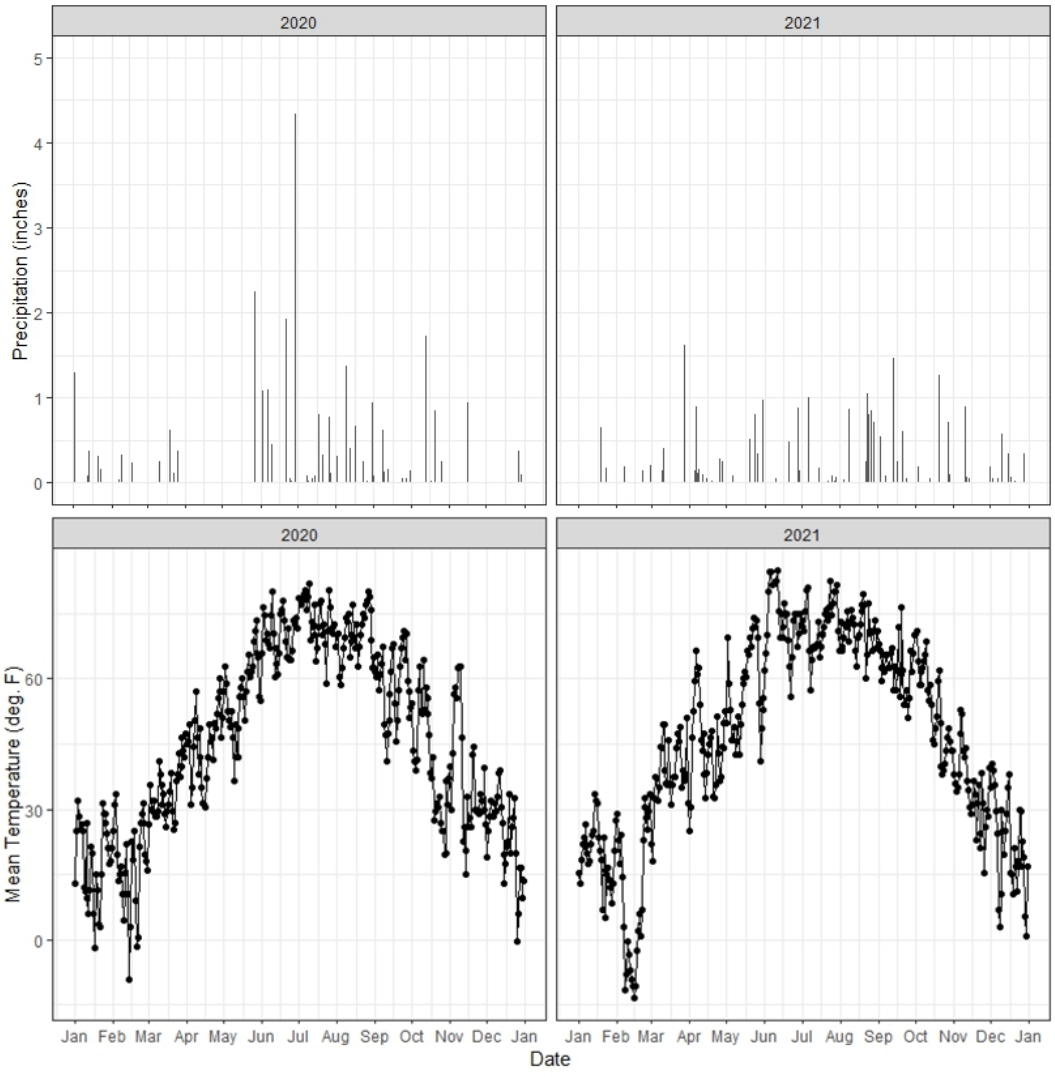

Figure 1.2 Conceptual diagram depicting sequential core extraction, ingrowth core installation/extraction, total root production, and calculation of root decomposition and root production rate. Total root production is represented by the cumulative mass of roots collected from each ingrowth core across the growing season. Root decomposition is represented as the total root production subtracted from the difference in initial and final standing root stock. The root production rate is the mass of roots collected between each growth stage divided by the ingrowth period.

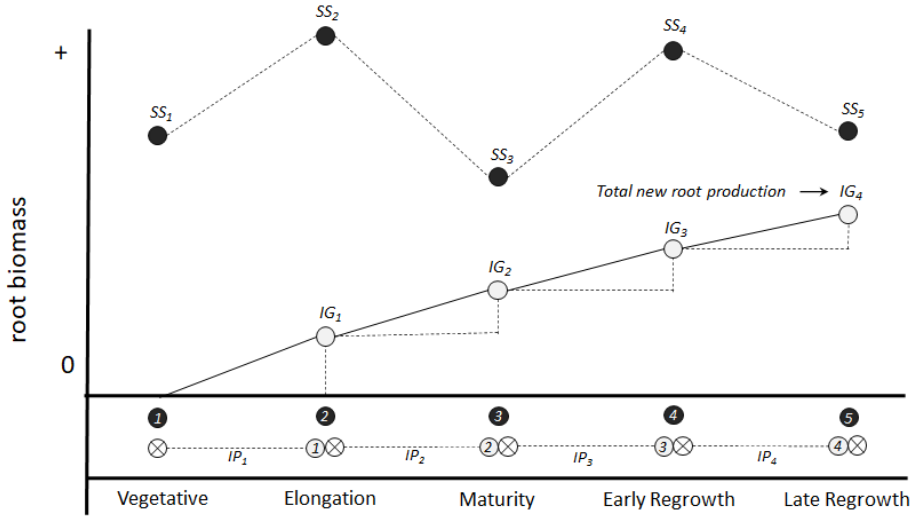

n Sequential core extraction

n Ingrowth core extraction

Ingrowth core installation

IP_n Ingrowth period (days)

$$Root\ Producation\ Rate = \frac{IG_n}{IP_n}$$

$$Decomposed\ Root\ Biomass = (SS_5 - SS_1) - IG_4$$

Figure 1.3 Means and standard error of standing root stock for three cropping systems when: a) grouped by crop growth stage and b) grouped by experiment year. In panel a, means with different lowercase letters are significantly different within a growth stage ($p < 0.05$), and means with different uppercase letters are significantly different within a cropping system ($p < 0.05$). In panel b, different lowercase letters denote significant differences between cropping systems within an experiment ($p < 0.05$). In panel a, the vertical dotted line represents the point at which aboveground biomass was removed at maturity for grain harvest.

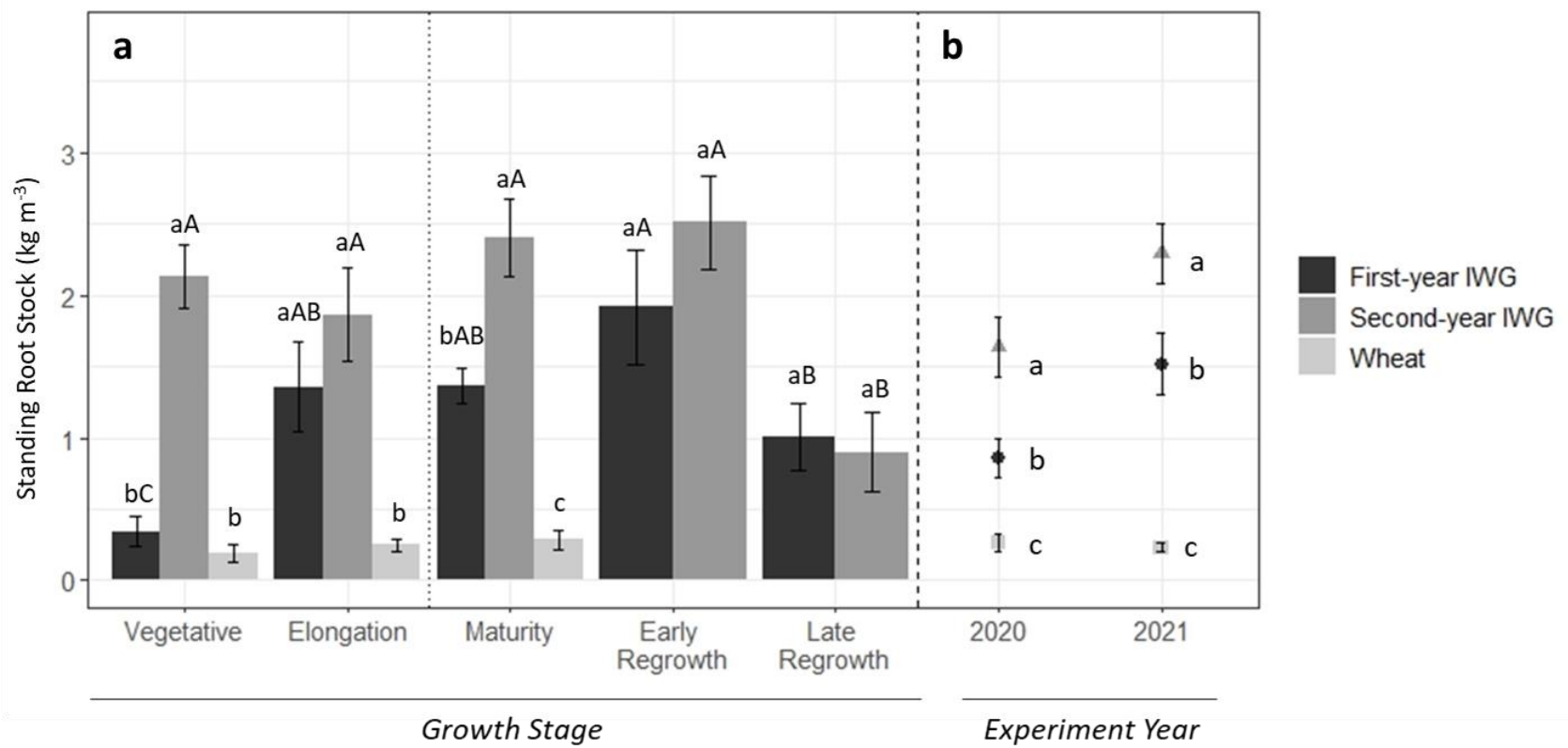

Figure 1.4 Means and standard error of root production rate for three cropping systems when: a) grouped by crop growth stage and b) grouped by experiment year. In panel a, means with different lowercase letters are significantly different within a growth stage ($p < 0.05$), and means with different uppercase letters are significantly different within a cropping system ($p < 0.05$). In panel b, different lowercase letters denote significant differences between cropping systems within an experiment ($p < 0.05$). In panel a, the vertical dotted line represents the point at which aboveground biomass was removed at maturity for grain harvest.

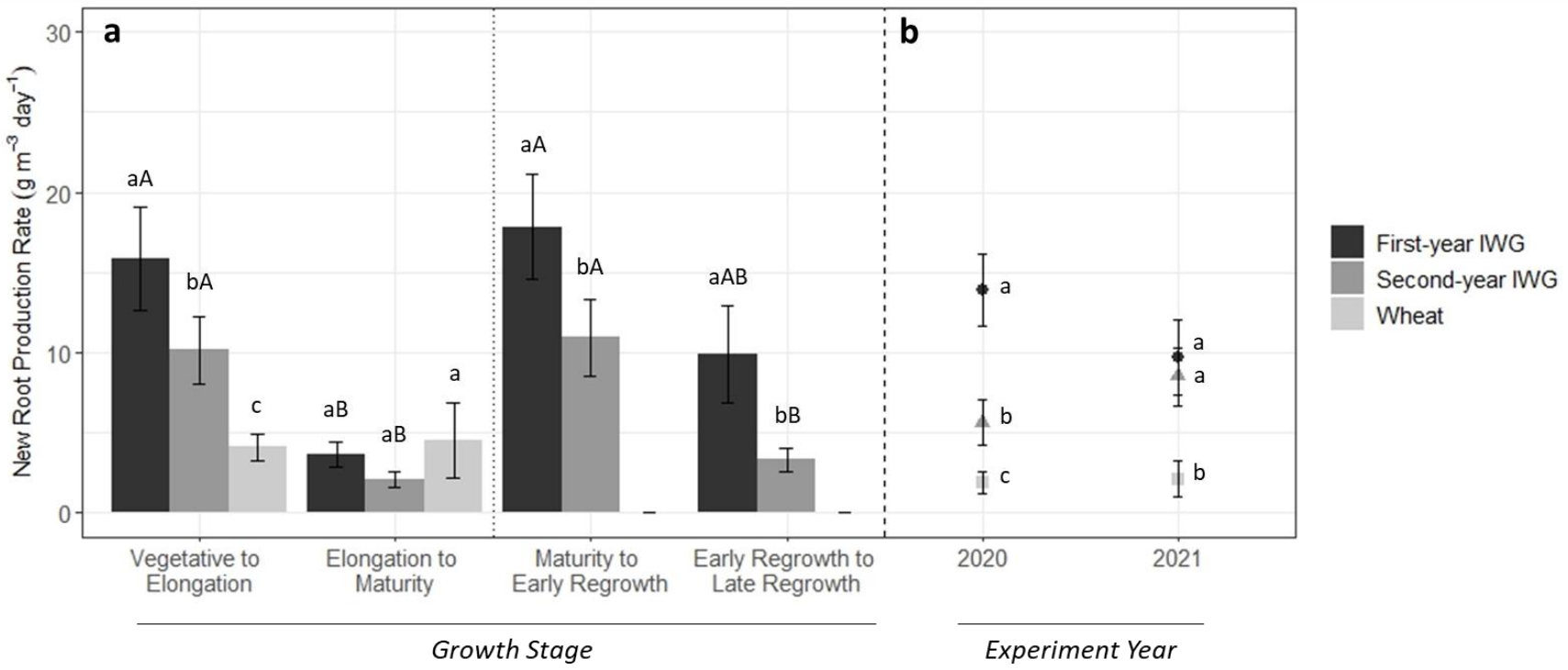

Chapter 2 : Stand Age-related Changes in Carbon Uptake and Partitioning May Limit Potential for Belowground Carbon Storage in a Perennial Grain Cropping System

Synopsis

Contrary to expectations, many perennial crops yield little to no increase in soil carbon (C) stocks, and it remains unclear the extent to which perennial age-related changes in crop physiological traits such as C uptake and crop-microbial-soil C partitioning underly this pattern. As soil C stocks respond slowly to land use changes, experimental designs that directly track C fluxes and C incorporation into crop-microbial-soil pools will shed light on the role C uptake and partitioning play in constraining soil C accrual. We conducted a ^{13}C isotope-tracer study to compare C uptake and crop-microbial-soil C partitioning patterns between a 1-year-old (IWG-1) and 2-year-old (IWG-2) perennial grain crop, intermediate wheatgrass (IWG; *Thinopyrum intermedium* (Host) Barkworth and Dewey), and compared these to an annual grain crop, spring wheat (*Triticum aestivum* L.). Crop shoots, roots, soil, and soil respired-C were sampled 10 times over a 90-day chase period to track the fate of recently assimilated ^{13}C into crop-soil pools. In addition, the incorporation of recently assimilated ^{13}C into soil microbial biomass (^{13}C PLFA) and functional groups was determined over the first 7 days post-label application. Results indicated IWG ineffectively partitioned new C to soil pools, with only 12% and 8% of total assimilated C recovered from soil in IWG-1 and IWG-2 when averaged across the study period, compared to the almost 25% of total assimilated C recovered from wheat soil. Instead of new C being mobilized to soil pools, the

relatively large proportion of new C stored in IWG1-1 roots (14%) and arbuscular mycorrhizal fungi compared to that of wheat or IWG-2 suggests IWG invests more heavily in the development of root-mycorrhizal networks during its first production year. By the second production year, very little new C was allocated belowground, with almost 50% of total assimilated C retained in aboveground tissues and over half of the assimilated C lost via soil respiration by the end of the study period. IWG-2 also had a larger proportion of microbial C accounted for by saprotrophic fungi than seen in the other wheat or IWG-1. We expect the changes in C partitioning are due to a shift from an acquisitive to conservative growth strategy that occurs between the first and second IWG production years, which may substantially limit the potential contributions to soil C accrual as IWG stands age.

Introduction

Cropland soil management plays a critical role in regulating the flux of carbon (C) between atmospheric and terrestrial pools. Over the past 12,000 years, land cultivation has already released an estimated 116 – 154 Pg C from soil now managed for agriculture, with half of this soil carbon loss attributable to cropland management (Sanderman et al., 2016). Most croplands continue to act as a net source of CO_2 to the atmosphere, especially in systems dominated by annual crop species (West et al., 2010; IPCC, 2022), which are predicted to lose approximately 0.3% of their C stocks each year over the coming decades due to annual cropland management practices such as frequent tillage and in-field disturbances (Molotoks et al., 2020; Garnier et al., 2022). Establishing

cropland management systems that prevent soil C loss and ideally restore C stocks through soil C sequestration on just a small fraction of the over 556 million hectares of land area occupied by annual maize, soybean and wheat will have substantial implications for mitigating climate change and maintaining long-term productivity of cropland soils (Amelung et al., 2020; FAO, 2021).

The perennialization of croplands is often proposed as a strategy to increase the potential for soil C sequestration without sacrificing cropland productivity (Gutknecht et al., 2023). Perennial grasses, including those domesticated for biofuel, forage, and grain production, are expected to enhance soil C accrual compared to the annual species monocultures more typically seen in croplands (Tieman and Grandy, 2015; Augarten et al., 2023). Under perennial grass crops, soil C accrual is promoted by extensive and dense root networks, greater belowground C inputs and reduced soil disturbance. However, there have been inconsistent results regarding the capacity of perennial grass cropping systems to build soil C. While some perennial grass crops significantly increased soil C stocks relative to annual grains within 5 years of establishment, others such as emerging perennial grain crops show no evidence of increasing total soil C stocks during their 3 – 5-year production period (Zan et al., 2001; Sprunger et al., 2018). These discrepancies challenge our understanding of whether perennial grass cropping systems will predictably build soil C in agricultural landscapes and raise questions regarding the mechanisms that underlie the inconsistent response of soil C stocks to perennial grass crop establishment.

A variety of mechanisms regulating the balance of soil C inputs and soil C losses that drive changes in soil C stocks have been investigated, including the priming of native

organic matter (Ye and Hall, 2019), the stabilization of C in mineral-organo complexes (Tiemann and Grandy, 2015), and crop physiological controls over C uptake (i.e., the total C assimilated via photosynthesis during a given time period) or C partitioning to crop-microbial-soil pools. Crop physiological traits such as C uptake and C partitioning are often stronger regulators of soil C dynamics and accrual than edaphic or climatic factors (Fujisaki et al., 2018; Ji et al., 2022; Janzen et al., 2022), but we lack a clear understanding of how perennial grass crop C uptake and C partitioning to crop-microbial-soil pools differ from that of annual crops. Separate studies suggest perennial crops allocate a larger proportion of recently assimilated C belowground (Woeltjen, 2023, Chapter 1), but almost no studies directly compared these findings to annual crop C allocation patterns. Further, almost no studies evaluated age-related changes in herbaceous perennial crop C partitioning, despite clear age-related change in C partitioning in woody perennials (Genet et al., 2010; Bruggerman et al., 2011). These gaps in research hamper the ability to predict soil C accrual in perennial grass cropping systems and thwart efforts to establish perennial crops to build C in cropland soils.

Beyond crop physiological controls, root-microbial-soil interactions strongly regulate soil C accrual. The transfer of root-derived C into soil microbial pools, and subsequent deposition of microbially-derived C into soil pools is increasingly recognized as a primary pathway through which stable soil C is accrued (Cotrufo et al., 2013; Liang et al., 2017; Buckeridge et al., 2020). Over 76% of the new soil C accrued following the conversion from annual to perennial cropping systems is estimated to be derived from soil microbial byproducts and tissues (Zhu et al., 2020), underscoring the importance of

incorporating new C into soil microbial communities to enhance the potential for soil C accrual. However, few studies directly traced the movement of C through the root-microbe-soil continuum in perennial cropping systems, leaving a gap in our understanding of how perennial crops will contribute to soil C storage.

To better understand the potential mechanisms limiting soil C accrual in perennial cropping systems, we established a ^{13}C-tracer study to directly quantify the uptake, partitioning, and belowground respiratory losses of new C through time. This study compared C uptake and partitioning patterns between two cool-season grasses utilized in grain production: 1-year-old and 2-year-old intermediate wheatgrass (IWG), a perennial grass domesticated for grain and forage production, and spring wheat, a common annual grain. Including these three cropping systems allowed us to isolate the age-related changes in C uptake and partitioning that occur within the first two years of IWG establishment, while comparing C use dynamics more broadly between perennial and annual grain crops.

Given the higher photosynthetic rate of perennial grains compared to annual grains during the early growing season (Jaikumar et al., 2013), we expected total C uptake during the labelling period in the IWG systems would exceed that of wheat. The total mass and proportion of recovered ^{13}C recovered from root pools were expected to be greater in IWG than Wheat, given the higher standing root stocks and root production observed in IWG compared to wheat (Sprunger et al., 2018; Woeltjen, 2023, Chapter 1) Since there is little difference in total soil C stocks between IWG and wheat (Culman et al., 2013; Sprunger et al., 2018), despite the larger root stock and root production rates

(see Woeltjen, 2023, Chapter 1), we expected less new C would be transferred from root to soil pools in IWG than wheat. Along these lines, we expected a greater proportion of assimilated C to be lost to soil respiration in the IWG system when compared to wheat. We expected C partitioning patterns would be similar between the first- and second-year IWG systems, though overall C uptake would be reduced in the older IWG stand (Jaikumar et al., 2013; Jaikumar et al., 2016).

Materials and Methods

Site Description and Experimental Design

This study was established at the Rosemount Research and Outreach Center located in southeast Minnesota (44˚42′ N, 93˚05′ W). Mean annual temperature and precipitation were 11.1 C and 864 mm, respectively. Soils were deep, well-drained silt loams classified as Typic Hapludolls.

We used a modified staggered-start approach with repeated measures to isolate the effect of life strategy and stand age on C uptake and C partitioning over the growing season in two perennial and one annual grain cropping systems. The two perennial systems were a 1-year-old intermediate wheatgrass (IWG-1; *Thinopyrum intermedium*, (Host) Barkworth and Dewey) and a 2-year-old intermediate wheatgrass (IWG-2) stand. The annual grain system was represented by annual spring wheat (Wheat). All fields in

this study were within a 1.45 km radius and were verified to have similar site conditions, including soil texture and hillslope position.

Agronomic management details are summarized in table 2.1. IWG-1 was planted in September 2019 on 38 cm rows and seeded at a rate of 13 kg pure live seed ha^{-1}. IWG-2 was planted in September 2018 on 41 cm rows and seeded at a rate of 13 kg pure live seed ha^{-1}. Both the IWG-1 and IWG-2 stands were established with 'MN-Clearwater' seed and were fertilized with urea at a rate of 80 kg N ha^{-1} each year at the onset of spring regrowth (early April) and harvested for grain annually in August or September when crops were approaching physiological maturity (see Heineck et al., 2022). In the year of this study, the IWG-1 and IWG-2 fields were harvested for grain on August 3, 2020. After grain harvest, the remaining IWG straw was mowed to a height of 10 cm and removed from the field. Spring wheat was planted in April 2020 on 15 cm rows at a seeding rate of 2.7 million seeds ha^{-1}. Wheat was spring-fertilized with urea at a rate of 80 kg N ha^{-1} in 2020 and harvested for grain on July 24, 2020, at which point all aboveground biomass was cut to 10 cm and removed from the study area.

Experimental Design and ^{13}C-CO_2 Pulse-Labeling

Four replicate 1-m^2 plots in each field were randomly designated for *in situ* ^{13}C pulse labeling. Replicate plots within each field were separated by at least 5 m and were visually verified to contain crops of similar health and canopy density.

In situ ^{13}C pulse labeling took place in May 2020, when belowground C allocation for both perennial and annual grains was expected to be maximal (Pugliese et al., 2019). Replicate plots were labeled on four consecutive days between 10:00am and 2:00pm, with the first labeling event in each field commencing on May 11. In total we conducted 12 labeling events (3 fields x consecutive labeling events in each of 4 plots per field), labeling one replicate from each field per day for four consecutive days. For each labeling event, a clear polycarbonate chamber (1 m x 1 m x 1 m; see supplemental material in Appendix 2) was installed on one replicate plot in each field. Each chamber was equipped with a closed loop copper coil cooling/dehumidification system, a temperature / humidity sensor, and a CO_2 sensor. Prior to chamber deployment, openings or junctures on the chamber walls were sealed with silicone caulk, and wet soil was mounded at the base of the chamber to prevent the exchange of gases between the chamber and ambient atmospheres. Chamber temperature and humidity were monitored throughout the labeling period to ensure they were consistent with ambient atmospheric conditions.

To avoid elevating chamber CO_2 concentrations excessively beyond ambient levels, crops were allowed to draw down chamber CO_2 concentrations until stable (about 250 ppm) after sealing the chamber to the soil surface. Then, a pulse of ^{13}C-enriched CO_2 (^{13}C-CO_2) was released into the chamber by injecting 20 mL acetic acid (10% v/v) into beakers within the chamber containing 2 g ^{13}C-enriched sodium bicarbonate (99 atom%, Cambridge Isotope Laboratories, Inc., Andover, MA). Longitudinal fans placed above the beakers distributed and mixed the ^{13}C-CO_2 label across the chamber area. Each pulse

increased chamber CO_2 concentrations to approximately 550 ppm. Following the first pulse, chamber CO_2 concentrations were again allowed to be drawn down to a plateau of around 250 ppm before a second pulse of ^{13}C-CO_2 was released using the same protocol as with the first pulse. Chambers were removed once chamber CO_2 concentrations once again plateaued near ~250 ppm following the second pulse. In total, each plot was exposed to 612 mg ^{13}C through the acidification of 4 g ^{13}C-enriched sodium bicarbonate over a time interval of approximately 120 minutes.

Crop Tissue and Soil Samplings

Following the labeling period, crop tissue and soil samples were collected from each labeled replicate 10 times over a 90-day chase period. The samples were collected immediately after chamber removal (0 h), 1.5 h, 18 h, 24 h, 3 d, 7 d, 14 d, 30 d, 60 d, and 90 d after label application. At each sampling event, whole plants were excavated to a depth of 15 cm from a randomly selected 20 cm x 10 cm section of row within each labeled plot. Due to space constraints, sampled sections were separated by at least 10 cm.

Crop shoots, or aboveground biomass tissue, were clipped from the excavated section immediately by cutting a portion of healthy, living tissue to 10 cm above the soil surface. Along with the remainder of the excavated section, the clipped crop shoot samples were placed in a cooler and transported to the laboratory, where they were stored at 4 C until further processing.

In the laboratory, crop shoots were gently washed with DI water to remove adhering soil particles and dried at 60 C. The remainder of the excavated sections were

subsampled for root and soil analysis. Soil samples, which were further separated into bulk and rhizosphere soils, were collected from the excavated section first. Bulk soil represented non-root associated soil and was collected from root-free sections of the excavated section. Rhizosphere soil samples were isolated by gently shaking the excavated section to remove non-rhizosphere soil, with soil that adhered to roots collected as rhizosphere soil. Bulk soil and rhizosphere soil samples were freeze-dried in preparation for elemental and lipid analysis. The roots remaining on the excavated section were then clipped at the crop crown, rinsed in DI water to remove soil particles, then dried at 60 C for 48 h.

In preparation for elemental analysis, the dried crop shoot, root, and soil samples were ground to a fine powder using a ball mill and packaged into tin capsules. The C content and ^{13}C abundance ($\delta^{13}C$, ‰) were determined by dry combustion of each sample using an elemental analyzer coupled to a continuous-flow Isoprime 100 isotope ratio mass spectrometer (Elementar Pyrocube, Elementar Americas, Inc.) .

The C pool size of each compartment (g C m^{-2}) was estimated for each of the 10 sampling events as:

$$Pool\ Size\ (g\ C\ m^{-2}) = compartment\ size\ (g\ m^{-2}) * C\ content\ (\%)$$

where compartment size was either predicted (crop shoots, crop roots) or directly measured (soil, soil microbial biomass) and C content was the measured C content of the compartment. Though shoot and root samples were collected at each sampling event, the limited size of the sampling area precluded the collection of samples large enough for

direct measurement of the compartment size. Instead, the shoot and root compartment sizes were predicted using predictive models. These models are detailed in Table 2.2 and are described briefly as follows. A logistic model previously developed to predict IWG shoot biomass (g m^{-2}) as a function of growing degree days was used to predict the IWG-1 and IWG-2 shoot biomass present at each of the 10 sampling events (Jungers et al., 2018). The asymptote of the model represented peak shoot biomass at physiological maturity, and therefore we substituted peak shoot biomass values determined in August 2020 from an adjacent experiment (Bowden, 2023) into the model to calibrate it to our field study. A similar process was used to predict shoot biomass at each of the 10 sampling events for wheat. A linear model described in Bauer et al. (1987) and Bauer (1984) was used to estimate wheat shoot biomass as a function of growing degree days in our study. Total shoot biomass values collected at wheat physiological maturity in 2020 from an adjacent experiment (Woeltjen, 2023, Chapter 1) were substituted into the model to calibrate it to our study.

Similarly, representative root biomass samples for compartment size measurement could not be collected directly from labeled areas due to maximum size restrictions of the labeling chamber. Therefore, models were developed to predict root biomass in each cropping system at each of the 10 sampling events (table 2.2). We used root biomass values collected between April and August 2020 from an adjacent experiment (Woeltjen, 2023, Chapter 1) to develop three models that predicted root biomass to a depth of 15 cm as a function of the day of year. Wheat and IWG-1 root biomass trends were best predicted by quadratic models, and therefore quadratic equations were used to estimate

root biomass in these fields (table 2.2). IWG-2 root biomass trends were best predicted by a linear equation (table 2.2).

The soil compartment size was directly measured as the sum of bulk and rhizosphere soil compartments. Bulk density samples collected in each field in April 2020 were used to determine the bulk and rhizosphere soil compartment sizes. Since bulk density did not differ significantly across cropping systems, bulk density was averaged across fields (1.3 g cm^{-3}) and multiplied by the sampling depth (15 cm) to estimate the soil compartment size. Further, since a given core of soil contains both rhizosphere and bulk soil, the sizes of the bulk soil and rhizosphere soil compartments were estimated by multiplying the whole soil pool by 0.75 and 0.25, respectively, preventing the overestimation of C recovery from the whole soil pool (Butler et al., 2001; Pausch et al., 2016). In this paper, we present trends in ^{13}C recovery from the whole soil pool, which is the sum of ^{13}C in bulk and rhizosphere soils at any given sampling event.

Cumulative Soil Respiration

Following Mou et al. (2018) and Hafner et al. (2012), the^{13}C carbon released from the crop-soil system via soil respiration was captured at each sampling event using the alkali trap method. Briefly, in each labeled plot an opaque cylinder (8 cm diameter by 25 cm tall) was driven to a depth of 10 cm below the soil surface. A polypropylene specimen cup filled with 40 mL of 1 M sodium hydroxide solution (the alkali trap) was placed inside the cylinder and an opaque lid was sealed to the top of the cylinder immediately

thereafter. Alkali traps were deployed immediately after the labelling chambers were removed from the field and were replaced with new cups at 1.5, 18 h and 24 h after chamber removal, yielding 1.5 h, 16.5 h and 6 h trapping periods, respectively. A new cup was placed in the chamber at the time of sampling at the 24 h, 3 d, 7 d, 14 d, 30 d, 60 d, 90 d and natural abundance sampling events and removed from the cylinder after a 24 h trapping period. At the end of the trapping period, the lid was removed from the opaque cylinder and alkali traps were removed, capped, sealed, and stored at 4 C until further processing.

In the laboratory, the sodium hydroxide solution in each specimen cup was reacted with excess 1 M strontium chloride to produce strontium carbonate. The strontium carbonate was rinsed repeatedly with DI water until the pH of the rinsate was neutral. Then, the strontium carbonates and rinsate were placed in an oven at 60 C until all rinsate was evaporated and strontium carbonates were dry. The dried carbonates were weighed to determine the pool size, or the mass of CO_2-C (g C m^{-2}) respired during each trapping period, then ground into a fine powder using a ball mill. The $\delta^{13}C$ (‰) of the dried carbonate samples was determined using a MultiCarb system in line with a dual-inlet mass spectrometer (GV Isoprime) at the University of California – Berkeley Center for Stable Isotope Biogeochemistry. As the trapping period varied slightly between individual traps, the mass of CO_2-C collected from each trap was divided by the trapping period duration to determine the rate of CO_2-C respiration (g C m^{-2} day^{-1}). Soil CO_2-C respiration rates measured at each sampling event were plotted over time, and cumulative trapezoidal integration was then used to estimate the cumulative mass of soil respired

CO_2-C accumulated by each of the 10 sampling events. This method of estimating cumulative soil respiration may not account for large pulses of CO_2 released following precipitation events or other in-field disturbances, and therefore represents a conservative estimate of cumulative soil CO_2 respiration.

Soil Microbial Biomass and Soil Microbial Community Functional Groups

Microbial biomass was extracted from rhizosphere soil samples from the 0 h – 7 d sampling events using the PLFA (Phospholipid Fatty Acid Analysis) method modified from the Bligh and Dyer (1959) method for δ^{13}C-PLFA analysis (Herman et al., 2012). To prepare rhizosphere soil for extraction, rhizosphere soil was freeze dried, and 8 g +/- 0.05 freeze-dried soil was weighed into hexane-rinsed centrifuge tubes. An initial extraction was performed three times from each soil sample using a 0.9:1:2 ratio of citrate buffer:chloroform ($CHCl_3$):methanol (MeOH). Citrate buffer and $CHCl_3$ were added to the extract to bring the final ratio of buffer:$CHCl_3$:MeOH to 0.9:1:1 to allow for phase separation overnight. The $CHCl_3$ layer was then evaporated, and the phospholipid fraction was collected using silica column chromatography. Phospholipids were then methylated using an alkaline methylation procedure (Herman et al., 2012) and analyzed using an Agilent (Santa Clara, California) 7790A GC coupled with an Elementar (Langenselbold, Germany) IsoPrime100 IRMS system. 1,2-dinonadecanoyl-sn-glycero-3-phosphocholine (19:0 PC; Avanti Polar Lipids, Alabaster, Alabama, cat # 850367P) was used as a surrogate standard and tridecanoic acid methyl ester (C 13:0; Sigma-Aldrich,

St. Louis, Missouri, cat # T062) was used as an internal standard used for converting peak areas to nmol fatty acid g dry soil^{-1}.

Signature fatty acids (biomarkers) that indicate the microbial groups included here are: Gram positive bacteria (G+ Bacteria; 15:0 iso and 15:0 anteiso), Gram negative bacteria (G- Bacteria; 18:1 ω9t and 16:1 ω7c), saprotrophic fungi (18:2 ω6,9c) and arbuscular mycorrhizal fungi (AMF, 18:1 ω9c), actinomycetes (Actino; 16:0 10 me and 18:0 10me), and anaerobic bacteria (Anaerobic Bacteria; 19:0 cyclo) (Zelles, 1999). When more than one lipid was used as an indicator for a given group, they were summed to determine abundance and relative abundance. Total microbial biomass was determined by summing lipids equal to or less than 20:0 carbons in length.

Raw $\delta^{13}C$ data for each lipid were first normalized using USGS40 international reference material (L-glutamic acid; $\delta^{13}C = –26.39 \pm 0.04$ ‰) and reported relative to Vienna Pee Dee Belemnite (VPDB). These data were then corrected for the additional carbon molecule added during the methylation of fatty acids to fatty acid methyl esters (FAME), by using the following formula: $\delta^{13}C_{PLFA} = [(C_{PLFA} + 1) \prime \delta^{13}C_{FAME} - \delta^{13}C_{MeOH}]/ C_{PLFA}$, where C_{PLFA} is the number of carbons in each individual lipid before methylation, $\delta^{13}C_{FAME}$ is the corrected $\delta^{13}C$ value of each measured individual lipid, and $\delta^{13}C_{MeOH}$ is the corrected $\delta^{13}C$ of the methanol used for the methylation steps determined using elemental combustion analysis (Butler et al., 2003). The methanol used during methylation had a measured $\delta^{13}C$ signature of -43.63‰ and -52.36‰. The amount of extracted microbial lipids (nmol g soil^{-1}) for each lipid class was multiplied by a

correction factor to compute g lipid C (g soil)$^{-1}$. These values were then multiplied by the soil bulk density (1.3 g m^{-2}) and sampling depth (15 cm) to yield units of g lipid C m^{-2}.

Natural Abundance Samples

Four replicate crop shoot, root, bulk soil, rhizosphere soil, soil respiration and rhizosphere microbial biomass samples were collected from a non-labeled portion of each field for determination of ^{13}C natural abundance. These samples were collected and processed according to the methods described above for labeled samples.

Isotopic Calculations

The ^{13}C from each cropping system compartment (shoots, roots, soil, soil respiration and rhizosphere soil microbial biomass) is expressed as both the absolute mass of recovered ^{13}C per unit area (mg ^{13}C m^{-2}, or the areal density) and the proportion of peak total ^{13}C recovered (%). The absolute mass of recovered ^{13}C allows for the evaluation of the total contribution of new C to different crop-soil compartments, while the proportional ^{13}C recovery allows for the assessment of C use patterns independent of agronomic factors that differ between perennial and annual grain cropping systems, such as row spacing and plant density.

To obtain these metrics, the δ^{13}C (‰) values obtained from the mass spectrometer were first converted to the isotopic ratio (R_{sample}) as follows:

$$R_{sample} = \left(\left(\frac{\delta^{13}C}{1000}\right) + 1\right) + R_{PDB}$$

where $R_{PDB} = 0.011237$, the ^{13}C / ^{12}C of the Vienna Pee-Dee Belemnite standard. The fractional abundance of ^{13}C ($^{13}C_{atom\%}$, %) in each sample was then determined as:

$$^{13}C_{atom\%} = \frac{R_{sample}}{R_{sample} + 1} * 100$$

The $^{13}C_{atom\%}$ excess of labelled samples ($^{13}C_{atom\% \text{ excess}}$, %) was then calculated by subtracting the $^{13}C_{atom\%}$ of labelled samples ($^{13}C_{atom\% \text{ sample}}$) from that of the unlabeled natural abundance samples ($^{13}C_{atom\% \text{ natural abundance}}$):

$$^{13}C_{atom\% \, excess} = {}^{13}C_{atom\% \, sample} - {}^{13}C_{atom\% \, natural \, abundance}$$

Negative $^{13}C_{atom\% \text{ excess}}$ indicated no detectable tracer was recovered from the sample, and therefore negative $^{13}C_{atom\% \text{ excess}}$ values were replaced by zeros. The absolute mass of excess ^{13}C (mg ^{13}C m-2) contained in each crop-soil compartment (shoots, roots, soil, soil respiration) was then estimated using the following equation:

$$^{13}C \; amount = Compartment \; size * compartment \; \%C * (^{13}C_{atom\% \, excess} / 100) * 1000$$

where compartment size is the estimated mass of the compartment (g m^{-2}), C content is the carbon content (%) of the compartment, $^{13}C_{atom\% \text{ excess}}$ is divided by 100 to give the proportion ^{13}C in the compartment, and 1000 is a conversion factor used to convert units from g to mg.

The proportion of ^{13}C recovered from each pool (% recovered ^{13}C) is further expressed as the ^{13}C amount in each compartment per total tracer ^{13}C recovered from the whole crop-soil system of a given plot shortly after chamber were removed:

$$\%\ recovered\ ^{13}C\ = \frac{^{13}C_{\ compartment,SE}}{^{13}C_{\ total,Peak}}$$

where the $^{13}C_{\text{ compartment, SE}}$ (mg ^{13}C m^{-2}) represents the mass of ^{13}C recovered from a compartment at a given sampling event. The $^{13}C_{\text{ total, Peak}}$ (mg ^{13}C m^{-2}) represents the total mass of ^{13}C recovered from the whole crop-soil system (sum of ^{13}C recovered from aboveground tissues, roots, and soil) in the corresponding plot replicate at the time of peak tracer recovery. The time of peak tracer recovery varied between plot replicates but was observed at either the first (0 h post-label application) or second (1.5 h post-label application) sampling event in all plot replicates.

Statistical Analysis

To account for the spatial and temporal autocorrelation induced by repeated sampling, the effect of cropping system and time on the mass and proportion of ^{13}C recovered from each carbon compartment were assessed using random intercept linear mixed effects models (Bradford et al., 2012; Fang et al., 2016). Models were first specified with cropping system (IWG-1, IWG-2, Wheat), time since tracer addition (time, as categorical variable; 0 h, 1.5 h, 18 h, 24 h, 3 d, 7 d, 14 d, 30 d, 60 d, 90 d), C compartment (shoots, roots, soil and cumulative respiration), and their interactions as

fixed effects. A significant three-way interaction between cropping system, time and carbon compartment was detected in all models (supplemental table 2.2), and therefore we investigated the effect of cropping system and time (and their interaction) on the mass and proportion of ^{13}C recovered within each separate C compartment. Random effects were defined using a nested structure with time nested in plot replicate. The same model structure weas used to evaluate the effect of cropping system and time on the mass and proportion of new C recovered from microbial biomass, and the effect of (IWG-1, IWG-2, Wheat), time since tracer addition (time, as categorical variable; 0 h, 1.5 h, 18 h, 24 h, 3 d, 7 d) and microbial functional group (actinomycetes, anaerobic bacteria, gram negative bacteria, gram positive bacteria, saprotrophic fungi and arbuscular mycorrhizal fungi) on the proportion of microbial biomass recovered from each functional group.

When significant effects were detected, we used least-squares comparison to evaluate significant differences within levels of cropping system and time. Differences were considered significant when Tukey-adjusted *p*-values were less than 0.05. Although linear mixed effects models are robust to minor violations of assumptions, model fits were visually inspected to confirm the assumptions were reasonably met prior to performing post-hoc tests (Schielzeth et al., 2020). All statistical analysis was performed with the R software (R Development Core Team, 2022; version 4.2.2) using the *nlme* (Pinheiro et al., 2022; version 3.1-160), *emmeans* (Lenth, 2023; version 1.8.4-1), and *multcomp* (Hothorn et al., 2008; version 1.4-17) packages.

Results

Areal Density of ^{13}C Recovery

In total, each replicate was exposed to 612 mg ^{13}C m^{-2}. Peak assimilated ^{13}C recovery from the whole system (sum of ^{13}C recovered in shoot, root, soil plus the cumulative soil respiration) measured shortly after completing the labeling event ranged from 199 - 387 mg ^{13}C m^{-2} (fig. 2.1). Whole-system ^{13}C recovery did not differ significantly across the study period in any cropping system, though trends suggest whole system ^{13}C recovery generally declined over the growing season in Wheat and IWG-1. Whole-system ^{13}C was just 4% different between peak tracer recovery and harvest in IWG-2, suggesting nearly all assimilated tracer carbon was accounted for in our sampling.

The effect of cropping system on the mass of ^{13}C recovered from crop-soil compartments (sum of shoots, roots, and soil) varied over time, as indicated by a significant two-way interaction between cropping system and time. Within 1.5 h of assimilation, crop-soil ^{13}C peaked at 387 mg m^{-2} in IWG-1, nearly 1.7 and 1.9 times greater than Wheat and IWG-2 (fig. 2.1). However, by 30 d post-assimilation, no significant differences in crop-soil ^{13}C were detected between IWG-1, IWG-2, or Wheat. In each cropping system, crop-soil ^{13}C declined over time as expected (fig. 2.1).

The decline in crop-soil ^{13}C was accompanied by a significant increase in cumulative soil respiration over time (fig. 2.1, table 2.3). Cumulative soil respiration also differed significantly by cropping system (table 2.3). Averaged across the study period,

Wheat (43.9 mg ^{13}C m^{-2}) respired significantly less new C than IWG-1 (58.4 mg ^{13}C m^{-2}), though IWG-2 did not significantly differ from either system (fig. 2.1).

The effect of cropping system on shoot ^{13}C recovery changed significantly over time (table 2.3, table 2.4). Whereas IWG-1 initially retained a higher mass of ^{13}C in shoots when compared to IWG-2 or Wheat, few significant differences in shoot ^{13}C were detected between any cropping systems by 60 d post-assimilation. Further, the mass of ^{13}C recovered from shoots in IWG-1 and Wheat declined by 86% and 82%, respectively, between 0 h and 60 d, after which all aboveground biomass was removed from fields during grain harvest. This same trend was not observed in the IWG-2 system, where there was no significant change in the mass of ^{13}C recovered from aboveground tissues during the same period.

Like shoots, root ^{13}C was significantly affected by cropping system, time, and their interaction (table 2.3, table 2.4). However, across the study period, IWG-1 consistently retained a larger mass of ^{13}C in roots than IWG-2 or Wheat. By 18 h post-assimilation, IWG-1 already retained significantly more ^{13}C in roots (36.35 mg ^{13}C m^{-2}) than IWG-2 (7.56 mg ^{13}C m^{-2}) or Wheat (12.02 mg ^{13}C m^{-2}). In all cropping systems a lag between the first sampling event (0 h) and peak root ^{13}C was observed, though this trend was only significant in IWG-1. Between 0 h and 3 d post-assimilation, IWG-1 root ^{13}C increased by nearly 185% and continued to rise to a peak of 66 mg ^{13}C m^{-2} 14 d post-assimilation. Following this peak, root ^{13}C declined rapidly towards initial values. A similar trend was noted in Wheat, where peak root ^{13}C was reached around 30 d post-assimilation followed by a drop in root ^{13}C as values approached those of initial

samplings. IWG-2 maintained similar root ^{13}C across the study period, with a minor peak in root ^{13}C occurring within the first 24 h post-assimilation.

The ^{13}C recovered from soil and rhizosphere soil microbial biomass varied significantly between cropping systems, but neither were affected by sampling time or the cropping system x time interaction (table 2.3). Averaged across the study period, ^{13}C recovered from soil was significantly greater in IWG-1 and Wheat than IWG-2 (table 2.4). Nearly 95% and 112% more soil ^{13}C was recovered on average from IWG-1 and Wheat when compared to IWG-2. Similarly, rhizosphere soil microbial biomass ^{13}C was on average highest in Wheat (0.38 mg ^{13}C m^{-2}) followed by IWG-1 (0.19 mg ^{13}C m^{-2}) and IWG-2 (0.07 mg ^{13}C m^{-2}) in the first 7 d post-assimilation (fig 2.3a). Though not significant, trends suggest ^{13}C incorporation in rhizosphere soil microbial biomass peaked 18 h to 24 h post-assimilation across all systems.

Proportional ^{13}C Recovery

The effect of cropping system on the proportion of assimilated ^{13}C recovered from shoots differed significantly by sampling time (table 2.3). At 0 h post-assimilation, the highest proportion of assimilated C retained in shoots was observed in IWG-1 (84%) and Wheat (64%) (fig. 2.2). IWG-2 (53%) retained a significantly lower proportion of new C in shoots at 0 h than IWG-1 (fig. 2.2). The proportion of ^{13}C recovered from shoots declined substantially across the study period in both IWG-1 and Wheat, with the proportion of ^{13}C remaining in shoots 60 d post-assimilation nearly 7.6 and 4.7 times

lower than at the 0 h sampling, respectively. Contrasting these trends, the proportion of assimilated C recovered from IWG-2 shoots remained relatively constant, averaging 43% across the study period. By the 30 d sampling event, IWG-2 (50%) retained a significantly higher proportion of ^{13}C in shoots compared to either IWG-1 or Wheat, and by the 60 d sampling event (just prior to grain harvest and aboveground biomass removal) IWG-2 still retained nearly 40% of its total assimilated carbon in aboveground tissues, a significantly greater proportion than the 10% and 11% observed in IWG-1 and Wheat, respectively. Following the 60 d sampling event, all ^{13}C in shoots was removed from the field with grain harvest and aboveground biomass removal. Less than 1% of total assimilated ^{13}C was recovered from the shoot regrowth in the IWG-1 and IWG-2 at 90 d sampling.

Similar to shoots, the effect of cropping system on the proportion of assimilated ^{13}C recovered from roots differed significantly by sampling time (table 2.3). Although all cropping systems initially retained just 2% - 5% of total assimilated C in roots, a significant effect of cropping system on the proportional ^{13}C recovery was identified within 3 d of assimilation (fig 2.2). At 3 d post-label application, 14% of total assimilated ^{13}C was recovered from IWG-1 roots compared to the 5% and 3% in Wheat and IWG-1, respectively. IWG-1 maintained 14-17% of total assimilated ^{13}C in roots until 14 d post-assimilation, after which the proportion of new C in roots declined significantly towards initial levels. While the proportion of total ^{13}C recovered at the 3 d (14%), 7 d (13%) and 14 d (17%) was significantly greater than that recovery at the initial sampling event (5%), there was no significant difference between the proportion of ^{13}C initially recovered and

the proportion recovered from roots by the end of the study period (7%). Although trends suggest ^{13}C recovery peaked at the 14 d and 30 d sampling events in IWG-2 (7%) and Wheat (8%), respectively, no significant change in ^{13}C recovery from roots was detected across the study period in these systems.

The proportion of ^{13}C recovered from soil varied between cropping systems but was not affected significantly by sampling time (table 2.3). Averaged across the study period, Wheat (25%) retained a significantly greater proportion of ^{13}C in soil than either IWG-1 (12%) or IWG-2 (8%) (fig. 2.2). The proportion of ^{13}C recovered from soil did not differ significantly between IWG-1 and IWG-2 when averaged across the study period.

The proportion of ^{13}C recovered from cumulative soil respiration varied between cropping systems and increased significantly over time in each cropping system (table 2.3). On average, IWG-2 lost nearly twice as much assimilated C to soil respiration than in either IWG-1 or Wheat (fig. 2.2). By the end of the study period, the proportion of assimilated C lost to soil respiration was nearly 87% in IWG-2, significantly greater than the 49% and 39% in Wheat and IWG-1.

The proportion of ^{13}C recovered from total rhizosphere soil microbial biomass was significantly affected by cropping system (table 2.3). The proportion of assimilated C recovered from soil microbial biomass in the first week following assimilation was less than 0.5% in all cropping systems (fig. 2.3b). The proportion of ^{13}C recovered from soil microbial biomass was significantly greater in Wheat than IWG-1 or IWG-2. Between the

0 h and 7 d samplings, an average of 0.17% of total assimilated ^{13}C was recovered from Wheat rhizosphere soil microbial biomass compared to the 0.05% and 0.04% of IWG-1 and IWG-2.

Proportion of New Microbial C Recovered in Microbial Functional Groups

Overall, gram negative and saprotrophic were the dominant consumers of new C across all cropping systems (table 2.5). Cropping systems diverged in the primary soil microbial functional groups consuming assimilated carbon (table 2.5). In IWG-1, a significantly higher proportion of microbial ^{13}C was accounted for by AMF than was seen in IWG-2 or Wheat. In contrast, a significantly higher proportion of microbial C was accounted for by saprotrophic fungi in IWG-2 than in IWG-1 or Wheat.

Discussion

Total C Uptake Declines with IWG Stand Age

Total ^{13}C uptake, measured as the sum of ^{13}C recovered from crop tissue and soil pools at the time of peak tracer recovery, was higher in IWG during the first production year but declined to similar levels as wheat by the IWG second production year. Since we applied the ^{13}C tracer in mid-May, we expected the first-year IWG to take up more C than wheat. Photosynthetic rates of wheat between late April and mid-May have been seen to range from 15 to 20 μmol m^{-2} s^{-1} in wheat, compared to nearly 20 to 27 μmol m^{-2} s^{-1} in

first-year IWG stands during the same time period, marking a nearly 61% and 44% higher photosynthetic rate in IWG-1 than wheat in late April and mid-May (Jaikumar et al., 2013). Results from our study aligned closely with observations made by Jaikumar et al. (2013), with ^{13}C uptake during the mid-May labeling period being 76% higher in IWG-1 than wheat.

Age-related changes in C uptake and partitioning were observed in IWG. Nearly twice as much ^{13}C was recovered from IWG-1 at peak crop-soil ^{13}C recovery than in IWG-2, suggesting the C uptake capacity of IWG declined as stands aged. Early-season IWG photosynthetic rates have been reported to decline between the first and second IWG production years (Jaikumar et al., 2013; Jaikumar et al., 2016), so the drop in total ^{13}C uptake observed between IWG-1 and IWG-2 was unsurprising. These results are also well-supported by other studies, which similarly demonstrated age-related changes in photosynthesis and leaf gas exchange across perennial crop production years. For example, Jaikumar et al. (2016) and Tejera et al. (2022) found the photosynthetic rate of IWG and miscanthus declined by 18 – 30% between the first and third production years. In these studies, age-related differences in C assimilation rates were particularly pronounced in late April and mid-May (see also Jaikumar et al., 2013), the same period of time when the ^{13}C tracer was assimilated in this study.

Wheat Transferred New C to Soil and Rhizosphere Soil Microbial Biomass, Potentially Contributing to Stable C Formation

Despite the lower total C uptake, wheat retained an amount of C in belowground pools that was comparable to that of the first-year IWG, and greater than that of the second-year IWG. This trend was largely due to differences in C partitioning and short-term C storage patterns observed between wheat and IWG systems. Wheat retained a relatively low proportion of new C in roots (2 - 8%) and high proportion of new C in soil (3 - 37%) across the growing season, with the average proportion recovered from soil 2 – 3 times greater than that of either of the IWG systems. These results contribute to a similar group of studies that demonstrate the effectiveness with which wheat transfers assimilated C from plant parts to soil pools. In a global meta-analysis evaluating crop-soil C fluxes, wheat retained the lowest amount of new C in roots (0.2 Mg C ha^{-1}) but transferred the second highest amount of new C to soil annually (0.8 Mg C ha^{-1} yr^{-1}), superseded only by maize and perennial ryegrass which each transferred 1.0 Mg C ha^{-1} yr^{-1} to soil each year (Mathew et al., 2020). Others similarly showed wheat retained most new belowground C in soil, with wheat labeled during the early part of its growing season retaining almost 65% of belowground C in soil compared to just 17% in roots (Sun et al., 2019). The relatively rapid transfer of new C from plant parts to soil is critical for building stable soil C during the production period of the crop and suggests wheat production may be more well-suited to contribute positively to soil carbon accumulation than crops that less readily move carbon between plant tissues and soil pools.

In terms of evaluating longer-term trends in C storage, however, both the amount *and stability* of new C retained in Wheat soils should be evaluated. Though we did not

directly measure new C stabilization in this study, our measurements of C retention in soil microbial communities in combination with evidence from emerging frameworks describing soil C stabilization pathways shed light on the potential stability of new C in wheat soils (Cotrufo et al., 2013). Soil C stabilization is largely dependent on the efficiency with which new C is allocated to belowground pools and assimilated into microbial biomass (Cotrufo et al., 2013; Liang et al., 2017). Both the byproducts of microbial C cycling and direct contributions of microbial tissue turnover are expected to be primary pathways through which C is stabilized (Buckeridge et al., 2020), with microbial tissue turnover accounting for an estimated 76 – 92% of new soil C in annual and perennial systems (Zhu et al., 2020). In wheat soils, incorporation of new C into microbial biomass has been seen to correspond to an increase in new C retained in stabilized, mineral-associated organic matter pools (Fang et al., 2016). Therefore, the incorporation of new C into wheat soil microbial communities observed in our study suggests wheat may have an advantage in terms of building stable soil C, compared to systems that retain lower proportion of C in soil microbial biomass.

Low and Slow: Potential for Lower but Longer-Term C Inputs by 1-year IWG

Important differences in C cycling were noted between the Wheat and first-year IWG, especially with regards to belowground C storage. Though both systems effectively translocated new C belowground, demonstrated by a steady decline and increase in new C recovered from aboveground tissues and belowground pools, respectively, IWG-1 tended to store a larger amount of C in root tissues compared with wheat. The higher root

C storage in IWG-1 is likely due to the high investment in root biomass production observed in first-year IWG stands (Woeltjen, 2023, Chapter 1). At peak root ^{13}C recovery the proportion of total ^{13}C recovered from wheat roots was 5 – 7%, closely aligning with studies showing annual grains such as maize and wheat retain just 6 - 7% of total assimilated C in roots (An et al. 2015, Sun et al. 2019). In contrast, the first-year IWG retained 14 – 17% of new C in roots, supporting studies showing IWG stores more C in roots than wheat (Sprunger et al., 2018; Sprunger et al., 2019). However, the proportion of new C recovered from roots within 30 days of assimilation in IWG-1 was on the lower end of the values typically reported for other perennial systems, which can range from 63 – 70% in first-year switchgrass and *Kobresia* grasslands (Wu et al., 2010; Chaudhary et al., 2012) to 10 – 55% in grazed perennial grass pastures (Wei et al., 2016; Ma et al., 2021). The relatively low recovery of new C in first-year IWG roots compared to other perennial grass systems may relate to the breeding and selection of IWG for grain production. In breeding for maximum grain yields, the selection of IWG crops that maximize aboveground biomass and reproductive development at the expense of belowground C could drive the relatively low root ^{13}C allocation observed in IWG-1 (Poffenbarger et al., 2023). However, few, if any, studies have evaluated the effect of breeding and selection on root-soil interactions in IWG, and additional studies should assess changes in root and soil C dynamics associated with breeding perennial grasses for maximal grain production.

Coupled with the nearly 30% of applied tracer that was not recovered from the crop-soil system by the end of the study period, the unexpectedly low proportion of new

C recovered from first-year IWG roots also suggests new C was retained in a pool not sampled by our design. It is well known that IWG roots extend below the 15 cm depth to which our samples were collected (Sprunger et al., 2018; Sprunger et al., 2019), with an estimated 40% and 52% of IWG coarse-root C and fine-root C contained below a 10 cm sampling depth (Sprunger et al., 2018). In a ^{13}C-labelling study, Peixoto et al. (2020) further found IWG deposited new C as deep as 3.6 m below the soil surface through rhizodeposition. Therefore, we expect a portion of the unrecovered tracer to be allocated to deeper (i.e., below 15 cm) root tissues and soil pools. The deposition of new C in deeper soil layers reduces exposure to oxygen and soil microbial activity, suggesting that in its first production year, IWG may contribute to the accrual of organic matter that is protected from decomposition.

IWG-1 retained a higher proportion of new microbial C accounted for by AMF than in wheat, supporting studies evidencing the development of robust mycorrhizal networks in perennial grain systems (Bergquist, 2019; Duchene et al., 2020; Rakkar et al., 2023). In other non-woody systems, the density of AMF hyphae was estimated to be two orders of magnitude larger than that of roots in the upper 30 cm of soil, with an estimated AMF hyphal density of nearly 2700 cm cm^{-3} compared to the 19.2 cm cm^{-3} density measured for fine roots (See et al., 2022). As AMF receive C from the host plant in exchange for nutrients mined from soil organic matter, the movement of C along AMF hyphal networks serves to extend the spatial extent over which first-year IWG influences C storage. AMF networks extend the movement of new C into bulk soil that is inaccessible to roots alone and potentially more protected from microbial decomposition

than C inputs deposited into the rhizosphere. It is important to note that, while the movement of new C along hyphal networks could increase the volume of soil in which new C can be deposited (via the decomposition of AMF hyphae), Johnson et al. (2002) showed new C traveling through AMF hyphal networks bypasses soil pools, being exported directly from the system in soil CO_2 efflux rather than being deposited into soil C pools.

Together, the storage of new C in roots and AMF in first-year IWG adds an important perspective to studies comparing soil C stocks in IWG and wheat. As root and AMF hyphal tissues can take 1 – 2 years to decompose (Gill and Jackson 2000; Leifeld et al., 2015; Zhang et al., 2020), storage of new C in root and AMF hyphal tissues may lead to slower, longer-term contributions of C derived from first-year IWG crops to soil C storage. Traditional methods of monitoring soil C stocks that assess soil C stocks between IWG and annual grains up to the year of IWG termination do not quantify root- and hyphal-derived contributions to soil C pools that occur after IWG termination, and therefore may underestimate the potential of IWG-derived C inputs to contribute positively to soil C storage.

Shifts in Growth Strategy May Limit Soil C Contributions by 2-year IWG

Clear age-related changes in crop-microbial-soil C partitioning patterns were observed between the first- and second-year IWG systems. The reduction in C uptake and belowground C allocation in the second-year IWG marks a shift in C economy, building

on a growing body of evidence showing herbaceous perennial crops transition from an acquisitive to conservative growth strategy between the first and second production years (Woeltjen, 2023, Chapter 1). An evaluation of C uptake and growth in Miscanthus biofuel systems revealed 1-year-old crops employed an acquisitive growth strategy, rapidly acquiring C and allocating it to support tissue development and promote crop establishment (Tejera et al., 2021). Comparatively, C uptake and growth rates were substantially reduced by the second Miscanthus production year, marking a shift towards a more conservative growth strategy (Tejera et al., 2021). In Miscanthus and IWG alike, the shift towards a more conservative growth strategy aligns with greater investment in stress tolerant plant structures or carbohydrate storage tissues rather than tissue growth as stands age (Jaikumar et al., 2016; Tejera et al., 2021).

The exact processes driving the age-related shift in IWG growth strategy remain unclear, as these changes are attributable to a myriad of interconnected physiological and environmental factors. For example, Tejera et al. (2022) partially restored the C uptake capacity of 3-year-old Miscanthus stands by ameliorating nitrogen limitation. However, since the photosynthetic activity of 3-year-old Miscanthus leaves remained lower than 1 year old leaves even after nitrogen addition, the authors posited physiological constraints on C sink strength rather than nutrient limitation alone drove the age-related decline in C uptake. In IWG, age-related declines in photosynthetic capacity were a trade-off for investing in compounds that increased protection against abiotic stressors (Jaikumar et al., 2016). Furthermore, others postulated older perennial stands shift C allocation towards structures that allow the plant to overcome the most limiting nutrient or resource

(Xia et al., 2017; Dayrell et al. 2018). As some contend increasing aboveground vegetation density in aging IWG stands leads to sunlight-limited conditions, the increased aboveground C allocation we observed in the second-year IWG may be spurred by an attempt to maximize photosynthetic tissue development to overcome light-limitation (Pinto et al., 2021). Additional research is needed to disentangle the environmental and physiological drivers underlying the shift in IWG growth strategy.

Regardless of the mechanisms underlying age-related shifts in IWG growth strategy, this transition has important implications for C cycling and the longer-term C storage potential in IWG stands (Henneron et al., 2020). Specifically, the transition from acquisitive to conservative growth between the first and second IWG production years may limit the capacity for IWG to make large contributions to stable SOC formation over its lifespan. For example, in woody perennials, resource-acquisitive species were associated with greater MAOM production than conservative growth species, which is expected to be a precursor to stable SOC formation (Xu et al., 2021). Similar results were found across a panel of 12 perennial grassland species, where the acquisitive rather than conservative growth strategy was linked to the stable MAOM formation derived from root C inputs (Henneron et al., 2020). Further, the shift towards storing assimilated C in aboveground rather than belowground pools further limits the potential for stable soil C storage in IWG systems characterized by regular aboveground biomass cutting and removal. As much as half of the assimilated newly assimilated C was retained in aboveground tissues in the second-year IWG across the growing season, and therefore the cutting and removal of aboveground biomass from older IWG stands serves to displace

almost 50% of assimilated C from IWG fields. These results underscore the importance of employing agronomic practices that keep aboveground tissue C in-field to maximize the potential for belowground C transfer. For example, combing the grain from standing plants and chopping the remaining straw for equal distribution over the field may present an opportunity to retain C contained in straw to the field following grain harvest.

Age-related changes in new C recovery from rhizosphere soil microbial biomass, with a relatively high proportion of soil microbial C accounted for by saprotrophic fungi, similarly have important implications for C cycling and storage. As saprotrophic fungal communities are decomposers, sourcing their C from the breakdown of soil organic matter, the increase in saprotrophic fungi observed in this study supports other research that has shown root decomposition in second-year IWG is 1.7 times higher than in first-year IWG (Woeltjen, 2023, Chapter 1). Increases in fungal abundance are linked to reductions in microbial community C use efficiency and increased heterotrophic respiration (Whitaker et al., 2014; Soares and Rousk, 2019), aligning with our observations of substantially greater soil respiratory losses of new C in IWG-2 compared to either IWG-1 or Wheat. Therefore, the greater use of new C by saprotrophic fungal communities in second-year IWG may lead to increased loss of new C to respiration and reduced contributions to soil C. However, the chemical composition of fungal biomass is widely believed to more readily contribute to the formation of stable soil C than bacterial biomass, presenting a trade-off between increased respiration and potentially greater stable soil C contributions in aging IWG stands (Buckeridge et al. 2020).

Conclusions

Wheat exhibited a lower C uptake than IWG systems, but more effectively transferred assimilated C from shoot to soil and rhizosphere soil microbial pools. First-year IWG systems were characterized by high C uptake and transfer of new C into roots and rhizosphere arbuscular mycorrhizal networks, potentially allowing belowground C inputs derived from 1st-year IWG crops to contribute to longer-term C storage in IWG systems. However, these trends were not maintained across stand age. A significant decrease in C uptake and belowground C partitioning was accompanied by an increase in aboveground C partitioning, belowground respiratory losses, and consumption of new C by rhizosphere saprotrophic fungi in the second-year IWG compared to the first-year IWG. These age-related trends in C uptake and partitioning demonstrate a transition from acquisitive to conservative growth between the first and second IWG production years, shedding light on the mechanisms underlying limited soil C accrual in IWG stands. Additional research of C uptake and partitioning patterns in other cool- and warm-season grass is needed to further investigate the ability of these results to explain limited and inconsistent C accrual in other perennial grass cropping systems.

Table 2.1 Agronomic management details for each cropping system.

		IWG-1	IWG-2	Wheat
2020	Field ID	R34	V17	R90
	Planting date	September 2019	September 2018	April 2020
	Seeding rate	13 kg live seed ha^{-1}	13 kg live seed ha^{-1}	2.7 million seeds ha^{-1}
	Row spacing	38 cm	41 cm	15 cm
	N fertilization date(s)	April 2020	April 2019, April 2020	April 2020
	N fertilization rate	80 kg N ha^{-1}	80 kg N ha^{-1}	80 kg N ha^{-1}
	N fertilizer type	Urea	Urea	Urea
	Harvest date	August 3	August 3	July 24

Table 2.2 Model parameters used to predict shoot and root compartment sizes.

		Model form	Citation
Shoot Biomass	IWG-1	$Shoot\ biomass\ (g\ m^{-2}) = \frac{797.73}{1 + e^{\frac{1734 - GDD}{509.3}}}$	Jungers et al., 2018
	IWG-2	$Shoot\ biomass\ (g\ m^{-2}) = \frac{797.73}{1 + e^{\frac{1734 - GDD}{509.3}}}$	Jungers et al., 2018
	Wheat	$Shoot\ biomass\ (kg\ ha^{-1}) = 4.007 * GS^2$	Bauer et al., 1987
Root Biomass	IWG-1	$Root\ biomass\ (g\ m^{-2}) = (9.01 * DOY) + (-0.02 * DOY^2) - 814$	Woeltjen, 2023
	IWG-2	$Root\ biomass\ (g\ m^{-2}) = (-1.12 * DOY) + 483$	Woeltjen, 2023
	Wheat	$Root\ biomass\ (g\ m^{-2}) = (4.84 * DOY) + (-0.01 * DOY^2) - 415$	Woeltjen, 2023

Table 2.3 Analysis of variance and probability of significance for the mass of ^{13}C and proportion of ^{13}C recovered from five C compartments: shoots, roots, soil, cumulative respiration, and total rhizosphere microbial biomass.

	Shoots	Roots	Soil	Cumulative Respiration	Total Rhizosphere Microbial Biomass
Mass of ^{13}C					
Cropping System (CS)	**<0.001**	**<0.001**	**<0.001**	**0.019**	**<0.001**
Time (T)	**<0.001**	**0.003**	0.9275	**<0.001**	0.108
CS x T	**<0.001**	**0.001**	0.1805	0.518	0.154
Proportion of ^{13}C					
Cropping System (CS)	0.2511	**<0.001**	**<0.001**	**<0.001**	**<0.001**
Time (T)	**<0.001**	**0.004**	0.935	**<0.001**	0.200
CS x T	**0.009**	**0.044**	0.139	**0.028**	0.636

Table 2.4 Mean and standard error of ^{13}C (mg ^{13}C m^{-2}) recovered from shoots, roots, and soil at each of the 10 sampling events. Means not sharing any lowercase letters indicate significant differences between cropping systems at a given sampling event ($p<0.05$). Means not sharing any uppercase letters indicate significant differences between sampling events within a given cropping system ($p<0.05$). When no cropping system x time interaction was present, values were averaged across the study period prior to performing means comparison analysis.

		Time since tracer added										
		0 h	1.5 h	18 h	24 h	3 d	7 d	14 d	30 d	60 d	90 d	Study Period
Shoots	IWG-1	326±36 aA	327±42 aA	234±26 aB	202±27 aBC	204±41 aBC	156±21 aBC	121±23 CD	57±8 abDE	43±20DE	0±0 E	
	IWG-2	103±19 bA	93±2 bA	92±8 bA	83±6 bAB	70±5 cAB	65±3 bAB	79±4 AB	88±5 aA	60±16 AB	1±0 B	
	Wheat	146±38 bA	140±29 bA	122±22 bA	109±19 bAB	129±27 bA	82±15 bABC	72±10 ABC	28±5 bBC	27±5 BC	0±0 C	
Roots	IWG-1	20±4 C	21±5 C	36±10 aBC	35±10 aBC	57±14 aAB	55±15 aAB	66±8 aA	32±5 aBC	35±9 aBC	32±10 aBC	
	IWG-2	9±1	11±1	8±2 b	11±4 b	6±1 b	5±2 b	9±5 b	9±3 b	5±2 b	3±1 b	
	Wheat	5±1	5±1	12±6 b	10±3 b	11±2 b	14±2 b	16±4 b	18±4 ab	14±5 b	6±2 b	
Soil	IWG-1	20±5	39±12	59±8	42±9	69±21	57±11	36±16	33±10	43±9	51±10	45 a
	IWG-2	87±26	8±8	17±14	9±7	4±3	2±1	6±6	11±11	1±0	10±10	16 b
	Wheat	7±4	80±21	95±54	63±30	47±21	92±80	43±19	57±46	40±15	43±20	57 a

Table 2.5 Analysis of variance and estimated marginal means of the proportion of total rhizosphere soil microbial biomass ^{13}C accounted for by actinomycetes (Actino), anaerobic bacteria, gram positive bacteria, gram negative bacteria, saprotrophic fungi and arbuscular mycorrhizal fungi (AMF) when averaged over cropping system (CS) and sampling time (T). Means followed by different lowercase letters are significantly different within levels of either cropping system of sampling time.

		Actino	**Anaerobic bacteria**	**Gram - bacteria**	**Gram + bacteria**	**Saprotrophic fungi**	**AMF**
ANOVA	Cropping system (CS)	**< 0.001**	**< 0.001**	**0.002**	**<0.001**	**<0.001**	**0.001**
	Time (T)	0.166	0.131	**0.008**	0.136	**0.015**	0.290
	CSxT	0.476	0.165	0.147	0.225	0.106	0.074
		---------- % Total microbial biomass ^{13}C ----------					
CS	IWG-1	3.80 a	5.07 a	26.0 b	6.66 a	30.4 b	5.17 a
	IWG-2	0.36 c	0.88 b	29.8 a	1.36 b	40.1 a	3.37 b
	Wheat	2.43 b	3.99 a	30.0 a	6.12 a	28.3 b	2.07 b
T	0 h	3.05	4.93	29.4 ab	5.84	29.8 b	2.62
	1.5 h	2.32	2.8	33.3 a	5.47	30.5 b	2.76
	18 h	1.5	2.11	28.0 ab	3.66	32.3 ab	4.16
	24 h	1.86	3.03	27.1 b	3.62	33.5 ab	4.12
	3 d	2.07	3.60	27.8 b	3.58	35.2 ab	4.36
	7 d	2.38	3.42	26.0 b	6.13	36.6 a	3.18

Figure 2.1 Mean and standard error of ^{13}C (mg ^{13}C m^{-2}) recovered from the whole system (solid red line; sum of all measured pools), crop-soil pools (dotted black line; sum of shoot, root and soil pools) and cumulative soil respiration (dashed black line). Lowercase letters indicate the effect of cropping system on crop-soil ^{13}C recovery within each sampling event, where means not sharing any lowercase letters are significantly different ($p<0.05$). Uppercase letters indicate the effect time on crop-soil ^{13}C recovery within each cropping system, where means not sharing any uppercase letters are significantly different ($p<0.05$).

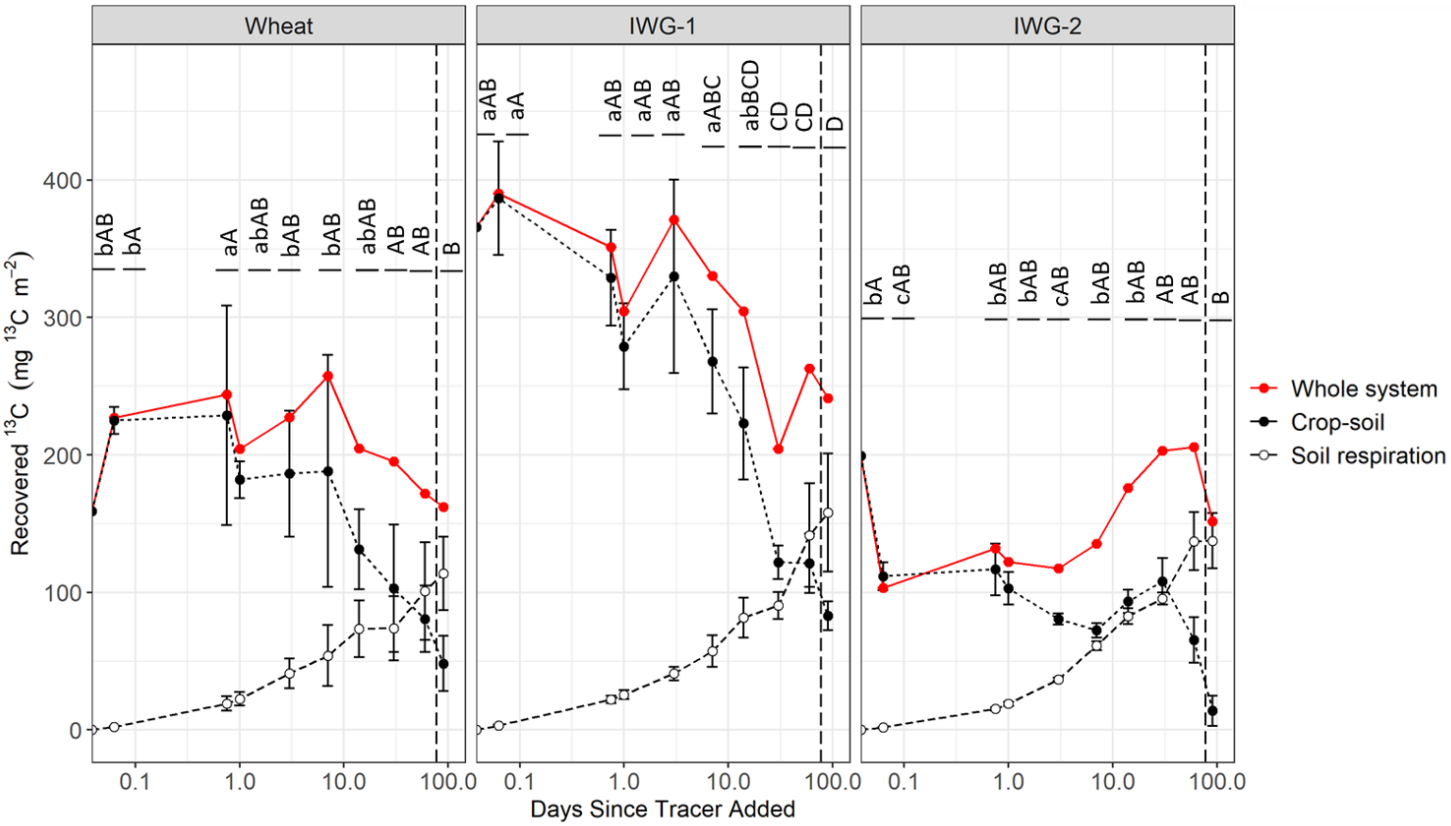

Figure 2.2 Proportion of total assimilated ^{13}C recovered from shoots, roots, soil, and cumulative soil respiration. Data are presented as means ± standard error. Means with asterisks indicate significant differences between cropping systems were detected within a sampling event. The vertical dashed lines indicate the point at which aboveground biomass was cut and removed from fields during grain harvest.

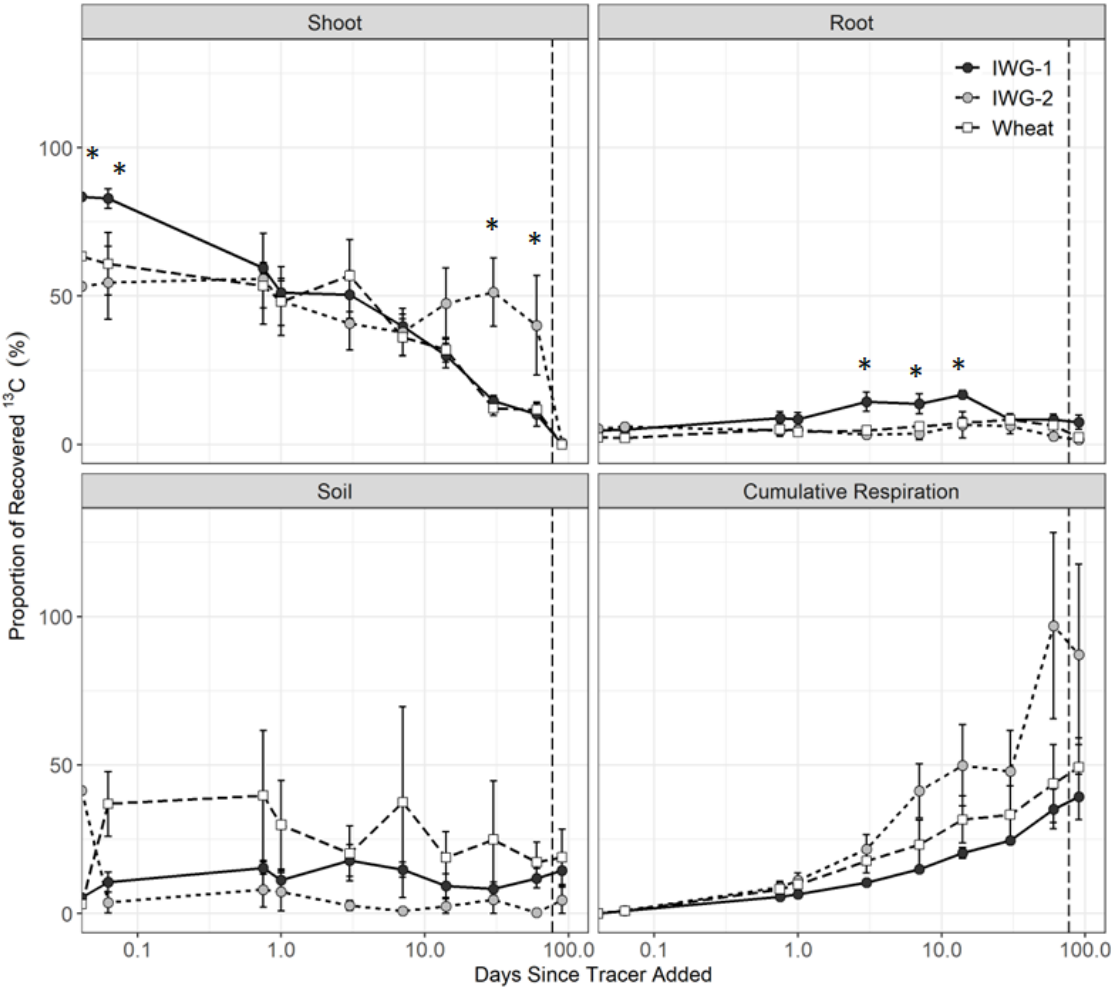

Figure 2.3 The a) ^{13}C (mg m^{-2}) and b) proportion of total assimilated ^{13}C (%) recovered from rhizosphere soil total microbial biomass. Points to the right of the vertical solid line represent mean and standard error when averaged across sampling time and means followed by different lowercase letters are significantly different ($p < 0.05$). The x-axis scale was log-transformed to improve readability.

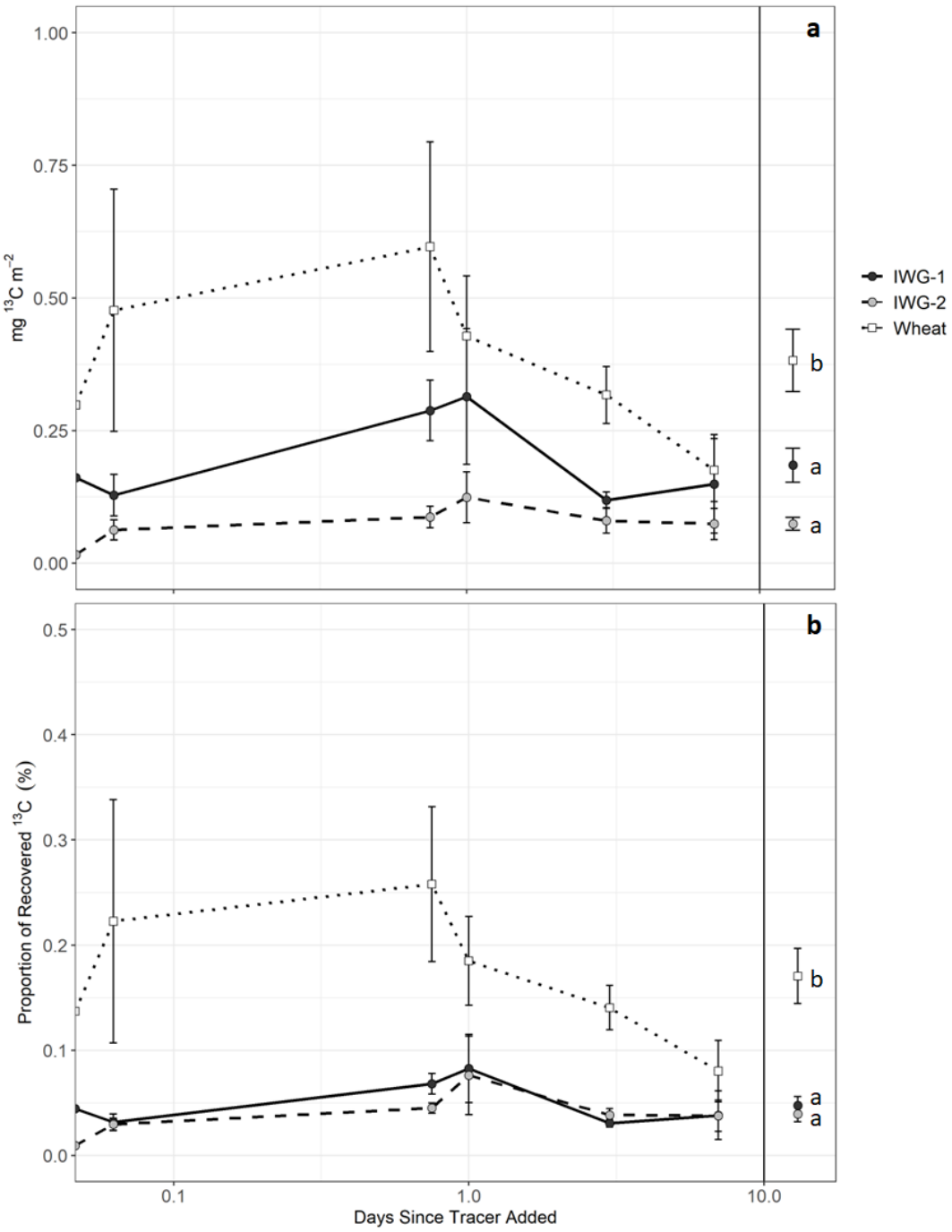

Chapter 3 : Evaluating Effect of Stand Age and Grain Harvest on Nitrogen Sources and Nitrogen Conservation in Intermediate Wheatgrass Systems

Synopsis

Perennial grasses often rely on well-developed internal nitrogen (N) translocation and conservation mechanisms to support growth and development, but little is known about the extent to which perennial grain crops like intermediate wheatgrass (IWG, *Thinopyrum intermedium* (Host) Barkworth and Dewey) utilize N conservation to meet the N demands of tissue growth, and the effect of perennial grain harvest and biomass removal at physiological maturity on N conservation remains unclear. We hypothesized that harvesting perennial grains at physiological maturity would disrupt N conservation and translocation dynamics, potentially contributing to the development of N-limiting conditions over time as IWG crops deplete soil N reserves to meet aboveground tissue N growth demands. To test these hypotheses, we established a ^{15}N-urea tracer study to track the fate of fertilizer N through aboveground tissue, root, and soil pools in IWG stands that were 1 year old (IWG-1), 2 years old (IWG-2) and 3 years old (IWG-3). We measured indicators of N availability (aboveground tissue N content and soil NO_3-N), N translocation and conservation, and fertilizer-derived N uptake. Results indicated that aboveground tissue N concentration fell by nearly 0.2% each year, alongside a significant decline in soil NO_3-N observed between the first and third IWG production years. While

these results suggested IWG stands may experience N limitation as they age, the age-related decline in tissue N content and soil NO_3-N was not accompanied by an increase in N translocation or N conservation, as would be expected if IWG were experiencing N limitation. Rather, net N translocation declined significantly with stand age, falling from nearly 4103 mg N m^{-2} in IWG-1 to 2636 mg N m^{-2} in IWG-3, suggesting IWG does not become more reliant on internally translocated N as stands age. Further, N derived from fertilizer (Ndff) represented only a small proportion of the N recovered from crop tissues at physiological maturity, accounting for just 14 – 26% and 18 – 21% of aboveground tissue N and root N, respectively, increasing with stand age and the fertilizer N recovery efficiency (FNR). Though the crop tissue FNR increased with stand age, it remained lower than previous observations in other perennial and annual cropping systems, suggesting fertilizer N management should be optimized to improve IWG fertilizer N uptake and ensure IWG systems remain profitable in the long-term.

Introduction

Agricultural landscapes in the upper Midwest, USA are largely dominated by annual grain row crops that are characterized by high fertilizer nitrogen (N) inputs and substantial N losses to the atmosphere, regional surface waterways and groundwater reservoirs (Jungers et al., 2019; Hussain et al., 2020; Vangeli et al., 2022). The consequences of diminished water quality are particularly threatening to the environmental and economic sustainability of agricultural regions. Some regions in the

upper Midwest pay an estimated US$4.8 billion annually to treat waters polluted by agriculturally-derived N and ensure affected communities have access to potable drinking water (Ribaudo et al., 2011). Establishing agroecosystems that minimize reliance on fertilizer N inputs, efficiently uptake fertilizer-applied N and conserve internal N is critical to ensuring long-term environmental and human health in agricultural communities.

Perennial grass crops are particularly well-suited to reduce the need for high fertilizer N inputs and therefore minimize N losses on agricultural landscapes. The high N uptake efficiency of perennial grass roots reduces the need for fertilizer N inputs and prevents the loss of N through leaching (Vadas et al., 2008; Jungers et al., 2017; Reilly et al., 2022). Additionally, many perennial grass crops employ effective N conservation strategies that recycle the N assimilated during one growing season to support aboveground tissue development during subsequent growing seasons (Jach-Smith and Jackson, 2015; Roley et al., 2020). These N conservation strategies rely on the translocation of N from aboveground tissues to belowground storage pools (i.e., N resorption) between the onset of physiological maturity and tissue senescence. Up to 30 - 70% of the N recovered from aboveground tissues can be sourced from N resorbed during the previous growing season, but the reliance on internally translocated N varies widely based on plant physiology and environmental conditions, such as N availability (Li et al., 1992, Li and Redmann, 1992; Wayman et al., 2014).

In intermediate wheatgrass (IWG), a cool-season perennial grass domesticated for grain and forage production, a high N use efficiency (Sprunger et al., 2018; Dobbratz et

al., 2023) and N conservation mechanisms (i.e., internal N translocation between aboveground and belowground crop tissues) have already been observed (Woeltjen, 2023, Chapter 2, unpublished data). These trends suggest IWG has evolved mechanisms to conserve N, indicating IWG is in part reliant on internally translocated N to meet the demands of aboveground and belowground tissue growth (Killingbeck 1996). Yet, it remains unclear to what extent IWG relies on translocation to meet N demands. Further, the effect of harvesting IWG grain at physiological maturity, rather than later in the season to allow for N translocation, remains unclear. Management recommendations for perennial grass cropping systems are often designed to allow for maximal N conservation via N translocation, even at the expense of yield reductions. For example, even though biomass yields peak at physiological maturity (i.e., August) in switchgrass and miscanthus biofuel crops, growers are recommended to harvest biomass later in the growing season (i.e., October-November) to allow for maximum N translocation (Heaton et al., 2009; Jach-Smith and Jackson, 2015). In these cases, growers accept a reduced biomass yield in exchange for the financial and environmental benefits imparted by N conservation mechanisms, with some suggesting that allowing crops to carry out their N conservation may save growers nearly US$9 ha^{-1} (Wayman et al., 2014). However, as IWG grain yields and nutritional content decline significantly after physiological maturity is reached, delaying crop harvest beyond physiological maturity is not viable because seeds shatter leading to grain yield losses (Heineck et al., 2022). A better understanding of the impact of IWG grain harvest on N conservation is needed to ensure N management plans are tailored to adequately meet IWG N demands and prevent depletion of soil N.

Evidence of N depletion and limitation have already been observed in aging IWG stands (Tautges et al., 2018; Crews et al., 2022), suggesting current agronomic recommendations are suboptimal for maintaining N availability in aging IWG stands. Others have shown IWG assimilated more N into crop tissues than was applied as fertilizer (Sprunger et al., 2018; Dobbratz et al., 2023). The discrepancy between fertilizer N application and fertilizer N uptake could be driven by inadequate fertilizer N application, or the disruption of internal N conservation mechanisms.

To address these knowledge gaps, we established a ^{15}N fertilizer tracer study to track the fate of fertilizer-derived N through aboveground tissues, roots, and soil organic N pools in IWG stands ranging from 1 – 3 years old. This study had three primary objectives. First, we aimed to evaluate evidence of N limitation in ageing grain-harvested IWG systems using proxies of N availability (aboveground tissue N content and soil nitrate-N concentration) and N conservation (net N translocation and nitrogen resorption efficiency). Second, we assessed primary N sources supplying the N that supports tissue growth and development in IWG. We evaluated three primary sources, including fertilizer N, non-fertilizer N (soil-derived N) and internally translocated N using the proxies of N conservation and the direct quantification of fertilizer-derived N in crop shoot and root tissues. Third, we measured the effect of stand age on fertilizer N uptake efficiency and quantified the amount of fertilizer N removed at harvest in the first, second and third IWG production years. We hypothesized that: 1) N limitation would be observed as IWG stands aged; 2) net N translocation would increase and N conservation proxies would indicate an increased reliance on internally translocated N as stands age,

alongside an increase in the proportion of N sourced from soil, due to suboptimal N fertilization causing IWG to rely on non-fertilizer-derived N sources to meet the N demands of tissue growth; and 3) fertilizer N uptake efficiency would be high across all stand ages, given the dense root stock and high leachate uptake, with almost all fertilizer-applied N assimilated into crop tissues during the growing season.

Materials and Methods

Experimental Design and Crop Management

This study was established at the University of Minnesota Rosemount Research and Outreach Center located in Rosemount, Minnesota (44˚42′ N, 93˚05′ W) between April and December of 2021. Mean annual temperature and precipitation were 11.1 C and 864 mm, respectively (NRCS, 2023). Mean temperature and daily precipitation in Rosemount, MN in 2021 are presented in figure 3.1. Soils were deep, well-drained silt loams classified as Typic Hapludolls (NRCS, 2023).

The details of each field and the associated agronomic management practices are included in table 3.1. To summarize, this study was conducted in three separate fields, each containing one IWG stand age: a 1-year-old (IWG-1), 2-year-old (IWG-2) and 3-year-old (IWG-3) IWG stand. All stands utilized in this study were located within a 1.45 km radius and were verified to have similar site conditions, including soil texture and hillslope position. The IWG-1, IWG-2 and IWG-3 stands were established in September

of 2020, 2019, and 2018, respectively. Within each stand, the study area was divided into four 3.3 m x 8.3 m blocks (fig. 3.2). Each block contained a 1 m^2 microplot (1.2 m x 0.8 m) designated for ^{15}N labeling (IAEA, 2008; Wood et al., 2020; Costa et al., 2021). Approximately 3 m from the long edge of the ^{15}N microplot, a 1.2 m x 5 m area was delineated for determination of crop biomass yield and ^{15}N natural abundance of crop tissue and soil samples (fig. 3.2; IAEA, 2008). Within this area, five 1.2 m x 0.8 m non-enriched sampling zones were established. Each non-enriched sampling zone was randomly assigned to one of the five sampling events carried out over the study period. Three of the sampling zones were assigned to a sampling that occurred during the growing season, aligning with IWG boot stage, maturity, and post-harvest regrowth. The remaining two non-enriched sampling zones were sampled at the end of the season (late November). One of these zones was harvested for grain at maturity and is referred to as EOS-harvested. The other zone was left unharvested and is referred to as EOS-unharvested. This study design allowed us to determine the maximum potential N translocated belowground between maturity and senescence in IWG, a process which occurs between maturity and senescence and required biomass to remain standing between these growth stages. Due to limited availability of boot stage and regrowth samples at the time this paper was written, only the data collected at the Maturity, EOS-harvested and EOS-unharvested samplings are presented here.

Application of Enriched and Non-Enriched Fertilizers

Each microplot was fertilized with a ^{15}N-enriched urea fertilizer (^{15}N-urea) solution at a rate of 80 kg N ha^{-1}. The ^{15}N-urea solution was enriched to 5 atom% excess by dissolving 102.96 g ^{15}N-urea (10 atom% excess) and 2988.23 g non-enriched urea fertilizer into 1 L deionized water (Readman et al., 2002; Harris et al., 2015; Spackman and Fernandez, 2019). The ^{15}N-urea solution was sprayed directly onto the soil surface using hand spray bottles to ensure the ^{15}N-urea solution was applied evenly across the microplot area (Huddell et al., 2023; supplemental figure 3.1). This method of fertilizer application produces similar results as when urea is broadcast in solid forms (Follett et al., 2001). While spraying the ^{15}N-urea solution onto the microplots, a wooden barrier was placed around the microplot edges to restrict airborne travel of water vapors carrying ^{15}N-urea and prevent contamination of the surrounding study area (supplemental figure 3.1).

As with the ^{15}N microplots, each 1.2 m x 5 m non-enriched sampling zone was fertilized with a urea solution at a rate of 80 kg N ha^{-1}. The urea solution applied to these non-enriched sampling zones was prepared as previously described for the ^{15}N-urea, except only non-enriched urea was used. The non-enriched urea solution was applied using a backpack sprayer to evenly distribute the fertilizer across the non-enriched sampling zones. The area extending 1 m beyond each ^{15}N microplot and non-enriched sampling zone edge was also fertilized with non-enriched urea solution using these application methods. Following local fertilizer application recommendations, all ^{15}N microplots and non-enriched sampling areas were irrigated to simulate a 0.64 cm (¼ in)

rainfall event immediately after fertilizer application (Spackman and Fernandez, 2019; Huddell et al. 2023; supplemental figure 3.2).

Plant Tissue and Soil Sampling

In each ^{15}N-enriched microplot, a 0.2 m^2 area was randomly selected for crop tissue and soil sampling at each sampling time. At least five healthy IWG shoots were clipped at the soil surface for analysis of the aboveground crop tissue elemental composition. In the same 0.2 m^2 area, a 5 cm diameter auger was used to extract one soil core at each of two depths (0 - 15 cm and 15 - 30 cm) for root biomass determination. A 2.5 cm diameter soil corer was used to collect 6 cores from each depth interval (6 cores x 2 depth intervals for 12 cores total). The 6 cores per depth interval were evenly spread between the position of the crop crown and the middle of the interrow to capture variability in soil nutrient concentrations between the interrow and row positions. The six soil cores were then composited to form one soil sample per depth interval and plot replicate for analysis of soil elemental composition.

The same methods were used to collect aboveground crop tissue, root, and soil samples in the non-enriched sampling areas, except all aboveground biomass in a 0.81 m x 0.61 m quadrat was clipped at the soil surface and collected for aboveground biomass yield determination. The root and soil cores were then collected from within this quadrat area as previously described for the ^{15}N-enriched microplot samplings.

All crop tissue and soil samples, from both the ^{15}N-enriched microplots and non-enriched sampling zones, were stored in a cooler and transported to a laboratory where

they were stored at 4 C until further processing. To limit the risk of cross-contamination during the collection of the ^{15}N-enriched and non-enriched samples, separate sets of tools were used to collect crop tissue and soil samples from the ^{15}N-enriched microplots and the non-enriched sampling zones. Further, crop tissue and soil sampling tools were rinsed with DI water and wiped clean between fields to limit the potential for cross-site contamination.

In the laboratory, aboveground crop tissue samples were immediately dried at 60 C for at least 48 h, weighed for dry matter determination and ground into a fine powder using a ball mill. Roots were isolated from the two cores collected for root biomass determination using hydropneumatic elutriation (Smucker et al., 1982). Briefly, the process uses compressed air and water to flush soil free from roots over a 410-micron mesh screen. Following elutriation, roots were dried at 60 C then further cleaned by hand to remove remaining organic debris and sand particles prior to weighing for dry matter determination and ground into a fine powder using a ball mill. Soil samples were sieved to 2 mm within 10 days of sample collection. A subsample of sieved soil was packaged into 4 mL microeppendorf tubes and allowed to air-dry for at least 48 hr. A steel bead was added to each microeppendorf tube, then tubes were sealed. Microeppendorf tubes were placed in metal capsules and loaded onto a ball mill to grind soil into a fine powder. Ground crop tissue and soil samples were packaged into tin capsules and analyzed to determine the N content (%) and isotopic signature ($\delta^{15}N$, ‰) by dry combustion of each sample using an elemental analyzer coupled to a continuous-flow Isoprime 100 isotope ratio mass spectrometer (Elementar Pyrocube, Elementar Americas, Inc.).

Within 10 days of sample collection, soil available NO_3-N was determined by weighing 10 g +/- 0.05 g of fresh soil (sieved to 2 mm) into acid-washed 50 mL centrifuge tubes. Then, 40 mL of 1 M KCl was added to each tube. Tubes were capped and shaken for 1 hr at 240 rpm. Afterwards, tubes were allowed to sit upright until all sediment had settled to the bottom of the tube. The extractant was filtered through pre-rinsed Whatman No. 1 filter paper into acid-washed scintillation vials, and vials were frozen until soil NO_3-N in each sample could be determined using a modified well plate assay method as described by Dobbratz et al., (2023).

In the Maturity and EOS-harvested sampling zones, grain harvest commenced when crops reached physiological maturity. At this time, grain was harvested, and all aboveground biomass was cut to a 10 cm stubble then removed from the sampling area. These methods are representative of common grain harvest practices used in larger scale IWG production fields. Samples were collected from each Maturity sampling zone for determination of grain yield using a 0.81 m x 0.61 m quadrat placed in the center of the Maturity non-enriched sampling zone. In the EOS-unharvested sampling zones, no biomass was cut or removed at the time of grain harvest, so all aboveground biomass was left standing in these sampling zones between crop maturity and the EOS-unharvested sampling time. Similar methods were replicated in the ^{15}N microplots, where aboveground biomass in a portion of the microplot was cut to a 10 cm stubble and removed from the field, and the remainder of the aboveground biomass was left standing for the EOS-unharvested sampling event. In the remainder of the experimental area,

aboveground biomass was cut to 10 cm stubble and removed from the field to eliminate the potential for shading effects on the plots.

Calculations

A list of abbreviated terms, their descriptions and calculations are provided in table 3.2. All measurements were calculated on a mass per area basis. Due to differences in row spacing between the IWG fields (see table 3.1), all data were scaled to a field with a 40 cm (16 inch) row spacing.

We evaluated N and ^{15}N dynamics in three compartments of the crop-soil system: aboveground biomass, roots (0 – 15 cm and 15 – 30 cm) and soil organic N (0 – 15 cm and 15 – 30 cm). The total N recovery (N_{pool}), proportion of plant or soil N derived from fertilizer (Ndff), amount of N derived from fertilizer (FDN), and proportion of applied fertilizer N recovered (FNR) were determined following equations presented in Spackman and Fernandez (2020) and Stevens et al. (2005). The total N recovered from each compartment (N_{pool}, g N m^{-2}) in each compartment was determined as:

$$N_{pool}(g\ N\ m^{-2}) = pool\ size\ (g\ m^{-2}) * \frac{N\ content\ (\%)}{100}$$

The proportion of plant or soil N derived from fertilizer (Ndff, %) was calculated as follows:

$$Ndff\ (\%) = \frac{A_{sample} - A_{background}}{A_{fertilizer} - A_{background}}$$

where A_{sample} and $A_{background}$ are the ^{15}N fractional abundance (atom %) of plant or soil samples collected from the labeled microplots or the unlabeled plot, respectively, and $A_{fertilizer}$ represents the ^{15}N fractional abundance of the labeled fertilizer.

The amount of N derived from fertilizer (FDN) in each pool was then calculated as:

$$FDN\ (mg\ N\ m^{-2}) = N_{pool} * Ndff$$

The fertilizer N recovery (FNR) was determined using the following equation:

$$FNR\ (\%) = \frac{FDN}{Applied\ fertilizer\ (mg\ N\ m^{-2})}$$

Net N translocation, or the maximum amount of N translocated from aboveground tissues to belowground N pools between maturity and senescence, was estimated for each stand age using the following equation (Wayman et al. 2014):

$$Net\ N\ translocation\ (mg\ N\ m^{-2}) = N_{pool,EOS-unharvested} - N_{pool,maturity}$$

where $N_{pool,EOS\text{-}unharvested}$ is the N_{pool} of the EOS-unharvested sampling and $N_{pool,maturity}$ is the N_{pool} at maturity for a given stand age.

We also evaluated three N conservation proxies: N_{green}, N resorption proficiency (NRP) and N resorption efficiency (NRE) (Jach-Smith and Jackson, 2015). The N_{green} (%) is the N content of only green leaves collected at maturity. NRP (%) is the N content of leaves collected after senescence (i.e., late November), and represents the lowest N content achieved by the leaf, with a higher NRP indicating a lower amount of N was translocated out of the leaf (or resorbed) during senescence. N_{green} and NRP differ from the N content (%) of the whole aboveground biomass pool at maturity and senescence,

respectively, in that they only represent the N content of leaves, rather than the N content of the whole aboveground biomass pool which contains leaves, stems, etc.

NRE was then calculated as:

$$NRE(\%) = 1 - \left(\frac{NRP}{N_{green}} * MLCF\right) * 100$$

where MLCF = 0.713 (Vergutz et al., 2012), a coefficient that accounts for the leaf mass loss that occurs between maturity and senescence. NRE indicates the extent to which plants withdraw nutrients from senescing leaves during plant senescence, with a higher NRE indicating plants translocate a greater supply of N into belowground root and soil pools (Killingbeck, 1996)

Statistical Analysis

All statistical analysis was performed using R software (R Core Team, 2023). The effect of stand age, sampling time and their interaction on aboveground tissue N content, N_{pool}, Ndff, FDN and FNR were evaluated using linear mixed effects models. Using the *lme* function from the nlme package (Pinheiro et al., 2022; version 3.1-160), random intercept models were created with a random effects structure of sampling time nested within plot replicate. The effect of stand age, sampling time, sampling depth and their interaction on root and soil N content, N_{pool}, Ndff, FDN and FNR were evaluated using random intercept models created with a random effects structure of sampling time nested within plot replicate nested within depth. The same model structure was used to evaluate the effect of stand age, sampling time, depth, and their interaction on soil available NO_3-N. The effect of stand age on N_{green}, NRP, NRE and grain yield were evaluated with one-

way ANOVA. When main effects or interactions were significant, a Tukey's-adjusted least-squares means comparison was performed using the *emmeans* function from the emmeans package (Lenth 2023; version 1.8.4-1). Compact letter displays were generated from the estimated means using the *cld* function from the multcomp package (Hothorn et al., 2008; version 1.4-17). Prior to post-hoc testing, all models were verified to meet model assumptions. When model assumptions were not met, data were transformed prior to means comparison. All significant differences were evaluated at $P < 0.05$.

Results

Soil NO_3-N

Soil available NO_3-N was significantly affected by sampling time and the two-way interactions between stand age x sampling time, stand age x depth, and sampling time x depth (table 3.3, fig. 3.3). At the Maturity sampling event, no significant differences in soil NO_3-N were detected between stand ages when averaged across depth, with 0.094 mg N kg soil^{-1} recovered from IWG-1 and no soil NO_3-N recovered from either other stand. The soil NO_3-N remained significantly higher in IWG-1 than IWG-3 at the EOS-harvested event when averaged across sampling depth, with soil NO_3-N in IWG-1 being 1.3 and 2.4 times higher in IWG-1 than IWG-2 or IWG-3 at EOS-harvested, respectively. Similar trends were seen at the EOS-unharvested event, though no significant differences between fields were detected when averaged across sampling depth.

When averaged across sampling time, similar trends were seen in the 0 – 15 cm depth interval, with IWG-1 maintaining a significantly higher soil NO_3-N (1.852 mg N kg soil^{-1}) than IWG-3 (0.612 mg N kg soil^{-1}). However, the opposite trend was seen in the 15 – 30 cm depth interval. A significantly higher mass of soil NO_3-N was recovered from IWG-3 than either other stand age, with the soil NO_3-N in the 15 – 30 cm depth interval in IWG-3 being 2.7 and 5.2 times higher than IWG-2 and IWG-1, respectively. When averaged across sampling depth, a similar soil NO_3-N concentration was recovered from the Maturity (0.06 mg N kg soil^{-1}) and EOS-unharvested (0.82 mg N kg soil^{-1}) samplings, both of which were significantly lower than that of the EOS-harvested (2.58 mg N kg soil^{-1}) sampling. Similar trends were seen in the 15 – 30 cm sampling depth, though no significant differences were detected.

N Content

Aboveground tissue N content (%) was significantly affected by stand age and sampling time, but not their interaction (table 3.4, fig. 3.4). Aboveground N content declined significantly between IWG-1 and IWG-2, falling by nearly 28% before plateauing around 1.25% in IWG-2 and IWG-3. On average, aboveground N content at Maturity declined by 0.22% each year. When averaged across stand age, aboveground N content was lowest at Maturity (1.0 %) and EOS-unharvested (0.8 %), both of which were significantly lower than EOS-harvested (1.6%), indicating a significant effect of grain harvest on the N content of aboveground tissues. Root N content was not significantly affected by stand age, sampling time, sampling depth or their interactions

(table 3.4, fig. 3.4), with trends showing root tissue N content ranged from 1.0 – 1.5% in the 0 – 15 cm interval, and 0.5 – 1.5% in the 15 – 30 cm interval. Total soil organic N content was significantly affected by stand age and sampling depth (table 3.4, fig. 3.4). The IWG-1 (0.21%) and IWG-3 (0.22%) on average had higher soil organic N content than IWG-2, each being 1.1 times greater than that of IWG-2. On average, the soil organic N content was significantly greater in the 0 – 15 cm layer (0.22%) than the 15 – 30 cm layer (0.20%).

N Pool

The aboveground biomass N_{pool}, or the total mass of N recovered from aboveground biomass, was significantly affected by stand age and sampling time, but not their interaction (table 3.4, fig.3.5). Aboveground N_{pool} in IWG-3 was on average 1.3 and 1.6 times greater than in IWG-1 and IWG-2, respectively. Across sampling times, aboveground N_{pool} at Maturity (5.47 g N m^{-2}) was significantly larger than that of the EOS-harvested (2.18 g N m^{-2}) or EOS-unharvested (3.51 g N m^{-2}) samplings. The root N_{pool} was smaller than that of the aboveground N_{pool} and varied little across the study period. In roots, N_{pool} was significantly affected by sampling depth only (table 3.4, fig. 3.5), where the root N_{pool} between 0 – 15 cm contained 8 times more root N than the 15 – 30 cm layer, declining on average from 1.00 to 0.13 g N m^{-2} between the 0 – 15 cm and 15 – 30 cm depth intervals. The soil organic N_{pool} was significantly affected by stand age and sampling depth (table 3.4, fig. 3.5). On average, IWG-1 and IWG-3 had 1.1 times more organic N in soil than IWG-2, marking a significantly lower soil N_{pool} in IWG-2

than either other stand age. Like the root N_{pool}, significantly more N was stored in the soil organic N_{pool} in the 0 – 15 cm depth interval (417 g N m^{-2}) than 15 – 30 cm depth interval (386 g N m^{-2}).

Net N Translocation

Net N translocation, or the maximum mass of N translocated from aboveground tissues to belowground pools between physiological maturity (i.e., August) and senescence (i.e., November), was significantly affected by stand age (fig. 3.6). Net N translocation in IWG-1 was 4324 mg N m^{-2}, representing 73% of the IWG-1 aboveground N pool at maturity. Net N translocation fell by nearly 44% between IWG-1 and IWG-2, and no significant differences were detected in net N translocation between IWG-2 (2429 mg N m^{-2}) and IWG-3 (2539 mg N m^{-2}). Net N translocation in IWG-2 and IWG-3 represented 49% and 40%, respectively, of the aboveground N_{pool} at maturity.

Fertilizer-Derived N

The mass of fertilizer-derived N (FDN) in aboveground tissues varied by stand age and sampling time (table 3.4, fig. 3.7). On average, aboveground FDN was 92% higher in IWG-3 than IWG-1, increasing by 65% between each consecutive stand age. Aboveground FDN at the EOS-unharvested sampling (327 mg N m^{-2}) was substantially higher than that of the EOS-harvested sampling (147 mg N m^{-2}), marking a significant effect of grain harvest on aboveground FDN at the end of the growing season. In roots,

FDN was significantly affected by sampling depth, but no significant effect of other main effects or interactions were detected (table 3.4, fig. 3.7). Across all sampling events, root FDN ranged from 91 to 139 mg N m^{-2}, 84 to 217 mg N m^{-2} and 95 to 204 mg N m^{-2} in the upper 0 – 15 cm soil layer in IWG-1, IWG-2, and IWG-3, respectively. Root FDN was 10.5 times higher in the 0 – 15 cm layer than the 15 – 30 cm layer, where root FDN ranged from 1 to 10 mg N m^{-2}, 1 to 38 mg N m^{-2} and 4 to 20 mg N m^{-2} across sampling times in IWG-1, IWG-2, and IWG-3, respectively. Soil FDN was significantly affected by sampling depth and the interaction between stand age and sampling depth (table 3.3, fig. 3.7). In the upper 0 – 15 cm, soil FDN was significantly greater in IWG-1 (2388 mg N m^{-2}) than IWG-3 (1681 mg N m^{-2}), with IWG-2 falling in between (2076 mg N m^{-2}). No significant differences between stand ages were found in soil FDN in the 15 – 30 cm layer, with FDN ranging from 500 mg N m^{-2} in IWG-1 to 892 mg N m^{-2} in IWG-3. On average, FDN was 4.2, 4.1 and 1.9 times greater in the 0 – 15 cm depth interval than the 15 – 30 cm depth interval in IWG-1, IWG-2 and IWG-3, respectively.

Proportion of IWG Tissue N Derived from Fertilizer or Soil

The proportion of the total N derived from fertilizer (Ndff) in aboveground tissues varied by stand age and sampling time (table 3.4, fig. 3.8). Averaged across sampling times, aboveground Ndff increased significantly with stand age, nearly doubling from an average of 7% to 16% between IWG-1 and IWG-3. At Maturity, aboveground Ndff ranged from 14 – 26%, and therefore the proportion of N derived from non-fertilizer sources at Maturity was 74% and 86% in IWG-3 and IWG-1, respectively, indicating the

N derived from non-fertilizer sources decreased with stand age. Aboveground Ndff at Maturity was on average 3 and 2.3 times higher than at the EOS-harvested or EOS-unharvested samplings, respectively. Aboveground Ndff was similar at both EOS samplings, ranging from 3 – 10% and 5 – 12% across stand ages at the EOS-harvested and EOS-unharvested sampling times. Root Ndff was affected significantly by sampling time and sampling depth, but varied little with stand age (table 3.3, fig. 3.8). On average root Ndff was highest at Maturity (15%), declining by nearly 38% between Maturity and the EOS samplings, though no significant differences were detected between the EOS-harvested (9%) or EOS-unharvested (9%) samplings. When averaged across sampling time and stand age, root Ndff was higher in the 0 – 15 cm layer (13%) compared to the 15 – 30 cm layer (9%).

Fertilizer N Recovery

FNR, measured as the proportion of FDN to applied fertilizer N, in the aboveground biomass varied by stand age and sampling time (table 3.4, fig. 3.9). Aboveground FNR was on average higher in IWG-3 (10%) than either IWG-2 (6%) or IWG-1 (4%), with FNR at maturity being 10% and 22% in IWG-1 and IWG-3, respectively. Aboveground FNR at Maturity was 8 and 4 times greater than at the EOS-harvested or EOS-unharvested samplings, respectively, though no significant differences in aboveground FNR were detected between either EOS sampling. Trends in root FNR varied across stand age and sampling time, though root FNR was significantly affected by sampling depth only (table 3.4, fig. 3.9), with FNR in the 0 – 15 cm layer (1.6%)

significantly greater than that of the 15 – 30 cm layer (0.2%). Soil FNR was significantly affected by sampling depth and the two-way interaction between stand age and depth (table 3.3, fig. 3.9). Soil FNR in IWG-1 (30%) was significantly higher than that of IWG-3 (21%) in the upper 0 – 15 cm soil layer, although no significant differences in soil FNR were detected between stand ages in the 15 – 30 cm layer (ranging from 6% – 11% across stand ages).

Nitrogen Conservation Indicators

The effect of stand age on N_{green} (the N content of green leaves at maturity), NRE (N resorption efficiency) and NRP (N resorption proficiency) was not significant (table 3.5), but trends suggest N_{green} declined with stand age. Similarly, trends suggested NRP increased sharply with stand age as indicated by a decline in the tissue N content in leaves at senescence with stand age. Although NRP was similar between IWG-1 (0.97%) and IWG-2 (0.90%), NRP in IWG-3 (0.64%) was nearly half that of IWG-1. NRE trends also declined with stand age, where IWG-1 (55.4%) had the highest NRE, followed by IWG-3 (49.3%) and IWG-2 (41.7%).

Grain Yield

Grain yield did not differ significantly across IWG stand age (table 3.5). Across all stand ages grain yield ranged from 399 to 421 lb $acre^{-1}$, decreasing marginally (not significant) between IWG-1 and IWG-3.

Discussion

N Availability in IWG Systems

We evaluated the hypothesis that IWG systems become N-limited as stands age using two common parameters linked to N availability: aboveground tissue N (%) and soil available NO_3-N. As expected, aboveground tissue N content at every sampling event was significantly lower in IWG-3 and IWG-2 compared to IWG-1. Declining tissue N content with stand age is commonly reported in IWG stands managed for grain production (Reilly et al., 2022; Crews et al., 2022). In a study conducted at five locations in which IWG was subjected to three different N fertilization regimes, IWG tissue N content declined by 40 - 46% between the second and fourth production years (Tautges et al., 2018). Interestingly, IWG aboveground tissue N contents were seen to decline on average by 0.2% each year (Jungers et al., 2017; Tautges et al., 2018), similar to the aboveground tissue N content decline of 0.2% yr^{-1} seen in our study. The steady decline in aboveground tissue N content seen across a variety of studies suggests a consistent management or physiological mechanism underlies the decline in aboveground tissue N, and identifying this mechanism will improve the ability to develop sustainable IWG N management practices.

Along with aboveground tissue N content, soil NO_3-N concentrations declined significantly between the first and third IWG production year. These results aligned closely with previous studies, which showed little change in soil NO_3-N between the first and second IWG production year but substantial (41 – 48%) declines in soil NO_3-N after

three IWG production years (Pugliese et al., 2019; Dobbratz et al., 2023). Since only 2.5 – 5.0 g N m^{-2} (25 – 50 kg N ha^{-1}) was removed in aboveground biomass at harvest, but 8 g N m^{-2} (80 kg N ha^{-1}) was applied at spring fertilization, the decline in soil NO_3-N suggests inadequate fertilizer N application rates are not solely responsible for the decline in soil NO_3-N. Rather, the decline may signal other suboptimal fertilizer application methods, including improper timing or placement, that may reduce the fertilizer uptake efficiency (FNR) and subsequently lead to reductions in soil NO_3-N as crops deplete soil available N pools due to lack of access to fertilizer N (Mahler et al., 1994; Thilakarathna et al., 2020). Taken together with the diminished aboveground tissue N contents, the age-related reduction in soil NO_3-N suggests N availability in IWG systems declines as stands age.

To compensate for reduced N availability, perennial grasses increase the conservation of internal N supplies through translocation of N from aboveground to belowground tissue N storage pools between physiological maturity and senescence (Jach-Smith and Jackson, 2015; Roley et al., 2020). Given the decline in aboveground tissue N content and soil NO_3-N availability, which can be a signal that N-limiting conditions are developing as IWG stands age, we expected net N translocation to increase with stand age. However, we found net N translocation declined significantly with stand age, contradicting our hypothesis that the development of N limiting conditions would drive an increase in net N translocation with IWG stand age as stands become more reliant on internally translocated N to support tissue growth and development. The marginal (non-significant) decline in NRE, which represents the proportion of

aboveground N translocated from green leaves to belowground N pools between maturity and senescence, further supports the trends we observed with net N translocation, suggesting IWG does not invest more heavily into internal N translocation and N conservation strategies as stands age. As other wheatgrass species have been shown to respond to the amelioration of N limitation by decreasing the reliance on internally translocated N (Li and Redman, 1991), the reduction in net N translocation and NRE draws into question whether the declining aboveground tissue N content and soil available NO_3-N indicate N limitation.

Reductions in tissue N content and soil N availability often signal the development of N-limiting conditions, but these changes can also result from other environmental and physiological factors. For example, aging perennial plants may shift N allocation towards non-structural plant components (i.e., stems) to overcome light limitation (Poorter et al., 2011; Liang et al. 2022). This strategy is particularly prevalent in perennial grass stands, which often experience light limitation due to greater levels of aboveground biomass developing per unit area as stands age. Therefore, the decrease in tissue N concentrations is not linked to nutrient availability per se, but rather to increased allocation to stems that maintain lower N concentrations than other aboveground parts, such as leaves. Although experimental evidence remains limited, Glover et al. (2004) showed the leaf to stem ratio of intermediate wheatgrass, tall wheatgrass, and slender wheatgrass declined with stand age when measured across two consecutive production years, and a similar trend may be apparent in IWG managed for grain production. In this study, a significant increase in aboveground biomass with stand age was noted, with

aboveground biomass per m row almost tripling between the first and third IWG production year (supplemental figure 3.3). This suggests light limitation could also play a role in the declining N content in IWG tissues, and there are likely several interconnected processes that drive the changes in aboveground tissue N content and soil NO_3-N availability we observed in this study and previous literature.

Primary N Sources Supporting IWG Tissue Growth

We evaluated the extent of N translocation and N fertilizer uptake in IWG crop tissues, as these are two primary sources of N that support tissue growth in perennial grasses (Li and Redman, 1991). Compared to other similarly-aged perennial grass biofuel crops, net N translocation across all IWG stand ages was relatively low. For example, the third-year IWG translocated just 40% of aboveground N belowground between maturity and senescence in this study, whereas 3-year-old, 5- to 7-year-old, and 8-year-old switchgrass respectively translocated 64%, 45% and 27% of aboveground N belowground between maturity and senescence (Dohleman et al., 2012; Heaton et al., 2008; Wayman et al., 2014). Similarly, 3- to 4-year-old miscanthus translocated nearly 63 - 75% of aboveground N belowground between maturity and senescence, falling to just 17% in 5- to 7-year-old stands (Dohleman et al., 2008; Heaton et al., 2008; Leroy et al., 2022). Although age-related declines in net N translocation can be seen in the switchgrass and miscanthus studies, similar to the decline noted in our study, switchgrass and miscanthus still translocated nearly two thirds of the aboveground N to belowground pools in their third production year. This suggests N translocation remained an important

source of N during the first several years following planting. The relatively low proportion of aboveground N translocated belowground in IWG relative to switchgrass and miscanthus of similar ages suggests that preventing IWG from translocating N belowground between maturity and senescence, due to grain harvest and biomass removal at maturity, may not be as consequential as it is for other perennial grass biofuel systems. Especially after the first year of IWG production, where the net N translocation falls from over 70% to 40%, the relatively low net N translocation suggests IWG likely primarily relies on N sources aside from internally translocated N to meet the demands of tissue growth and development.

These trends in whole aboveground biomass N translocation are supported when evaluating N translocation from green leaves alone to belowground pools (i.e., NRE), which is often used as a more sensitive indicator of N translocation than when evaluating the whole aboveground biomass pool (Jach-Smith and Jackson, 2015). NRE trended downwards as stands aged and was generally lower than seen in other wheatgrass and perennial biofuel grasses. The NRE between maturity and senescence for 1-year-old desert wheatgrass (*Agropyron desertorum*) and 1-year-old Siberian wheatgrass (*Agropyron fragile*) were 80% and 74% (Khasanova et al., 2013), respectively, compared to the 50% observed for 1-year-old IWG in this study. A 3-year-old miscanthus stand fertilized at 150 kg N ha^{-1} had an NRE of 60% (Jach-Smith and Jackson, 2015), higher than the 41% and 49% observed for 2- and 3-year-old IWG stands in this study. Along with the observations of reduced net N translocation, the slight age-related decline in NRE and overall lower NRE relative to similarly-aged wheatgrass and perennial grass

biofuel species further suggests IWG employs a lower degree of N translocation than other perennial grasses, and therefore delaying harvest beyond maturity to maximize N translocation to belowground tissues in IWG may not be as important as it is for other perennial grass crop species. Even so, our results showed that IWG translocated up to half of the aboveground biomass N to belowground pools between maturity and senescence in unharvested systems, and IWG N management recommendations should consider the effect grain N and biomass N removal at harvest has on the potential contributions internally translocated N makes to supporting the N demands of IWG tissue growth and maintenance.

Fertilizer N was also not a substantial pool of N supplying IWG aboveground tissue or root tissue growth during the growing season. In aboveground tissues, the proportion of fertilizer N was unexpectedly low relative to other cropping systems. For example, in three different 3-year-old miscanthus cultivars FDN accounted for nearly 36 – 72% of aboveground N at maturity (Leroy et al., 2022), compared to the 26% at maturity in the 3-year-old IWG stand in this study. Even compared to annual grain crops, the proportion of FDN in aboveground IWG tissues was considerably lower. A meta-analysis including maize, wheat and rice estimated the proportion of aboveground N derived from fertilizer at maturity was 36%, 42% and 42%, respectively (Yu et al., 2022), compared to the 14 – 26% we measured at maturity between the first and third IWG production years. Given the large root stocks and efficient uptake of soil leachate in IWG stands (Jungers et al., 2019; Reilly et al., 2022; Woeltjen, 2023, Chapter 1) we expected

IWG roots to be largely composed of fertilizer-derived N. However, as with aboveground tissues, the proportion of root N derived from fertilizer was relatively low.

Together, these results indicate non-fertilizer sources are the primary source of N used to support IWG tissue (both aboveground and root) production throughout the growing season across all IWG stand ages. As IWG did not demonstrate strong internal N translocation and conservation strategies relative to other crops, IWG has likely not developed to rely strongly on a large pool of internally translocated N to meet N demands under the fertilization and agronomic practices used in this study. Instead, we suggest that the mineralization of native soil organic N and IWG crop residues provides a large portion of the N used to support IWG tissue development. The reliance on the turnover of IWG residues aligns with observations that root decomposition and root N turnover increase with IWG stand age (Woeltjen, 2023, Chapter 1), suggesting IWG systems efficiently recycle N through decomposition of root tissues.

Efficiency of Fertilizer Uptake

The aboveground tissue fertilizer N recovery (i.e., FNR), measured as the proportion of fertilizer-N recovered to the fertilizer-N applied, was relatively low across all IWG stand ages compared to previously published FNR values for annual crops. FNR in IWG aboveground tissues ranged from 4 - 22% across stand age and sampling times, with peak FNR at IWG maturity being 13%, 16% and 22% in IWG-1, IWG-2, and IWG-3. These values were much lower than 36 - 50% reported for other annual grain and perennial biomass crops, and far lower than the estimated aboveground FNR of 40 - 75%

reported for IWG in other studies (Stout and Weaver, 2007; Sprunger et al., 2018; Frick et al., 2022). The discrepancy between FNR measured in this study compared to that of other IWG studies could be attributed in part to methodological differences between direct and indirect measures of FNR (Quan et al., 2020), but could also reflect suboptimal N management practices in which N fertilizer quality, rate or timing is poorly synchronized with N uptake by IWG crops. As the response of cropping systems to varied N fertilizer application is inconsistent, and cropping systems can respond differently to varied N rate and timing when grown in different environmental or soil conditions (Cambouris et al., 2008), studies evaluating optimal N uptake timing specific to IWG across a variety of growing environments are needed.

IWG may have a lower aboveground FNR compared to annual crops because it requires more N to support more root biomass. Others recovered nearly 50% of the 160 kg N applied to a 2-year-old IWG stand in crop tissues (Huddell et al., 2023), and up to half of total IWG tissue N can be accounted for by root tissues (Sprunger et al., 2018). Therefore, we expected the low aboveground FNR would be accompanied by a high root FNR. However, root FNR was on average just 1.8% in the upper 0 – 15 cm and less than 0.5% in the 15 – 30 cm soil layer. Although unexpected for the IWG system due to the rapid production of root biomass in the first production year and maintenance of root stocks in the second production years (Woeltjen, 2023, Chapter 1), these results align with others showing low FNR by roots in clover (2.5%), ryegrass (11%) and maize (1 – 2%) (Castle et al., 1999; Quan et al., 2018; Quan et al., 2020). The low root FNR in these cases is likely driven by a relatively limited root pool size compared to aboveground

biomass, which can be several orders of magnitude larger than that of roots (see supplemental figure 3.3). Since aboveground tissues and roots maintain similar N contents, the smaller root stock will lead to a smaller assimilation of N compared to standing biomass.

As off-site transport of FDN from agricultural systems contributes considerably to regional water quality, greenhouse gas emissions and air pollution, the low FNR from aboveground tissues and roots poses a concern for regional environmental health if the remaining fertilizer N is not retained in the IWG system. In the first year of production, an average of one third of the applied fertilizer remained in soil organic N pools, making it susceptible to mineralization and loss from the system. However, the soil FNR declined with stand age as the uptake of FDN into aboveground tissues increased, suggesting IWG more efficiently utilizes fertilizer N inputs to produce biomass as stands age.

Over one third of the applied fertilizer remained unaccounted for in our sampling, raising questions regarding the fate of the remaining FDN. Although it is possible our simulated irrigation caused a portion of the labelled fertilizer to travel below the 30 cm sampling depth via soil leachate, others using similar methods in IWG were able to recover nearly 100% of the applied fertilizer N and saw soil FDN did not increase with depth (Huddell et al., 2023), as would be expected if these methods washed the tracer below 30 cm. Further, ample literature shows IWG is highly effective at assimilating soil NO_3-N and preventing loss of fertilizer N through soil leaching (Culman et al., 2013; Jungers et al., 2019; Reilly et al., 2022), and data from this study similarly shows NO_3 losses through soil leaching were low in all stands across the study period (see

supplemental figure 3.4). Rather, future studies should explore alternative loss pathways for FDN such as denitrification, and storage of FDN in alternative pools including roots below 30 cm, crop crowns, rhizomes, and soil microbial biomass.

Removal of FDN at harvest

The stand age-related increase in aboveground FNR and FDN has important implications for IWG growers that harvest grain and remove the remaining standing biomass from fields. Since the same mass of fertilizer was applied to each IWG system, the increase in FNR with stand indicates a greater mass of applied fertilizer N is removed with grain harvest in each consecutive IWG production year. The decline in grain yield with IWG stand age suggests the potential financial loss associated with exporting a larger amount of fertilizer N from the system via grain harvest and aboveground biomass removal is not offset by economic gains from grain yield. Further development of dual-use of IWG systems, in which both grain and straw provide economic value, will therefore be especially important to ensuring IWG systems remain both economically and environmentally sustainable.

Effect of Drought during Study Year

This study was conducted during a moderate to severe drought that affected the upper Midwestern region of the USA during the 2021 growing season, with some affected areas receiving half as much precipitation as usual (see figure 3.1). Drought conditions severely limit soil water availability, and can consequently impact crop tissue

growth, N uptake capacity and N conservation dynamics (Fan and Li, 2001; Yang et al., 2011; Khasanova et al., 2013). Khasanova et al. (2013) found water-limited conditions were associated with reduced internal N translocation as indicated by $N_{green,}$ NRP and NRE in perennial grasses from the *Agropyron* and *Festuca* families. Although our results were usually in line with previous studies, and we believe our results are still representative of the IWG systems we studied, the effect of drought on IWG N cycling should be taken into consideration when interpreting our results.

Conclusions

In this study, a decline in aboveground tissue N content and soil NO_3-N with stand age was observed, which supported the hypothesis that IWG stands become N limited as they age. However, IWG did not translocate more N belowground or demonstrate stronger N conservation mechanics as stands aged, which would be expected if stands were experiencing N limiting conditions. Together, these results suggested a process other than N limitation is driving the decline in tissue N and soil NO_3-N. Though relatively less than other perennial cropping systems, all IWG stand ages translocated N belowground between maturity and senescence, and this translocated N pool should be considered when designing N management recommendations for growers. Fertilizer-derived N accounted for only a small proportion of the N in crop tissues, and the majority of fertilizer-applied N remained unrecovered from aboveground biomass or roots across all IWG stand ages, suggesting current urea fertilizer management recommendations are suboptimal for meeting the N demands of IWG tissue growth and maintenance. Future

research should explore the fate of fertilizer N through crop-soil pools when alternative N rates, timing and placements are applied in IWG grain systems. As aboveground fertilizer N recovery increased with stand age, indicating a greater mass of fertilizer N is removed at harvest with each consecutive production year, dual use systems in which economic value is assigned to both IWG grain and IWG straw will lead to the most cost-effective management in terms of fertilizer N.

Table 3.1 Agronomic management details for each field included in this study.

		IWG-1	IWG-2	IWG-3
2021	Field ID	R90	R34	R7-21
	Planting date	September 2020	September 2019	September 2018
	Seeding rate	13 kg live seed ha^{-1}	13 kg live seed ha^{-1}	13 kg live seed ha^{-1}
	Row spacing	30 cm	38 cm	40 cm
	N fertilization date	April 2021	April 2020, April 2021	April 2019, April 2020, April 2021
	N fertilization rate	80 kg N ha^{-1}	80 kg N ha^{-1}	80 kg N ha^{-1}
	N fertilizer type	Urea	Urea	Urea
	Harvest date	August 2	August 2	August 2

Table 3.2 List of abbreviated terms and their descriptions

Abbreviation	Description
N content	N content (%) of compartment or pool
N_{pool}	The total amount of N in a compartment (i.e., shoots, roots, soil)
Ndff	Proportion of N_{pool} derived from fertilizer
FDN	Mass of N_{pool} derived from fertilizer
FNR	Proportion applied fertilizer N recovered from the N_{pool} of a compartment
Net N Translocation	Net N translocated from whole aboveground biomass pool to belowground pools between maturity and senescence
N_{green}	N content (%) of only green leaves collected at maturity
NRE	Nitrogen resorption efficiency, or the ratio of N_{green} to NRP
NRP	Nitrogen resorption proficiency, or the lowest tissue N content achieved by leaves after senescence

Table 3.3 Analysis of variance and probability of significance for soil available NO_3-N. Significant p-values are bolded ($P < 0.05$).

	Soil available NO_3-N
Stand age (A)	0.330
Sampling time (S)	**0.002**
Depth (D)	0.766
AxS	**<0.001**
SxD	**0.018**
AxD	**<0.001**
AxSxD	0.182

Table 3.4 Analysis of variance and probability of significance for N content, Npool, FDN, Ndff and FNR of aboveground biomass tissues (AGB), roots and soil organic N (Soil). Significant p-values are bolded ($P < 0.05$).

		N content	N_{pool}	FDN	Ndff	FNR
AGB	Stand age (A)	**<0.001**	**0.0014**	**0.0018**	**0.0002**	**0.0018**
	Sampling time (S)	**0.002**	**0.0022**	**0.0006**	**0.0004**	**0.0006**
	AxS	0.3343	0.6627	0.2049	0.8488	0.2049
Roots	Stand age (A)	0.1003	0.8699	0.6160	0.9796	0.6160
	Sampling time (S)	0.1196	0.4582	0.7287	**0.0168**	0.7287
	Depth (D)	0.1088	**0.0022**	**0.0020**	**0.0033**	**0.0020**
	A x S	0.7235	0.2152	0.3961	0.6930	0.3961
	A x D	0.5563	0.6113	0.5367	0.2236	0.5367
	S x D	0.5223	0.5263	0.5054	0.0984	0.5054
	A x S x D	0.7196	0.6095	0.5513	0.4851	0.5513
Soil	Stand age (A)	0.4861	**0.0001**	0.4260	0.4861	0.4260
	Sampling time (S)	0.1313	0.4073	0.1320	0.1313	0.1320
	Depth (D)	**< 0.0001**	**0.0024**	**< 0.0001**	**<0.0001**	**< 0.0001**
	A x S	0.8181	0.7088	0.8324	0.8181	0.8324
	A x D	**0.0029**	0.2918	**0.0055**	**0.0029**	**0.0055**
	S x D	0.9111	0.5024	0.8473	0.9111	0.8473
	A x S x D	0.2147	0.8115	0.2493	0.2147	0.2493

Table 3.5 Analysis of variance and estimated marginal means of N_{green} (the N content of green leaves), nitrogen resorption proficiency (NRP; the tissue N content of senesced leaves), nitrogen resorption efficiency (NRE; the relative proportion of the leaf N pool resorbed during senescence) and grain yield.

		N_{green}	NRP	NRE	Grain Yield
ANOVA	Stand age (A)	0.546	0.058	0.774	0.973
		%	*%*	*%*	*lb acre*$^{-1}$
Stand age	IWG-1	1.67	0.97	55.4	421
	IWG-2	1.16	0.90	41.7	418
	IWG-3	1.28	0.64	49.3	399

Figure 3.1 Annual precipitation and temperature in Rosemount, MN for the 2021 study year.

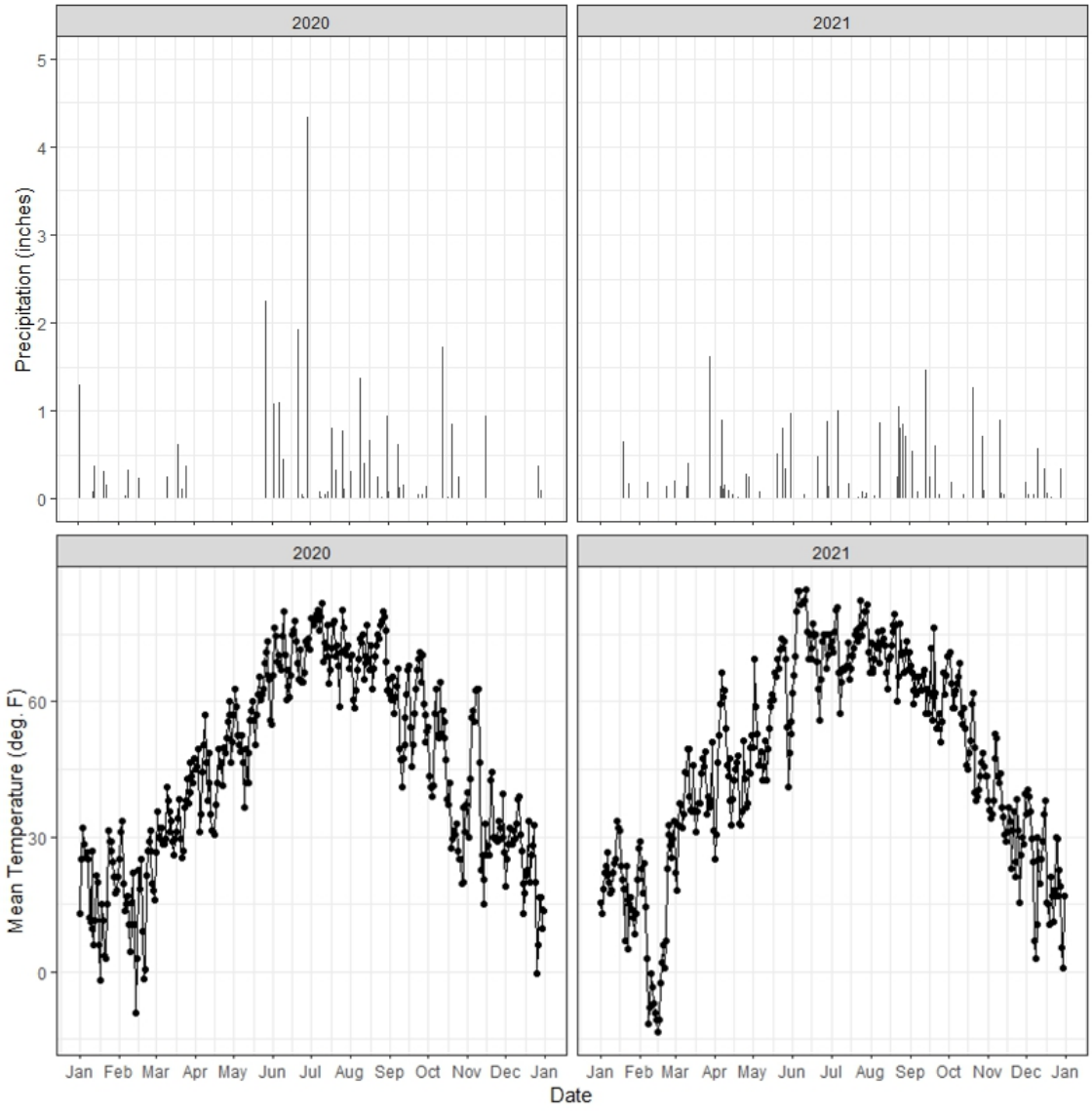

Figure 3.2 Plot layout and sampling zone delineation in ^{15}N-microplots and non-enriched sampling areas

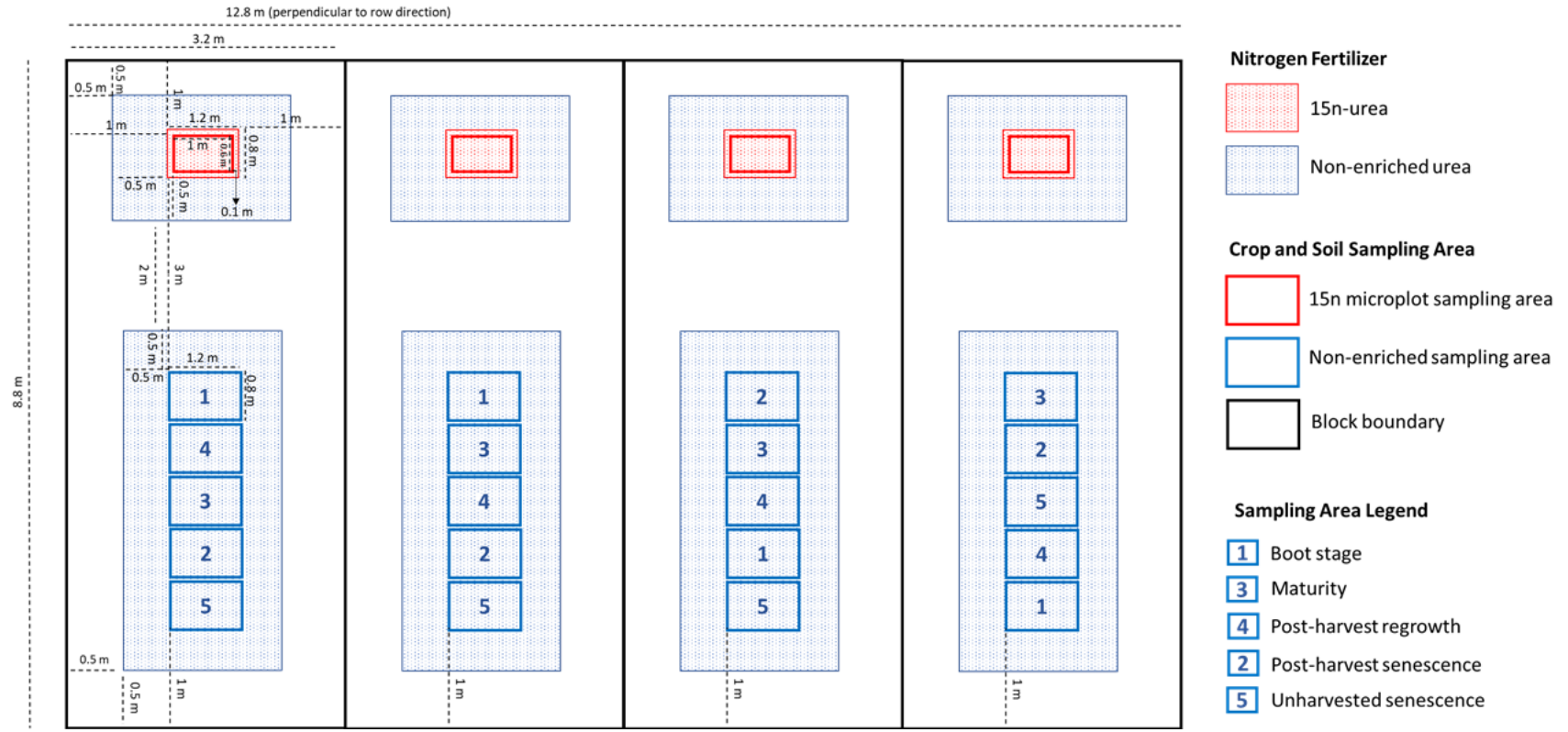

Figure 3.3 Mean and standard error of soil available NO_3-N in each stand age at two depths and three sampling times

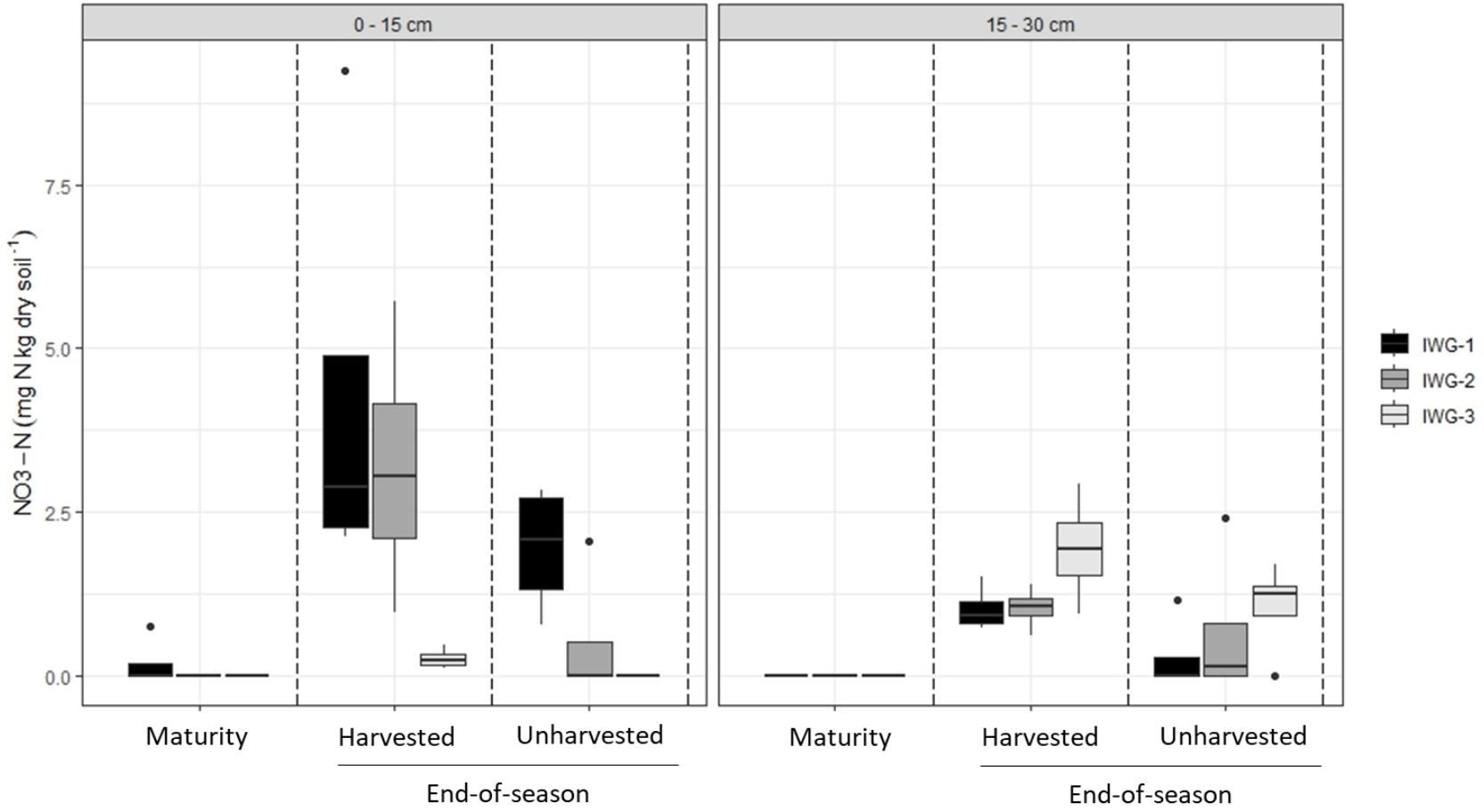

Figure 3.4 Mean and standard error of N content of compartments: a) aboveground biomass, b) roots (0 – 15 cm), c) roots (15 – 30 cm), d) soil (0 – 15 cm) and e) soil (15 – 30 cm). Groupings of horizontal bars associated with different lowercase letters indicate significant differences between stand age within a given compartment when averaged across sampling time. Asterisks following depth intervals indicate significant differences were detected between depth intervals when averaged across compartment and stand age.

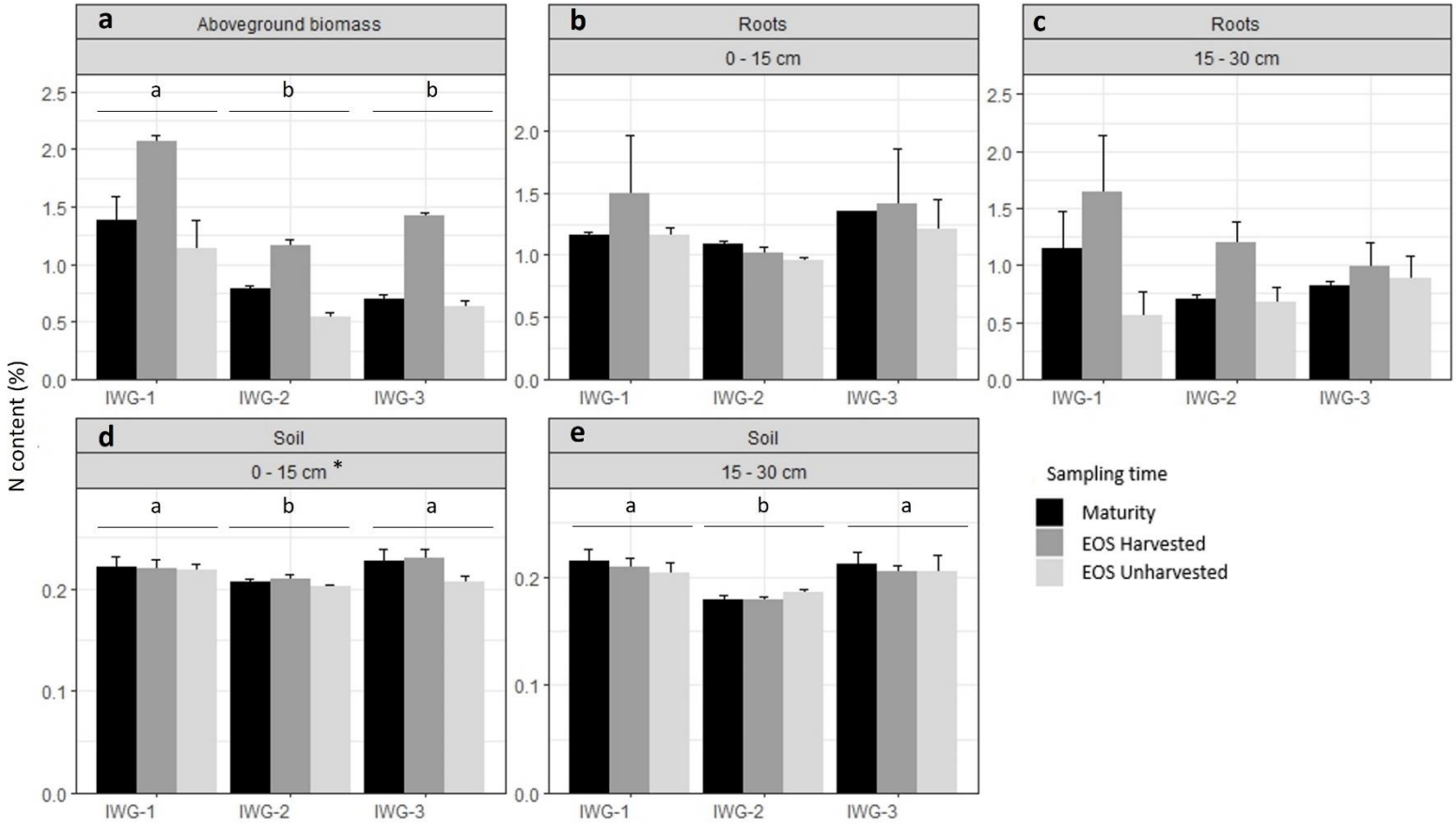

Figure 3.5 Mean and standard error of pool size (N_{pool}) of compartments: a) aboveground biomass, b) roots (0 – 15 cm), c) roots (15 – 30 cm), d) soil (0 – 15 cm) and e) soil (15 – 30 cm). Groupings of horizontal bars associated with different lowercase letters indicate significant differences between stand age within a given compartment when averaged across sampling time. Asterisks following depth intervals indicate significant differences were detected between depth intervals when averaged across compartment and stand age.

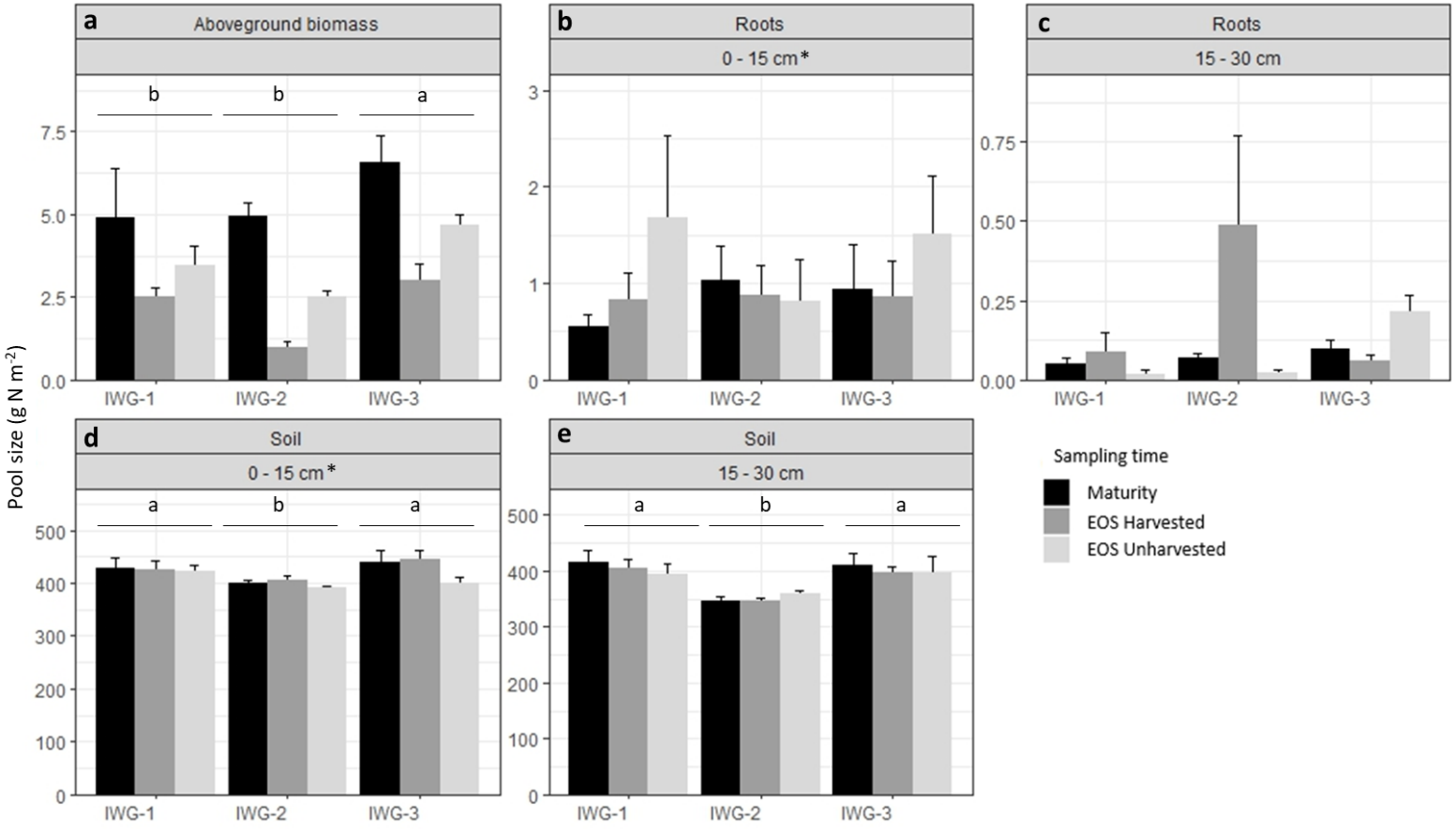

Figure 3.6 Mean and standard error of the net translocated N. Means not sharing any lowercase letters are significantly different ($P < 0.05$).

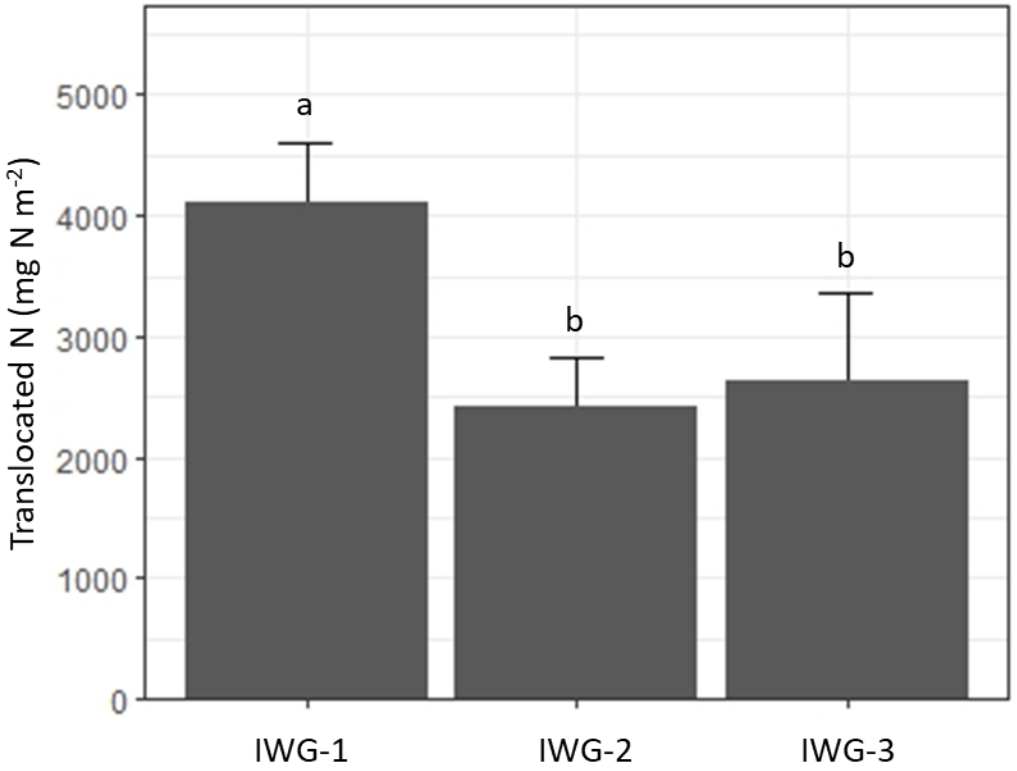

Figure 3.7 Mean and standard error of fertilizer-derived N (FDN) of compartments: a) aboveground biomass, b) roots (0 – 15 cm), c) roots (15 – 30 cm), d) soil (0 – 15 cm) and e) soil (15 – 30 cm). Groupings of horizontal bars associated with different lowercase letters indicate significant differences between stand age within a given compartment when averaged across sampling time. Asterisks following depth intervals indicate significant differences were detected between depth intervals when averaged across compartment and stand age.

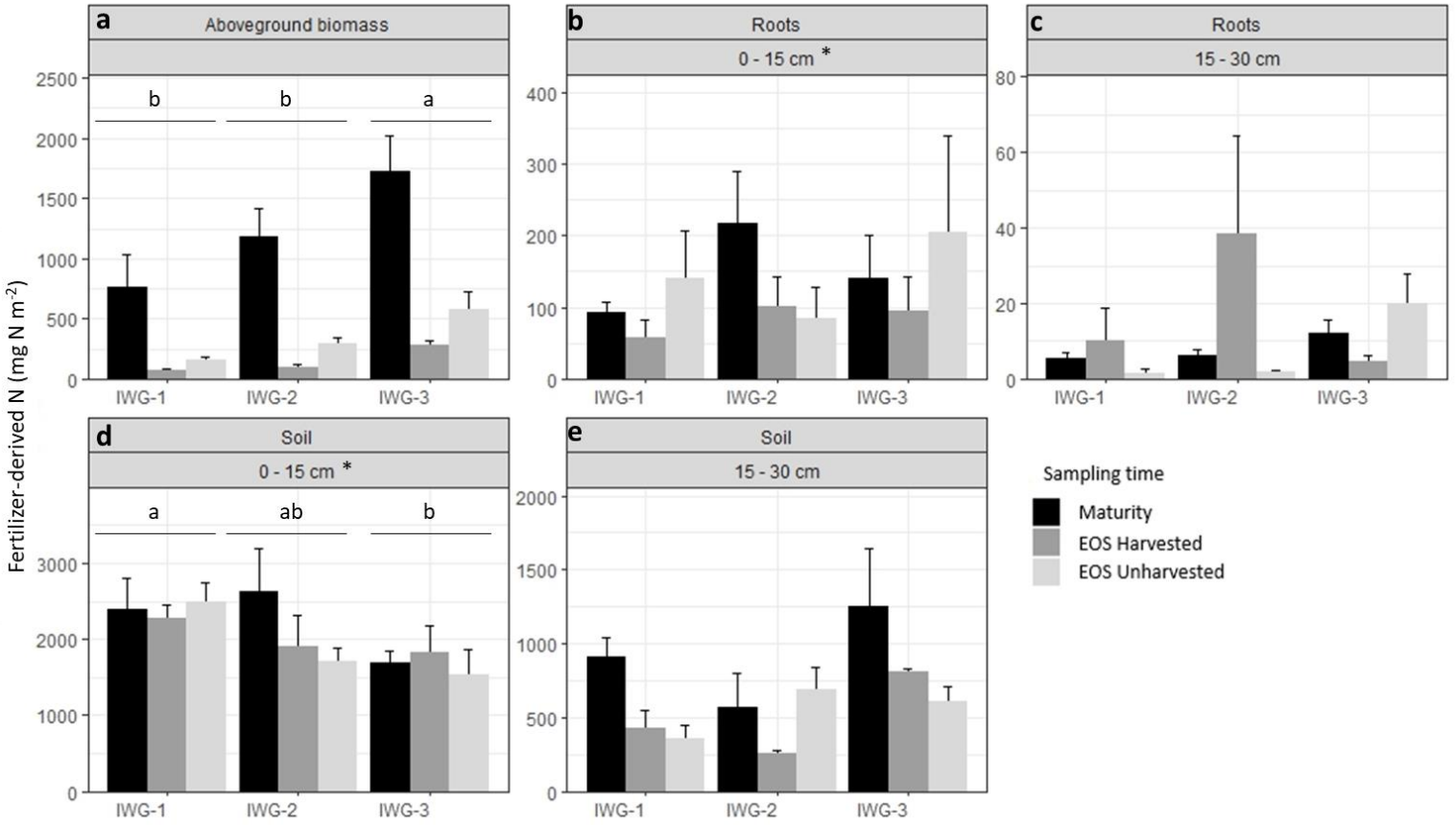

Figure 3.8 Mean and standard error of the proportion of N derived from fertilizer (Ndff) of compartments: a) aboveground biomass, b) roots (0 – 15 cm), c) roots (15 – 30 cm), d) soil (0 – 15 cm) and e) soil (15 – 30 cm). Groupings of horizontal bars associated with different lowercase letters indicate significant differences between stand age within a given compartment when averaged across sampling time. Asterisks following depth intervals indicate significant differences were detected between depth intervals when averaged across compartment and stand age.

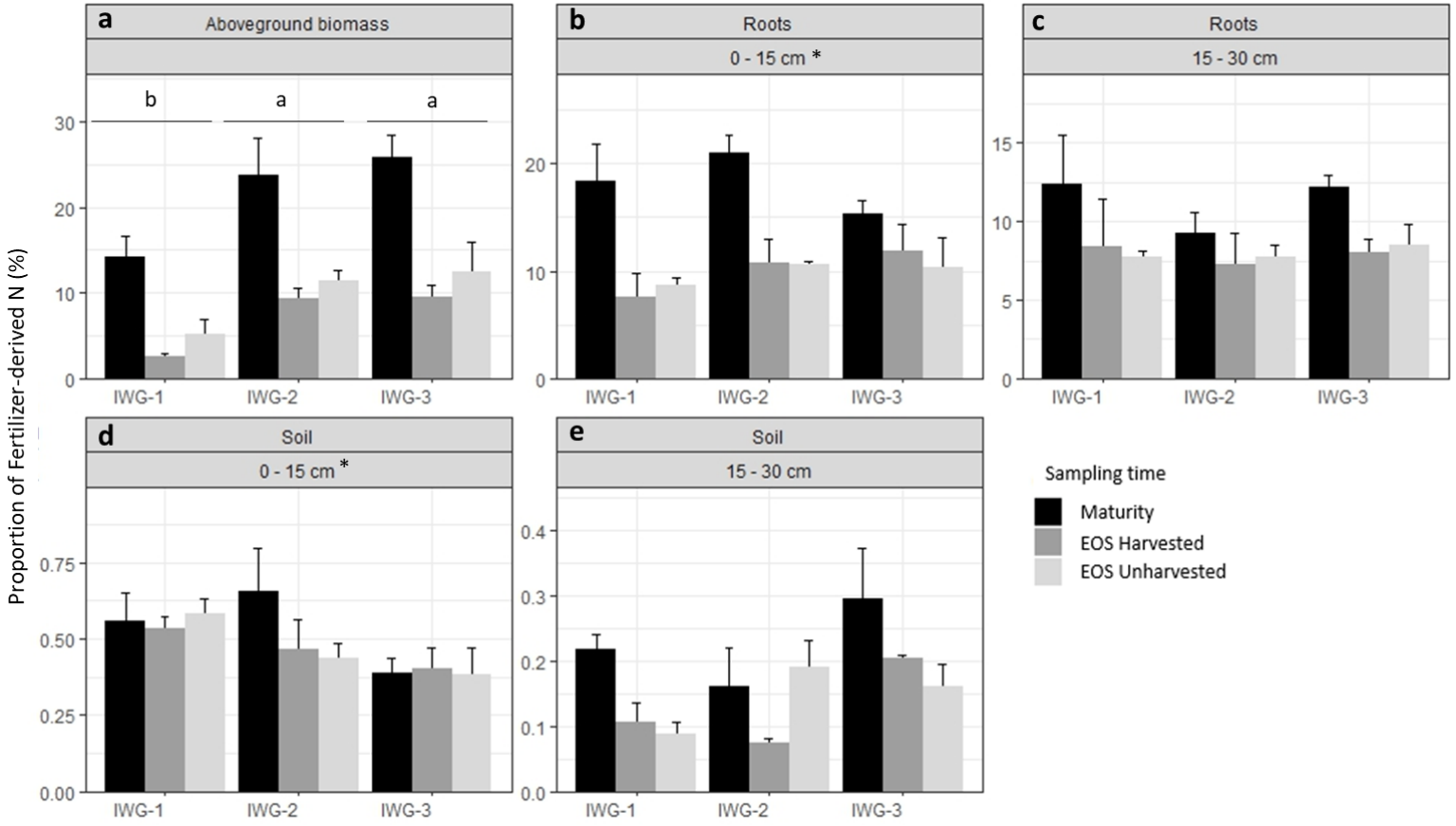

Figure 3.9 Mean and standard error of fertilizer N recovery (FNR) of compartments: a) aboveground biomass, b) roots (0 – 15 cm), c) roots (15 – 30 cm), d) soil (0 – 15 cm) and e) soil (15 – 30 cm). Groupings of horizontal bars associated with different lowercase letters indicate significant differences between stand age within a given compartment when averaged across sampling time. Asterisks following depth intervals indicate significant differences were detected between depth intervals when averaged across compartment and stand age.

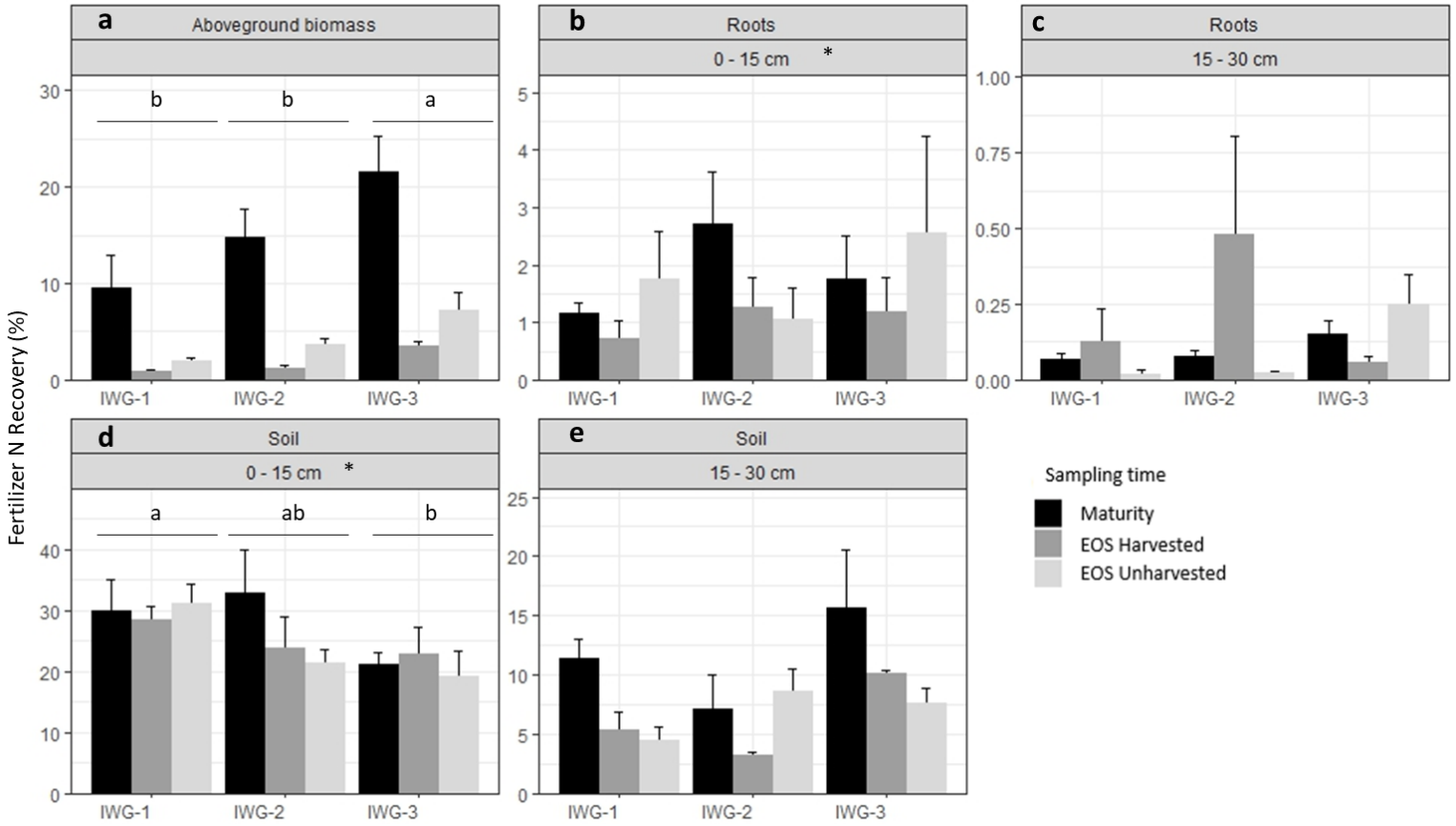

Bibliography

Acharya, B. S., Rasmussen, J., & Eriksen, J. (2012). Grassland carbon sequestration and emissions following cultivation in a mixed crop rotation. *Agriculture, Ecosystems & Environment*, *153*, 33–39. https://doi.org/10.1016/j.agee.2012.03.001

Amelung, W., Bossio, D., de Vries, W., Kögel-Knabner, I., Lehmann, J., Amundson, R., ... & Chabbi, A. (2020). Towards a global-scale soil climate mitigation strategy. Nature communications, 11(1), 5427.

Audu, V., Rasche, F., Dimitrova Mårtensson, L.-M., & Emmerling, C. (2022). Perennial cereal grain cultivation: Implication on soil organic matter and related soil microbial parameters. *Applied Soil Ecology*, *174*, 104414. https://doi.org/10.1016/j.apsoil.2022.104414

Augarten, A. J., Malone, L. C., Richardson, G. S., Jackson, R. D., Wattiaux, M. A., Conley, S. P., Radatz, A. M., Cooley, E. T., & Ruark, M. D. (2023). Cropping systems with perennial vegetation and livestock integration promote soil health. *Agricultural & Environmental Letters*, *8*(1), e20100. https://doi.org/10.1002/ael2.20100

Bauer, A., Frank, A. B., & Black, A. L. (1984). Estimation of Spring Wheat Leaf Growth Rates and Anthesis from Air Temperature1. *Agronomy Journal*, *76*(5), 829–835. https://doi.org/10.2134/agronj1984.00021962007600050027x

Bauer, A., Frank, A. B., & Black, A. L. (1987). Aerial Parts of Hard Red Spring Wheat. I. Dry Matter Distribution by Plant Development Stage1. *Agronomy Journal*, *79*(5), 845–852. https://doi.org/10.2134/agronj1987.00021962007900050019x

Bergquist, G., Gutknecht, J., Sheaffer, C., & Jungers, J. M. (2022). Plant Suppression and Termination Methods to Maintain Intermediate Wheatgrass (Thinopyrum intermedium) Grain Yield. *Agriculture*, *12*(10), Article 10. https://doi.org/10.3390/agriculture12101638

Bergquist, G. E. (2019.). Biomass yield and soil microbial response to management of perennial intermediate wheatgrass (Thinopyrum intermedium) as grain crop and carbon sink. Master's thesis, University of Minnesota Press.

Bligh, E. G. and Dyer, W. J.: A rapid method of total lipid extraction and purification, Can. J. Biochem. Physiol., 37, 911–917, 1959.

Bolinder, M. A., Angers, D. A., Bélanger, G., Michaud, R., & Laverdière, M. R. (2002). Root biomass and shoot to root ratios of perennial forage crops in eastern Canada. *Canadian Journal of Plant Science*, *82*(4), 731–737. https://doi.org/10.4141/P01-139

Bowden, J. (2023). Organically managed intermediate wheatgrass (Thinopyrum intermedium) as a dual-use grain and forage crop. Master's thesis, University of Minnesota Press, May 2023.

Bradford, M. A., Strickland, M. S., DeVore, J. L., & Maerz, J. C. (2012). Root carbon flow from an invasive plant to belowground foodwebs. *Plant and Soil*, *359*(1), 233–244. https://doi.org/10.1007/s11104-012-1210-y

Brüggemann, N., Gessler, A., Kayler, Z., Keel, S. G., Badeck, F., Barthel, M., Boeckx, P., Buchmann, N., Brugnoli, E., Esperschütz, J., Gavrichkova, O., Ghashghaie, J., Gomez-Casanovas, N., Keitel, C., Knohl, A., Kuptz, D., Palacio, S., Salmon, Y., Uchida, Y., & Bahn, M. (2011). Carbon allocation and carbon isotope fluxes in the plant-soil-atmosphere continuum: A review. *Biogeosciences*, *8*(11), 3457–3489. https://doi.org/10.5194/bg-8-3457-2011

Buckeridge, K. M., La Rosa, A. F., Mason, K. E., Whitaker, J., McNamara, N. P., Grant, H. K., & Ostle, N. J. (2020). Sticky dead microbes: Rapid abiotic retention of microbial necromass in soil. *Soil Biology and Biochemistry*, *149*, 107929. https://doi.org/10.1016/j.soilbio.2020.107929

Buckeridge, K. M., Mason, K. E., McNamara, N. P., Ostle, N., Puissant, J., Goodall, T., Griffiths, R. I., Stott, A. W., & Whitaker, J. (2020). Environmental and microbial controls on microbial necromass recycling, an important precursor for soil carbon stabilization. *Communications Earth & Environment*, *1*(1), Article 1. https://doi.org/10.1038/s43247-020-00031-4

Butler, J. L., Williams, M. A., Bottomley, P. J., & Myrold, D. D. (2003). Microbial Community Dynamics Associated with Rhizosphere Carbon Flow. *Applied and Environmental Microbiology*, *69*(11), 6793–6800. https://doi.org/10.1128/AEM.69.11.6793-6800.2003

Cai, H., Li, F., & Jin, G. (2019). Fine root biomass, production and turnover rates in plantations versus natural forests: Effects of stand characteristics and soil properties. *Plant and Soil*, *436*(1), 463–474. https://doi.org/10.1007/s11104-019-03948-8

Castle, M. L., Rowarth, J. S., Cornforth, I. S., & Sedcole, J. R. (1999). *The fate of 15N-labelled fertiliser applied in autumn or winter to white clover (Trifolium repens L.) or perennial ryegrass (Lolium perenne L.)*. 6.

Chaudhary, D. R., Saxena, J., Lorenz, N., & Dick, R. P. (2012).   Distribution of recently fixed photosynthate in a switchgrass plant-soil system. *Plant, Soil and Environment*, *58*(No. 6), 249–255. https://doi.org/10.17221/532/2011-PSE

Chen, S., Lin, S., Reinsch, T., Loges, R., Hasler, M., & Taube, F. (2016). Comparison of ingrowth core and sequential soil core methods for estimating belowground net primary production in grass–clover swards. *Grass and Forage Science*, *71*(3), 515–528. https://doi.org/10.1111/gfs.12214

Clément, C., Sleiderink, J., Svane, S. F., Smith, A. G., Diamantopoulos, E., Desbrøll, D. B., & Thorup-Kristensen, K. (2022). Comparing the deep root growth and water uptake of intermediate wheatgrass (Kernza®) to alfalfa. *Plant and Soil*. https://doi.org/10.1007/s11104-021-05248-6

Costa, N. R., Crusciol, C. A. C., Trivelin, P. C. O., Pariz, C. M., Costa, C., Castilhos, A. M., Souza, D. M., Bossolani, J. W., Andreotti, M., Meirelles, P. R. L., Moretti, L. G., & Mariano, E. (2021). Recovery of 15N fertilizer in intercropped maize, grass and legume and residual effect in black oat under tropical conditions. *Agriculture, Ecosystems & Environment*, *310*, 107226. https://doi.org/10.1016/j.agee.2020.107226

Cotrufo, M. F., Wallenstein, M. D., Boot, C. M., Denef, K., & Paul, E. (2013). The Microbial Efficiency-Matrix Stabilization (MEMS) framework integrates plant litter decomposition with soil organic matter stabilization: Do labile plant inputs form stable soil organic matter? *Global Change Biology*, *19*(4), 988–995. https://doi.org/10.1111/gcb.12113

Crews, T. E., Carton, W., & Olsson, L. (n.d.). Is the future of agriculture perennial? Imperatives and opportunities to reinvent agriculture by shifting from annual monocultures to perennial polycultures. *Global Sustainability*, 18.

Crews, T. E., Kemp, L., Bowden, J., & Murrell, E. (2022). How the Nitrogen Economy of a Perennial Cereal-Legume Intercrop Affects Productivity: Can Synchrony Be Achieved? *Frontiers in Sustainable Food Systems*, *6*, 755548. https://doi.org/10.3389/fsufs.2022.755548

Culman, S. W., Snapp, S. S., Ollenburger, M., Basso, B., & DeHaan, L. R. (2013). Soil

and Water Quality Rapidly Responds to the Perennial Grain Kernza Wheatgrass. *Agronomy Journal*, *105*(3), 735–744. https://doi.org/10.2134/agronj2012.0273

Dayrell, R. L. C., Arruda, A. J., Pierce, S., Negreiros, D., Meyer, P. B., Lambers, H., & Silveira, F. A. O. (2018). Ontogenetic shifts in plant ecological strategies. *Functional Ecology*, *32*(12), 2730–2741. https://doi.org/10.1111/1365-2435.13221

de Oliveira, G., Brunsell, N. A., Sutherlin, C. E., Crews, T. E., & DeHaan, L. R. (2018). Energy, water and carbon exchange over a perennial Kernza wheatgrass crop. *Agricultural and Forest Meteorology*, *249*, 120–137. https://doi.org/10.1016/j.agrformet.2017.11.022

Dijkstra, F. A., Zhu, B., & Cheng, W. (2021). Root effects on soil organic carbon: A double-edged sword. *New Phytologist*, *230*(1), 60–65. https://doi.org/10.1111/nph.17082

Dobbratz, M., Jungers, J. M., & Gutknecht, J. L. M. (2023). Seasonal Plant Nitrogen Use and Soil N pools in Intermediate Wheatgrass (Thinopyrum intermedium). *Agriculture*, *13*(2), Article 2. https://doi.org/10.3390/agriculture13020468

Dohleman, F. G., Heaton, E. A., Arundale, R. A., & Long, S. P. (2012). Seasonal dynamics of above- and below-ground biomass and nitrogen partitioning in Miscanthus × giganteus and Panicum virgatum across three growing seasons. *GCB Bioenergy*, *4*(5), 534–544. https://doi.org/10.1111/j.1757-1707.2011.01153.x

Duchene, O., Celette, F., Barreiro, A., Dimitrova Mårtensson, L.-M., Freschet, G. T., & David, C. (2020). Introducing Perennial Grain in Grain Crops Rotation: The Role of Rooting Pattern in Soil Quality Management. *Agronomy*, *10*(9), 1254. https://doi.org/10.3390/agronomy10091254

Fan, X. L., & Li, Y. K. (2001). Effect of drought stress and drought tolerance heredity on nitrogen efficiency of winter wheat. In W. J. Horst, M. K. Schenk, A. Bürkert, N. Claassen, H. Flessa, W. B. Frommer, H. Goldbach, H.-W. Olfs, V. Römheld, B. Sattelmacher, U. Schmidhalter, S. Schubert, N. v. Wirén, & L. Wittenmayer (Eds.), *Plant Nutrition: Food security and sustainability of agro-ecosystems through basic and applied research* (pp. 62–63). Springer Netherlands. https://doi.org/10.1007/0-306-47624-X_29

Fang, Y., Singh, B. P., Badgery, W., & He, X. (2016). In situ assessment of new carbon

and nitrogen assimilation and allocation in contrastingly managed dryland wheat crop–soil systems. *Agriculture, Ecosystems & Environment*, *235*, 80–90. https://doi.org/10.1016/j.agee.2016.10.010

Food and Agriculture Administration (FAO) (2021). *FAOSTAT - Statistics Division Food and Agriculture Organization of the United Nations*. Available online at: http://www.fao.org/faostat/en/#data/QC (accessed May 23, 2023).

Follett, R. F. (2001). Innovative 15n Microplot Research Techniques to Study Nitrogen Use Efficiency Under Different Ecosystems. *Communications in Soil Science and Plant Analysis*, *32*(7–8), 951–979. https://doi.org/10.1081/CSS-100104099

Fornara, D. A., Tilman, D., & Hobbie, S. E. (2009). Linkages between plant functional composition, fine root processes and potential soil N mineralization rates. *Journal of Ecology*, *97*(1), 48–56. https://doi.org/10.1111/j.1365-2745.2008.01453.x

Frick, H., Oberson, A., Frossard, E., & Bünemann, E. K. (2022). Leached nitrate under fertilised loamy soil originates mainly from mineralisation of soil organic N. *Agriculture, Ecosystems & Environment*, *338*, 108093. https://doi.org/10.1016/j.agee.2022.108093

Fujisaki, K., Chevallier, T., Chapuis-Lardy, L., Albrecht, A., Razafimbelo, T., Masse, D., Ndour, Y. B., & Chotte, J.-L. (2018). Soil carbon stock changes in tropical croplands are mainly driven by carbon inputs: A synthesis. *Agriculture, Ecosystems & Environment*, *259*, 147–158. https://doi.org/10.1016/j.agee.2017.12.008

Garnier, J., Billen, G., Tournebize, J., Barré, P., Mary, B., & Baudin, F. (2022). Storage or loss of soil active carbon in cropland soils: The effect of agricultural practices and hydrology. *Geoderma*, *407*, 115538. https://doi.org/10.1016/j.geoderma.2021.115538

Genet, H., Breda, N., & Dufrene, E. (2010). Age-related variation in carbon allocation at tree and stand scales in beech (Fagus sylvatica L.) and sessile oak (Quercus petraea (Matt.) Liebl.) using a chronosequence approach. *Tree Physiology*, *30*(2), 177–192. https://doi.org/10.1093/treephys/tpp105

Gill, R. A., & Jackson, R. B. (2000). Global patterns of root turnover for terrestrial ecosystems. *New Phytologist*, *147*(1), 13–31. https://doi.org/10.1046/j.1469-8137.2000.00681.x

Glover, D. E., Kielly, G. A., Jefferson, P. G., & Cohen, R. D. H. (2004). Agronomic characteristics and nutritive value of 11 grasses grown with irrigation on a saline soil in southwestern Saskatchewan. *Canadian Journal of Plant Science*, *84*(4), 1037–1050. https://doi.org/10.4141/P03-073

Guo, L. B., Wang, M., & Gifford, R. M. (2007). The change of soil carbon stocks and fine root dynamics after land use change from a native pasture to a pine plantation. *Plant and Soil*, *299*(1), 251–262. https://doi.org/10.1007/s11104-007-9381-7

Hafner, S., Unteregelsbacher, S., Seeber, E., Lena, B., Xu, X., Li, X., Guggenberger, G., Miehe, G., & Kuzyakov, Y. (2012). Effect of grazing on carbon stocks and assimilate partitioning in a Tibetan montane pasture revealed by 13CO2 pulse labeling. *Global Change Biology*, *18*(2), 528–538. https://doi.org/10.1111/j.1365-2486.2011.02557.x

Harris, R., Armstrong, R., & Wallace, A. (2015). *Recovery of 15N urea fertiliser applied to wheat under different management strategies, in the High Rainfall Zone of south western Victoria*. 4.

Heaton, E. A., Dohleman, F. G., & Long, S. P. (2009). Seasonal nitrogen dynamics of Miscanthus×giganteus and Panicum virgatum. *GCB Bioenergy*, *1*(4), 297–307. https://doi.org/10.1111/j.1757-1707.2009.01022.x

Heineck, G. C., Schlautman, B., Law, E. P., Ryan, M. R., Zimbric, J. W., Picasso, V., Stoltenberg, D. E., Sheaffer, C. C., & Jungers, J. M. (2022). Intermediate wheatgrass seed size and moisture dynamics inform grain harvest timing. *Crop Science*, *62*(1), 410–424. https://doi.org/10.1002/csc2.20662

Henneron, L., Cros, C., Picon-Cochard, C., Rahimian, V., & Fontaine, S. (2020). Plant economic strategies of grassland species control soil carbon dynamics through rhizodeposition. *Journal of Ecology*, *108*(2), 528–545. https://doi.org/10.1111/1365-2745.13276

Herman, D. J., Firestone, M. K., Nuccio, E., and Hodge, A.: Interactions between an arbuscular mycorrhizal fungus and a soil microbial community mediating litter decomposition, FEMS Microbiol Ecol, 80, 236–247, https://doi.org/10.1111/j.1574-6941.2011.01292.x, 2012.

Hothorn, T, F. Bretz and P. Westfall (2008). Simultaneous Inference in General Parametric Models. Biometrical Journal 50(3), 346--363.

Huddell, A., Ernfors, M., Crews, T., Vico, G., & Menge, D. N. L. (2023). Nitrate leaching losses and the fate of 15N fertilizer in perennial intermediate wheatgrass and annual wheat—A field study. *Science of The Total Environment*, *857*, 159255. https://doi.org/10.1016/j.scitotenv.2022.159255

Hussain, M. Z., Robertson, G. P., Basso, B., & Hamilton, S. K. (2020). Leaching losses of dissolved organic carbon and nitrogen from agricultural soils in the upper US Midwest. *Science of The Total Environment*, *734*, 139379. https://doi.org/10.1016/j.scitotenv.2020.139379

International Atomic Energy Agency. (2018). *Rice production guidelines: Best farm management practices and the role of isotopic techniques.* IAEA. https://www-pub.iaea.org/books/IAEABooks/12310/Rice-Production-Guidelines-Best-Farm-Management-Practices-and-the-Role-of-Isotopic-Techniques

Intergovernmental Panel On Climate Change (IPCC). (2022). *Climate Change and Land: IPCC Special Report on Climate Change, Desertification, Land Degradation, Sustainable Land Management, Food Security, and Greenhouse Gas Fluxes in Terrestrial Ecosystems* (1st ed.). Cambridge University Press. https://doi.org/10.1017/9781009157988

Jach-Smith, L. C., & Jackson, R. D. (2015). Nitrogen conservation decreases with fertilizer addition in two perennial grass cropping systems for bioenergy. *Agriculture, Ecosystems & Environment*, *204*, 62–71. https://doi.org/10.1016/j.agee.2015.02.006

Jaikumar, N. S., Snapp, S. S., & Sharkey, T. D. (2013). Life history and resource acquisition: Photosynthetic traits in selected accessions of three perennial cereal species compared with annual wheat and rye. *American Journal of Botany*, *100*(12), 2468–2477. https://doi.org/10.3732/ajb.1300122

Jaikumar, N. S., Snapp, S. S., & Sharkey, T. D. (2016). Older *Thinopyrum intermedium* (Poaceae) plants exhibit superior photosynthetic tolerance to cold stress and greater increases in two photosynthetic enzymes under freezing stress compared with young plants. *Journal of Experimental Botany*, *67*(15), 4743–4753. https://doi.org/10.1093/jxb/erw253

Janzen, H. H., van Groenigen, K. J., Powlson, D. S., Schwinghamer, T., & van

Groenigen, J. W. (2022). Photosynthetic limits on carbon sequestration in croplands. *Geoderma*, *416*, 115810. https://doi.org/10.1016/j.geoderma.2022.115810

Ji, Y., He, Y., Shao, J., Liu, H., Fu, Y., Chen, X., Chen, Y., Liu, R., Gao, J., Li, N., Zhou, G., Zhou, L., & Zhou, X. (2022). Dissolved Organic Carbon Flux Is Driven by Plant Traits More Than Climate across Global Forest Types. *Forests*, *13*(7), Article 7. https://doi.org/10.3390/f13071119

Johnson, D., Leake, J. R., Ostle, N., Ineson, P., & Read, D. J. (2002). In situ13CO2 pulse-labelling of upland grassland demonstrates a rapid pathway of carbon flux from arbuscular mycorrhizal mycelia to the soil. *New Phytologist*, *153*(2), 327–334. https://doi.org/10.1046/j.0028-646X.2001.00316.x

Jungers, J. M., DeHaan, L. H., Mulla, D. J., Sheaffer, C. C., & Wyse, D. L. (2019). Reduced nitrate leaching in a perennial grain crop compared to maize in the Upper Midwest, USA. *Agriculture, Ecosystems & Environment*, *272*, 63–73. https://doi.org/10.1016/j.agee.2018.11.007

Jungers, J. M., DeHaan, L. R., Betts, K. J., Sheaffer, C. C., & Wyse, D. L. (2017). Intermediate Wheatgrass Grain and Forage Yield Responses to Nitrogen Fertilization. *Agronomy Journal*, *109*(2), 462–472. https://doi.org/10.2134/agronj2016.07.0438

Jungers, J. M., Frahm, C. S., Tautges, N. E., Ehlke, N. J., Wells, M. S., Wyse, D. L., & Sheaffer, C. C. (2018). Growth, development, and biomass partitioning of the perennial grain crop Thinopyrum intermedium. *Annals of Applied Biology*, *172*(3), 346–354. https://doi.org/10.1111/aab.12425

Khasanova, A., James, J. J., & Drenovsky, R. E. (2013). Impacts of drought on plant water relations and nitrogen nutrition in dryland perennial grasses. *Plant and Soil*, *372*(1), 541–552. https://doi.org/10.1007/s11104-013-1747-4

Killingbeck, K. T. (1996). Nutrients in Senesced Leaves: Keys to the Search for Potential Resorption and Resorption Proficiency. *Ecology*, *77*(6), 1716–1727. https://doi.org/10.2307/2265777

Leifeld, J., Meyer, S., Budge, K., Sebastia, M. T., Zimmermann, M., & Fuhrer, J. (2015). Turnover of Grassland Roots in Mountain Ecosystems Revealed by Their Radiocarbon Signature: Role of Temperature and Management. *PLOS ONE*, *10*(3), e0119184. https://doi.org/10.1371/journal.pone.0119184

Lenth R (2023). _emmeans: Estimated Marginal Means, aka Least-Squares Means_. R package version 1.8.4-1, <https://CRAN.R-project.org/package=emmeans>.

Leroy, J., Ferchaud, F., Giauffret, C., Mary, B., Fingar, L., Mignot, E., Arnoult, S., Lenoir, S., Martin, D., Brancourt-Hulmel, M., & Zapater, M. (2022). Miscanthus Sinensis is as Efficient as Miscanthus × Giganteus for Nitrogen Recycling in spite of Smaller Nitrogen Fluxes. *BioEnergy Research*, *15*(2), 686–702. https://doi.org/10.1007/s12155-022-10408-2

Li, Y. S., & Redmann, R. E. (1992). Nitrogen Budget of Agropyron dasystachyum in Canadian Mixed Prairie. *The American Midland Naturalist*, *128*(1), 61–71. https://doi.org/10.2307/2426413

Li, Y. S., Redmann, R. E., & van Kessel, C. (1992). Nitrogen Budget and 15N Translocation in a Perennial Wheatgrass. *Functional Ecology*, *6*(2), 221–225. https://doi.org/10.2307/2389758

Liang, C., Jesus, E. da C., Duncan, D. S., Jackson, R. D., Tiedje, J. M., & Balser, T. C. (2012). Soil microbial communities under model biofuel cropping systems in southern Wisconsin, USA: Impact of crop species and soil properties. *Applied Soil Ecology*, *54*, 24–31. https://doi.org/10.1016/j.apsoil.2011.11.015

Liang, C., Schimel, J. P., & Jastrow, J. D. (2017). The importance of anabolism in microbial control over soil carbon storage. *Nature Microbiology*, *2*(8), Article 8. https://doi.org/10.1038/nmicrobiol.2017.105

Liang, Y., Cossani, C. M., Sadras, V. O., Yang, Q., & Wang, Z. (2022). The Interaction Between Nitrogen Supply and Light Quality Modulates Plant Growth and Resource Allocation. *Frontiers in Plant Science*, *13*. https://www.frontiersin.org/articles/10.3389/fpls.2022.864090

Luo, Y., Wang, X., Cui, M., Wang, J., & Gao, Y. (2021). Mowing increases fine root production and root turnover in an artificially restored Songnen grassland. *Plant and Soil*, *465*(1), 549–561. https://doi.org/10.1007/s11104-021-05017-5

Ma, Z., Bork, E. W., Li, J., Chen, G., & Chang, S. X. (2021). Photosynthetic carbon allocation to live roots increases the year following high intensity defoliation across two ecosites in a temperate mixed grassland. *Agriculture, Ecosystems & Environment*, *316*, 107450. https://doi.org/10.1016/j.agee.2021.107450

Mahler, R. L., Koehler, F. E., & Lutcher, L. K. (1994). Nitrogen Source, Timing of Application, and Placement: Effects on Winter Wheat Production. *Agronomy Journal*, *86*(4), 637–642. https://doi.org/10.2134/agronj1994.00021962008600040010x

Mathew, I., Shimelis, H., Mutema, M., Minasny, B., & Chaplot, V. (2020). Crops for increasing soil organic carbon stocks – A global meta analysis. *Geoderma*, *367*, 114230. https://doi.org/10.1016/j.geoderma.2020.114230

McKenna, T. P., Crews, T. E., Kemp, L., & Sikes, B. A. (2020). Community structure of soil fungi in a novel perennial crop monoculture, annual agriculture, and native prairie reconstruction. *PLOS ONE*, *15*(1), e0228202. https://doi.org/10.1371/journal.pone.0228202

Molotoks, A., Stehfest, E., Doelman, J., Albanito, F., Fitton, N., Dawson, T. P., & Smith, P. (2018). Global projections of future cropland expansion to 2050 and direct impacts on biodiversity and carbon storage. *Global Change Biology*, *24*(12), 5895–5908. https://doi.org/10.1111/gcb.14459

Morales Ruiz, D. E., Aryal, D. R., Pinto Ruiz, R., Guevara Hernández, F., Casanova Lugo, F., & Villanueva López, G. (2021). Carbon contents and fine root production in tropical silvopastoral systems. *Land Degradation & Development*, *32*(2), 738–756. https://doi.org/10.1002/ldr.3761

Mou, X. M., Li, X. G., Zhao, N., Yu, Y. W., & Kuzyakov, Y. (2018). Tibetan sedges sequester more carbon belowground than grasses: A 13C labeling study. *Plant and Soil*, *426*(1–2), 287–298. https://doi.org/10.1007/s11104-018-3634-5

Naveed, M., Brown, L. K., Raffan, A. C., George, T. S., Bengough, A. G., Roose, T., Sinclair, I., Koebernick, N., Cooper, L., Hackett, C. A., & Hallett, P. D. (2017). Plant exudates may stabilize or weaken soil depending on species, origin and time. *European Journal of Soil Science*, *68*(6), 806–816. https://doi.org/10.1111/ejss.12487

Pastor-Pastor, A., González-Paleo, L., Vilela, A., & Ravetta, D. (2015). Age-related changes in nitrogen resorption and use efficiency in the perennial new crop Physaria mendocina (Brassicaceae). *Industrial Crops and Products*, *65*, 227–232. https://doi.org/10.1016/j.indcrop.2014.11.044

Pausch, J., Kramer, S., Scharroba, A., Scheunemann, N., Butenschoen, O., Kandeler, E.,

Marhan, S., Riederer, M., Scheu, S., Kuzyakov, Y., & Ruess, L. (2016). Small but active – pool size does not matter for carbon incorporation in below-ground food webs. *Functional Ecology*, *30*(3), 479–489. https://doi.org/10.1111/1365-2435.12512

Peixoto, L., Elsgaard, L., Rasmussen, J., Kuzyakov, Y., Banfield, C. C., Dippold, M. A., & Olesen, J. E. (2020). Decreased rhizodeposition, but increased microbial carbon stabilization with soil depth down to 3.6 m. *Soil Biology and Biochemistry*, *150*, 108008. https://doi.org/10.1016/j.soilbio.2020.108008

Pinheiro J, Bates D, R Core Team (2022). _nlme: Linear and Nonlinear Mixed Effects Models_. R package version 3.1-160, <https://CRAN.R-project.org/package=nlme>.

Pinto, P., De Haan, L., & Picasso, V. (2021). Post-Harvest Management Practices Impact on Light Penetration and Kernza Intermediate Wheatgrass Yield Components. *Agronomy*, *11*(3), Article 3. https://doi.org/10.3390/agronomy11030442

Poffenbarger, H., Castellano, M., Egli, D., Jaconi, A., & Moore, V. (n.d.). Contributions of plant breeding to soil carbon storage: Retrospect and prospects. *Crop Science*, *n/a*(n/a). https://doi.org/10.1002/csc2.20920

Poorter, H., Niklas, K. J., Reich, P. B., Oleksyn, J., Poot, P., & Mommer, L. (2012). Biomass allocation to leaves, stems and roots: Meta-analyses of interspecific variation and environmental control. *New Phytologist*, *193*(1), 30–50. https://doi.org/10.1111/j.1469-8137.2011.03952.x

Pugliese, J. Y., Culman, S. W., & Sprunger, C. D. (2019). Harvesting forage of the perennial grain crop kernza (Thinopyrum intermedium) increases root biomass and soil nitrogen cycling. *Plant and Soil*, *437*(1), 241–254. https://doi.org/10.1007/s11104-019-03974-6

Quan, Z., Li, S., Zhu, F., Zhang, L., He, J., Wei, W., & Fang, Y. (2018). Fates of 15N-labeled fertilizer in a black soil-maize system and the response to straw incorporation in Northeast China. *Journal of Soils and Sediments*, *18*(4), 1441–1452. https://doi.org/10.1007/s11368-017-1857-3

Quan, Z., Zhang, X., & Fang, Y. (2021). The undefined N source might be overestimated by 15N tracer trials. *Global Change Biology*, *27*(3), 467–468. https://doi.org/10.1111/gcb.15371

R Core Team (2022). R: A language and environment for statistical computing. R Foundation for Statistical Computing, Vienna, Austria. URL https://www.R-project.org/.

Rakkar, M., Jungers, J. M., Sheaffer, C., Bergquist, G., Grossman, J., Li, F., & Gutknecht, J. L. (2023). Soil health improvements from using a novel perennial grain during the transition to organic production. *Agriculture, Ecosystems & Environment*, *341*, 108164. https://doi.org/10.1016/j.agee.2022.108164

Readman, R. J., Beckwith, C. P., & Kettlewell, P. S. (2002). Effects of spray application of urea fertilizer at stem extension on winter wheat: N recovery and nitrate leaching. *The Journal of Agricultural Science*, *139*(1), 11–25. https://doi.org/10.1017/S0021859602002289

Reilly, E. C., Gutknecht, J. L., Sheaffer, C. C., & Jungers, J. M. (2022). Reductions in soil water nitrate beneath a perennial grain crop compared to an annual crop rotation on sandy soil. *Frontiers in Sustainable Food Systems*, *6*. https://www.frontiersin.org/articles/10.3389/fsufs.2022.996586

Resources Conservation Service, United States Department of Agriculture. 2023. Official Soil Series Descriptions. Available online. Accessed March 03, 2023.

Ribaudo, M., Hansen, L., Livingston, M. J., Mosheim, R., Williamson, J., & Delgado, J. (2011). Nitrogen in Agricultural Systems: Implications for Conservation Policy. *SSRN Electronic Journal*. https://doi.org/10.2139/ssrn.2115532

Robertson, G. P., Hamilton, S. K., Barham, B. L., Dale, B. E., Izaurralde, R. C., Jackson, R. D., Landis, D. A., Swinton, S. M., Thelen, K. D., & Tiedje, J. M. (2017). Cellulosic biofuel contributions to a sustainable energy future: Choices and outcomes. *Science*, *356*(6345), eaal2324. https://doi.org/10.1126/science.aal2324

Roley, S. S., Ulbrich, T. C., & Robertson, G. P. (2020). Nitrogen Fixation and Resorption Efficiency Differences Among Twelve Upland and Lowland Switchgrass Cultivars. *Phytobiomes Journal*, PBIOMES-11-19-0. https://doi.org/10.1094/PBIOMES-11-19-0064-FI

Sainju, U. M., Allen, B. L., Lenssen, A. W., & Ghimire, R. P. (2017). Root biomass, root/shoot ratio, and soil water content under perennial grasses with different nitrogen rates. *Field Crops Research*, *210*, 183–191. https://doi.org/10.1016/j.fcr.2017.05.029

Sainju, U. M., Allen, B. L., Lenssen, A. W., & Mikha, M. (2017). Root and soil total carbon and nitrogen under bioenergy perennial grasses with various nitrogen rates. *Biomass and Bioenergy*, *107*, 326–334. https://doi.org/10.1016/j.biombioe.2017.10.021

Sakiroglu, M., Dong, C., Hall, M. B., Jungers, J., & Picasso, V. (2020). How does nitrogen and forage harvest affect belowground biomass and nonstructural carbohydrates in dual-use Kernza intermediate wheatgrass? *Crop Science*, *60*(5), 2562–2573. https://doi.org/10.1002/csc2.20239

Sanderman, J., Hengl, T., & Fiske, G. J. (2017). Soil carbon debt of 12,000 years of human land use. *Proceedings of the National Academy of Sciences*, *114*(36), 9575–9580. https://doi.org/10.1073/pnas.1706103114

Schielzeth, H., Dingemanse, N. J., Nakagawa, S., Westneat, D. F., Allegue, H., Teplitsky, C., Réale, D., Dochtermann, N. A., Garamszegi, L. Z., & Araya-Ajoy, Y. G. (2020). Robustness of linear mixed-effects models to violations of distributional assumptions. *Methods in Ecology and Evolution*, *11*(9), 1141–1152. https://doi.org/10.1111/2041-210X.13434

See, C. R., Keller, A. B., Hobbie, S. E., Kennedy, P. G., Weber, P. K., & Pett-Ridge, J. (2022). Hyphae move matter and microbes to mineral microsites: Integrating the hyphosphere into conceptual models of soil organic matter stabilization. *Global Change Biology*, *28*(8), 2527–2540. https://doi.org/10.1111/gcb.16073

Smucker, A. J. M., McBurney, S. L., & Srivastava, A. K. (1982). Quantitative Separation of Roots from Compacted Soil Profiles by the Hydropneumatic Elutriation System1. *Agronomy Journal*, *74*(3), 500–503. https://doi.org/10.2134/agronj1982.00021962007400030023x

Soares, M., & Rousk, J. (2019). Microbial growth and carbon use efficiency in soil: Links to fungal-bacterial dominance, SOC-quality and stoichiometry. *Soil Biology and Biochemistry*, *131*, 195–205. https://doi.org/10.1016/j.soilbio.2019.01.010

Spackman, J. A., & Fernandez, F. G. (2020). Microplot Design and Plant and Soil Sample Preparation for ^{15}Nitrogen Analysis. *Journal of Visualized Experiments*, *159*, 61191. https://doi.org/10.3791/61191

Sprunger, C. D., Culman, S. W., Peralta, A. L., DuPont, S. T., Lennon, J. T., & Snapp, S.

S. (2019). Perennial grain crop roots and nitrogen management shape soil food webs and soil carbon dynamics. *Soil Biology and Biochemistry*, *137*, 107573. https://doi.org/10.1016/j.soilbio.2019.107573

Sprunger, C. D., Culman, S. W., Robertson, G. P., & Snapp, S. S. (2018a). Perennial grain on a Midwest Alfisol shows no sign of early soil carbon gain. *Renewable Agriculture and Food Systems*, *33*(4), 360–372. https://doi.org/10.1017/S1742170517000138

Sprunger, C. D., Culman, S. W., Robertson, G. P., & Snapp, S. S. (2018b). How Does Nitrogen and Perenniality Influence Belowground Biomass and Nitrogen Use Efficiency in Small Grain Cereals? *Crop Science*, *58*(5), 2110–2120. https://doi.org/10.2135/cropsci2018.02.0123

Sprunger, C. D., Oates, L. G., Jackson, R. D., & Robertson, G. P. (2017). Plant community composition influences fine root production and biomass allocation in perennial bioenergy cropping systems of the upper Midwest, USA. *Biomass and Bioenergy*, *105*, 248–258. https://doi.org/10.1016/j.biombioe.2017.07.007

Steingrobe, B., Schmid, H., & Claassen, N. (2001). The use of the ingrowth core method for measuring root production of arable crops – influence of soil and root disturbance during installation of the bags on root ingrowth into the cores. *European Journal of Agronomy*, *15*(2), 143–151. https://doi.org/10.1016/S1161-0301(01)00100-9

Steingrobe, B., Schmid, H., Gutser, R., & Claassen, N. (2001). Root production and root mortality of winter wheat grown on sandy and loamy soils in different farming systems. *Biology and Fertility of Soils*, *33*(4), 331–339. https://doi.org/10.1007/s003740000334

Stevens, W. B., Hoeft, R. G., & Mulvaney, R. L. (2005). Fate of Nitrogen-15 in a Long-Term Nitrogen Rate Study: II. Nitrogen Uptake Efficiency. *Agronomy Journal*, *97*(4), 1046–1053. https://doi.org/10.2134/agronj2003.0313

Stout, W. L., & Weaver, S. R. (2001). Effect of early season nitrogen on nitrogen fixation and fertilizer-use efficiency in grass-clover pastures. *Communications in Soil Science and Plant Analysis*, *32*(15–16), 2425–2437. https://doi.org/10.1081/CSS-120000382

Sun, Z., Wu, S., Zhang, Y., Meng, F., Zhu, B., & Chen, Q. (2019). Effects of nitrogen

fertilization on pot-grown wheat photosynthate partitioning within intensively farmed soil determined by 13C pulse-labeling. *Journal of Plant Nutrition and Soil Science*, *182*(6), 896–907. https://doi.org/10.1002/jpln.201800603

Tautges, N. E., Jungers, J. M., DeHaan, L. R., Wyse, D. L., & Sheaffer, C. C. (2018). Maintaining grain yields of the perennial cereal intermediate wheatgrass in monoculture *v.* bi-culture with alfalfa in the Upper Midwestern USA. *The Journal of Agricultural Science*, *156*(6), 758–773. https://doi.org/10.1017/S0021859618000680

Tejera, M., Boersma, N. N., Archontoulis, S. V., Miguez, F. E., VanLoocke, A., & Heaton, E. A. (2022). Photosynthetic decline in aging perennial grass is not fully explained by leaf nitrogen. *Journal of Experimental Botany*, *73*(22), 7582–7595. https://doi.org/10.1093/jxb/erac382

Tejera, M., Boersma, N., Vanloocke, A., Archontoulis, S., Dixon, P., Miguez, F., & Heaton, E. (2019). Multi-year and Multi-site Establishment of the Perennial Biomass Crop Miscanthus × giganteus Using a Staggered Start Design to Elucidate N Response. *BioEnergy Research*, *12*(3), 471–483. https://doi.org/10.1007/s12155-019-09985-6

Tejera, M. D., Miguez, F. E., & Heaton, E. A. (2021). The older plant gets the sun: Age-related changes in Miscanthus × giganteus phenology. *GCB Bioenergy*, *13*(1), 4–20. https://doi.org/10.1111/gcbb.12745

Thilakarathna, S. K., Hernandez-Ramirez, G., Puurveen, D., Kryzanowski, L., Lohstraeter, G., Powers, L.-A., Quan, N., & Tenuta, M. (2020). Nitrous oxide emissions and nitrogen use efficiency in wheat: Nitrogen fertilization timing and formulation, soil nitrogen, and weather effects. *Soil Science Society of America Journal*, *84*(6), 1910–1927. https://doi.org/10.1002/saj2.20145

Tiemann, L. K., & Grandy, A. S. (2015). Mechanisms of soil carbon accrual and storage in bioenergy cropping systems. *GCB Bioenergy*, *7*(2), 161–174. https://doi.org/10.1111/gcbb.12126

Vadas, P. A., Barnett, K. H., & Undersander, D. J. (2008). Economics and Energy of Ethanol Production from Alfalfa, Corn, and Switchgrass in the Upper Midwest, USA. *BioEnergy Research*, *1*(1), 44–55. https://doi.org/10.1007/s12155-008-9002-1

Vangeli, S., Posse, G., Beget, M. E., Otero Estrada, E., Valdettaro, R. A., Oricchio, P.,

Kandus, M., & Di Bella, C. M. (2022). Effects of fertilizer type on nitrous oxide emission and ammonia volatilization in wheat and maize crops. *Soil Use and Management*, *38*(4), 1519–1531. https://doi.org/10.1111/sum.12788

Vergutz, L., Manzoni, S., Porporato, A., Novais, R. F., & Jackson, R. B. (2012). Global resorption efficiencies and concentrations of carbon and nutrients in leaves of terrestrial plants. *Ecological Monographs*, *82*(2), 205–220. https://doi.org/10.1890/11-0416.1

Villarino, S. H., Pinto, P., Jackson, R. B., & Piñeiro, G. (2021). Plant rhizodeposition: A key factor for soil organic matter formation in stable fractions. *Science Advances*, *7*(16), eabd3176. https://doi.org/10.1126/sciadv.abd3176

von Haden, A. C., & Dornbush, M. E. (2014). Patterns of root decomposition in response to soil moisture best explain high soil organic carbon heterogeneity within a mesic, restored prairie. *Agriculture, Ecosystems & Environment*, *185*, 188–196. https://doi.org/10.1016/j.agee.2013.12.027

Wang, M., Bezemer, T. M., van der Putten, W. H., Brinkman, E. P., & Biere, A. (2018). Plant responses to variable timing of aboveground clipping and belowground herbivory depend on plant age. *Journal of Plant Ecology*, *11*(5), 696–708. https://doi.org/10.1093/jpe/rtx043

Wayman, S., Bowden, R. D., & Mitchell, R. B. (2014). Seasonal Changes in Shoot and Root Nitrogen Distribution in Switchgrass (Panicum virgatum). *BioEnergy Research*, *7*(1), 243–252. https://doi.org/10.1007/s12155-013-9365-9

Wei, J., Liu, W., Wan, H., Cheng, J., & Li, W. (2016). Differential allocation of carbon in fenced and clipped grasslands: A 13C tracer study in the semiarid Chinese Loess Plateau. *Plant and Soil*, *406*(1), 251–263. https://doi.org/10.1007/s11104-016-2879-0

Wei, L., Yao, P., Jing, G., Ye, X., & Cheng, J. (2019). Root production, mortality and turnover in soil profiles as affected by clipping in a temperate grassland on the Loess Plateau. *Journal of Plant Ecology*, *12*(6), 1059–1072. https://doi.org/10.1093/jpe/rtz039

West, T. O., Brandt, C. C., Baskaran, L. M., Hellwinckel, C. M., Mueller, R., Bernacchi, C. J., Bandaru, V., Yang, B., Wilson, B. S., Marland, G., Nelson, R. G., Ugarte, D. G. D. L. T., & Post, W. M. (2010). Cropland carbon fluxes in the United States:

Increasing geospatial resolution of inventory-based carbon accounting. *Ecological Applications*, *20*(4), 1074–1086. https://doi.org/10.1890/08-2352.1

Whitaker, J., Ostle, N., Nottingham, A. T., Ccahuana, A., Salinas, N., Bardgett, R. D., Meir, P., & McNamara, N. P. (2014). Microbial community composition explains soil respiration responses to changing carbon inputs along an Andes-to-Amazon elevation gradient. *Journal of Ecology*, *102*(4), 1058–1071. https://doi.org/10.1111/1365-2745.12247

Wood, J. H. A., Vitti, A. C., Risely, F.-A., Otto, R, Heitor, C. (2020). Long-term N fertilization reduces uptake of N from fertilizer and increases the uptake of N from soil. *Scientific Reports (Nature Publisher Group)*, *10*(1). http://dx.doi.org/10.1038/s41598-020-75971-0

Wu, Y., Tan, H., Deng, Y., Wu, J., Xu, X., Wang, Y., Tang, Y., Higashi, T., & Cui, X. (2010). Partitioning pattern of carbon flux in a Kobresia grassland on the Qinghai-Tibetan Plateau revealed by field 13C pulse-labeling. *Global Change Biology*, *16*(8), 2322–2333. https://doi.org/10.1111/j.1365-2486.2009.02069.x

Xia, J., Yuan, W., Wang, Y.-P., & Zhang, Q. (2017). Adaptive Carbon Allocation by Plants Enhances the Terrestrial Carbon Sink. *Scientific Reports*, *7*(1), Article 1. https://doi.org/10.1038/s41598-017-03574-3

Xu, H., Zhu, B., Wei, X., Yu, M., & Cheng, X. (2021). Root functional traits mediate rhizosphere soil carbon stability in a subtropical forest. *Soil Biology and Biochemistry*, *162*, 108431. https://doi.org/10.1016/j.soilbio.2021.108431

Yang, Y., Liu, Q., & Wang, G. X. (2011). Physiological behaviors of Acer mono under drought and low light. *Russian Journal of Plant Physiology*, *58*(3), 531–537. https://doi.org/10.1134/S1021443711030228

Ye, C., & Hall, S. J. (2020). Mechanisms underlying limited soil carbon gains in perennial and cover-cropped bioenergy systems revealed by stable isotopes. *GCB Bioenergy*, *12*(1), 101–117. https://doi.org/10.1111/gcbb.12657

Yu, X., Keitel, C., Zhang, Y., Wangeci, A. N., & Dijkstra, F. A. (2022). Global meta-analysis of nitrogen fertilizer use efficiency in rice, wheat and maize. *Agriculture, Ecosystems & Environment*, *338*, 108089. https://doi.org/10.1016/j.agee.2022.108089

Zadoks, J. C., Chang, T. T., & Konzak, C. F. (1974). A decimal code for the growth stages

of cereals. Weed research, 14(6), 415-421.

Zan, C. S., Fyles, J. W., Girouard, P., & Samson, R. A. (2001). Carbon sequestration in perennial bioenergy, annual corn and uncultivated systems in southern Quebec. *Agriculture, Ecosystems & Environment*, *86*(2), 135–144. https://doi.org/10.1016/S0167-8809(00)00273-5

Zelles, L. (1999). Fatty acid patterns of phospholipids and lipopolysaccharides in the characterisation of microbial communities in soil: A review. *Biology and Fertility of Soils*, *29*(2), 111–129. https://doi.org/10.1007/s003740050533

Zhang, H., Goll, D. S., Wang, Y.-P., Ciais, P., Wieder, W. R., Abramoff, R., Huang, Y., Guenet, B., Prescher, A.-K., Rossel, R. A. V., Barré, P., Chenu, C., Zhou, G., & Tang, X. (2020). Microbial dynamics and soil physicochemical properties explain large-scale variations in soil organic carbon. *Global Change Biology*, *26*(4), 2668–2685. https://doi.org/10.1111/gcb.14994

Zhu, X., Jackson, R. D., DeLucia, E. H., Tiedje, J. M., & Liang, C. (2020). The soil microbial carbon pump: From conceptual insights to empirical assessments. *Global Change Biology*, *26*(11), 6032–6039. https://doi.org/10.1111/gcb.15319

Appendix 1

Additional Details on Sampling Timeline and Methods Used in Chapter 1

Supplemental figure 1.1. Images documenting the methods used to install root ingrowth cores *in situ*. Clockwise from top left, the images depict: the guide system used to extract soil cores at an angle of 45-degrees to the soil surface; the pre-weighed root-free sand:soil mixture used to fill each ingrowth core once inserted into the cored hole; the extraction of root ingrowth cores from the surrounding soil using a cylinder and shovel; an ingrowth core incubating *in situ* for the duration of the ingrowth period.

Supplemental figure 1.2. Timeline of sequential core and root ingrowth core installation and extraction.

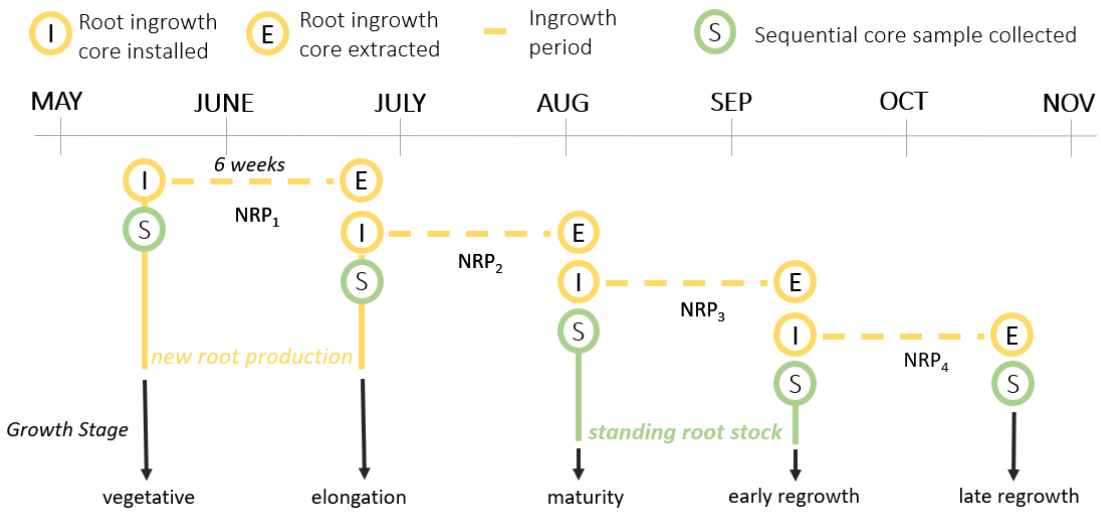

Appendix 2

Detailed Design of ^{13}C Labelling System Used in Chapter 2

Chamber Structure

The materials used to construct the chamber are listed in supplemental table 2.1. To construct the chambers, four clear Plexiglas panels (1/4" thick x 39.37" x 39.37") were attached to one another at 90-degree angles using aluminum angle (supplemental figure 2.1, supplemental figure 2.2). The aluminum angle was glued to the edge of each panel with a clear high-strength construction adhesive and secured with nine equally spaced machine screws/nuts. On two opposing panels, two furniture handles were screwed onto the panel walls approximately 10" (0.25 m) from the bottom panel edge (supplemental figure 2.1, supplemental figure 2.2). Construction adhesive was used to attach a fifth Plexiglas panel (1/4" thick) to one open edge of the four-walled panel structure, creating a cube-shaped chamber with one open side (supplemental figure 2.1, supplemental figure 2.2). A thin layer of clear silicone caulk was applied to all junctures between the aluminum angle, furniture handles and chamber panel edges.

Dehumidifier / Air Cooling and Label Application Systems

An original closed-system copper coil dehumidifier and air-cooling system was designed to control humidity and temperature inside the chamber (supplemental figure 2.1, supplemental figure 2.2, supplemental figure 2.3). The dehumidifier and cooling system consisted of 1) two 50 ft sections of soft copper tubing, 2) coil holders, 3) clear or opaque plastic tubing, 4) a submersible water pump, and 5) a cold-water reservoir (i.e., a cooler). The soft refrigerator tubing was hand-wrapped into 5" diameter coils, leaving approximately 1 ft. of copper tubing uncoiled on either end of the to form two straight "arms." Above the furniture handles, two 3/8" holes were drilled to center the coils around the center of the wall panel. One washer was centered and glued in place around this hole on both the outside- and inside-facing edge of the panel. A steel spacer was then inserted through the hole and washers and secured in place using construction adhesive. Together, the washers and steel spacer form a "coil holder" into which the arm of the copper coil dehumidifier can be inserted.

Once inserted into the coil holders, a piece of clear tubing was used to connect one coil arm on the first coil to the water pump (supplemental figure 2.1, supplemental figure 2.3). Another section of clear tubing was used to connect the exposed coil arm on the first coil to the coil arm on the second coil on the opposite panel. One end of a section of clear tubing was then attached to the exposed coil arm on the second coil, with the other end of the tube placed in the cold-water reservoir. When the tubing is installed correctly, the water pump will continuously circulate cold water through the tubes and copper coils.

This allows the circulating water to absorb heat from the chamber atmosphere through the copper coil, cooling the copper coil and surrounding air, which causes moisture from the inside the chamber to condense onto the copper coil surface. The circulating water will then be deposited back into the cold-water reservoir, where the absorbed heat is removed by the melting of ice. The cooled water is then recirculated throughout the copper coil system. The water pump is powered by a portable power station that has 120 V outlets.

On each of the adjacent wall panels to the copper coils, a fan and beaker shelf were installed for air circulation and label-application purposes (supplemental figure 2.1, supplemental figure 2.2). A longitudinal fan was centered around the middle of the panel and attached. Beneath the fan a plastic shelf was fixed to each wall. The shelf was large enough to hold four 150 mL beakers, which each could be filled with an isotopically enriched solid substrate. The solid substrate used in this experiment was ^{13}C-enriched sodium bicarbonate, which can be reacted with acetic acid to release the ^{13}C tracer as ^{13}C-CO_2. Four acid injection ports were therefore installed above each beaker position by drilling a 45-degree angle hole and inserting a section of chemical-resistant plastic tubing that extended into each of the beakers.

As with the chamber structure, all junctures between hardware, drilled holes, etc. were sealed with silicone caulk.

Chamber Atmosphere Sensor Unit

A microcontroller-based temperature, humidity and CO_2 sensor unit was designed and built to monitor the chamber atmosphere. The microcontroller was the Arduino Nano Every (ATMega4809 processor), the CO_2 sensor was the K30 10,000 ppm CO_2 Sensor (accuracy: +/- 30 ppm) and the temperature and relative humidity sensor was the DHT22 (accuracy: +/- 2% RH, +/- 0.2 C). An LCD display was wired to the microcontroller to allow for real-time viewing of CO_2 concentrations, temperature and relative humidity within the chamber. The wiring diagram can be found in supplemental figure 2.4, and the microcontroller operating code can be found below.

*Environmental Sensor Unit – Operation Code**
**This code is compatible with the Arduino IDE programming software*

```
// Code to Operate Environmental Sensing Unit
// Stella Woeltjen

// Some code borrowed from ladyada (public domain): sketch for various DHT humidity/temperature sensors

// REQUIRES the following Arduino libraries:
// - DHT Sensor Library: https://github.com/adafruit/DHT-sensor-library
```

```
// - Adafruit Unified Sensor Lib: https://github.com/adafruit/Adafruit_Sensor

#include "DHT.h"
#include "kSeries.h" //include kSeries Library
#include <LiquidCrystal.h>

#define DHTPIN 11     // Digital pin connected to the DHT sensor
#define DHTTYPE DHT22   // DHT 22  (AM2302), AM2321
//#define DHTTYPE DHT21   // DHT 21 (AM2301)

DHT dht(DHTPIN, DHTTYPE);
kSeries K_30(12,13); //Initialize a kSeries Sensor with pin 12 as Rx and 13 as Tx

// define pins connected to LCD display (pin # in blue)
const int rs = 5, en = 6, d4 = 7, d5 = 8, d6 = 9, d7 = 10;
LiquidCrystal lcd(rs, en, d4, d5, d6, d7);

void setup() {
  Serial.begin(9600);
  Serial.println(F("DHTxx test!"));

  dht.begin();
  lcd.begin(16, 2);
  lcd.print("Let's research!");
}

void loop() {
  // Reading temperature or humidity takes about 250 milliseconds
  // Sensor readings may also be up to 2 seconds 'old' (it's a very slow sensor)
 float h = dht.readHumidity();
  // Read temperature as Fahrenheit (isFahrenheit = true)
  float f = dht.readTemperature(true);

  // Check if any reads failed and exit early (to try again).
  if (isnan(h) || isnan(f)) {
    Serial.println(F("Failed to read from DHT sensor!"));
    return;
  }

//Read CO2 concentration from K30 sensor
double co2 = K_30.getCO2('p'); //returns co2 value in ppm ('p') or percent ('%')

  lcd.setCursor(0, 0);
   lcd.print("C: "); //print "CO2:" to LCD screen
```

```
  lcd.print(co2); //print CO2 in ppm to LCD screen
  lcd.print(" T:"); //print “T:” to LCD screen
   lcd.print(f); //print temperature in degrees F to LCD screen
  lcd.setCursor(0, 1); //add a space to previously printed line
   lcd.print("H: "); // print “H:” to LCD screen
   lcd.print(h); // print relative humidity (%) to LCD screen

 Serial.print("Co2 ppm = "); // print the same values as described above to serial display
  Serial.print(co2); //print value
 Serial.print(F(" Humidity: "));
  Serial.print(h);
 Serial.print(F("%  Temperature: "));
  Serial.print(f);
  Serial.println(F("°F "));

   // Take and print new measurement every 5 seconds.
  delay(5000); // enter time between measurements, in milliseconds
}
```

Testing the Chamber Design

The chamber atmosphere sensing unit and temperature- and relative humidity-logging Thermochrons were used to verify the dehumidifier and air-cooling system was capable of keeping chamber conditions consistent with ambient air. Field testing on this chamber design and cooling system were conducted throughout the summer of 2019. The copper coil dehumidifier and cooling system was shown to keep mean interior temperature and relative humidity within 12 – 24% and 28 – 40% of ambient conditions.

Supplemental table 2.1 Materials used to construct labelling chamber, air dehumidifier / cooling system and chamber atmosphere sensing unit.

Chamber component	Item	Quantity (per chamber)
Chamber structure	Polycarbonate panels (1/4” thick, 1m x 1 m)	5
	Furniture handles	4
	Aluminum Angle (1/8” x ¾” x 36”)	4
	#12-24 Steel Machine Screw and Nut, Round (1" long)	72
	Construction adhesive	As needed
	Silicone sealant	As needed
Dehumidifier / air cooler and label application system	Soft copper refrigeration tubing (3/8” OD, 50 ft. long)	2
	Flat steel washer (3/8" ID x 1" OD)	8
	Round steel spacer (3/8” ID x 2” long)	4
	Tygon tubing (3/8 ID, 8 ft. long)	As needed
	Crossflow fan (USB laptop cooling fan, 12” x 3” x 2.5”)	2
	400 GPH Submersible outdoor fountain water pump	1
	Cooler (48 qt)	1
	Portable power station (Stanley Fatmax or Yeti150)	1
	Tygon 2375 Ultra Chemical Resistant Tubing (1/8" ID x 1/4" OD x 1/16" Wall)	8 in. / port
	20 ml glass syringe	1
Chamber Atmosphere Sensing Unit	Arduino Nano Every, with headers	1
	K30 CO2 sensor module (10,000 ppm)	1
	DHT22 Temp/Humidity sensor	1
	16 x 2 lcd display (black on green, 3.3V)	1
	Trimpot 10K resistor	1
	22 awg solid hook-up wire	As needed
	4 x AA Battery Holder with On/Off Switch and 0.1” header pins	1
	6” Female to female jumper wires (20 ct.)	1
	Straight breakaway headers – 40 pins	1
	Heat shrink tubing	As needed
	Small plastic Tupperware (or other waterproof container)	1

Supplemental figure 2.1 Isotope labelling system: 1) Plexiglas chamber, 2) environmental sensing unit, 3) closed system copper coil dehumidifier and air cooler, 4) cold fluid reservoir, 5) longitudinal fans, 6) isotopically enriched substrate. Not pictured: power station (behind cooler) and water pump (inside cooler)

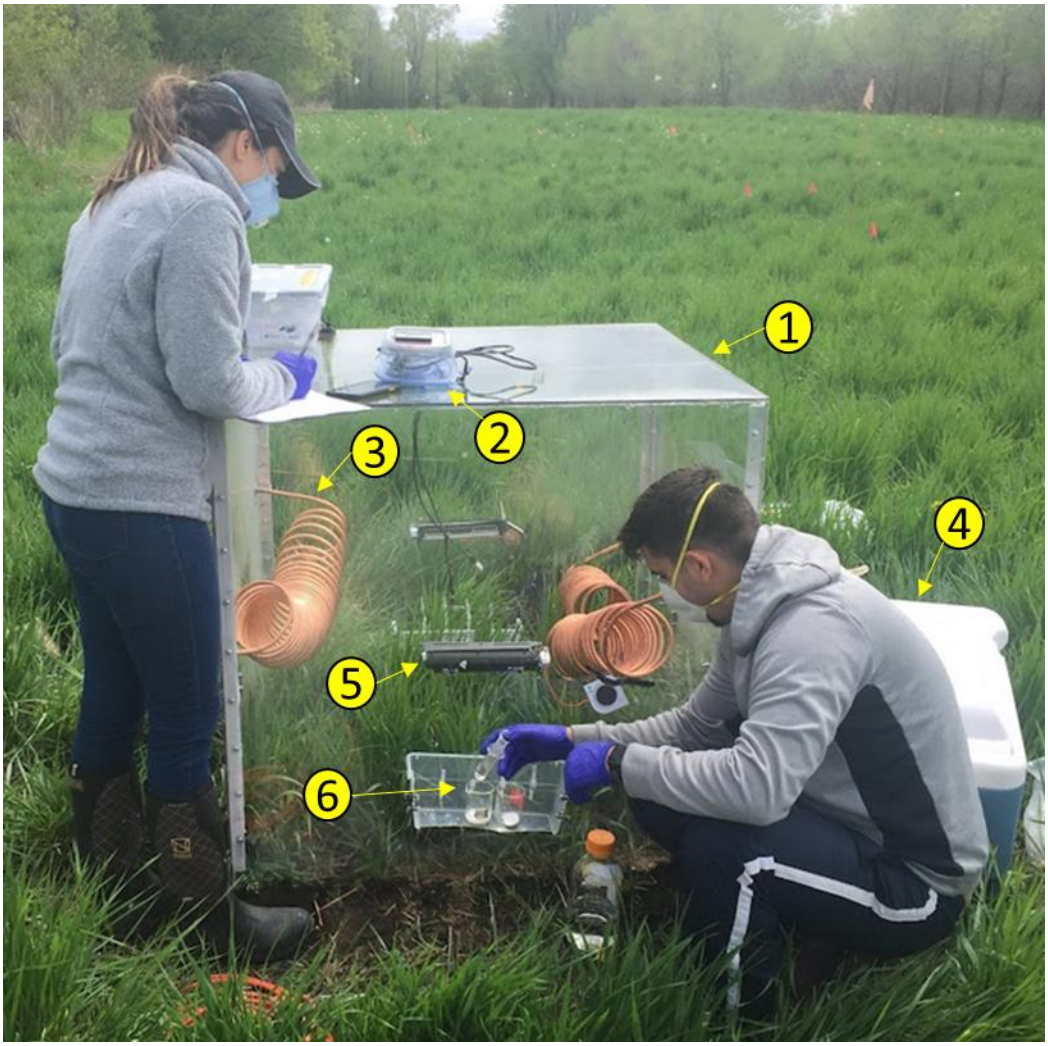

Supplemental figure 2.2 Schematic showing the layout of each wall panel on the labelling chamber.

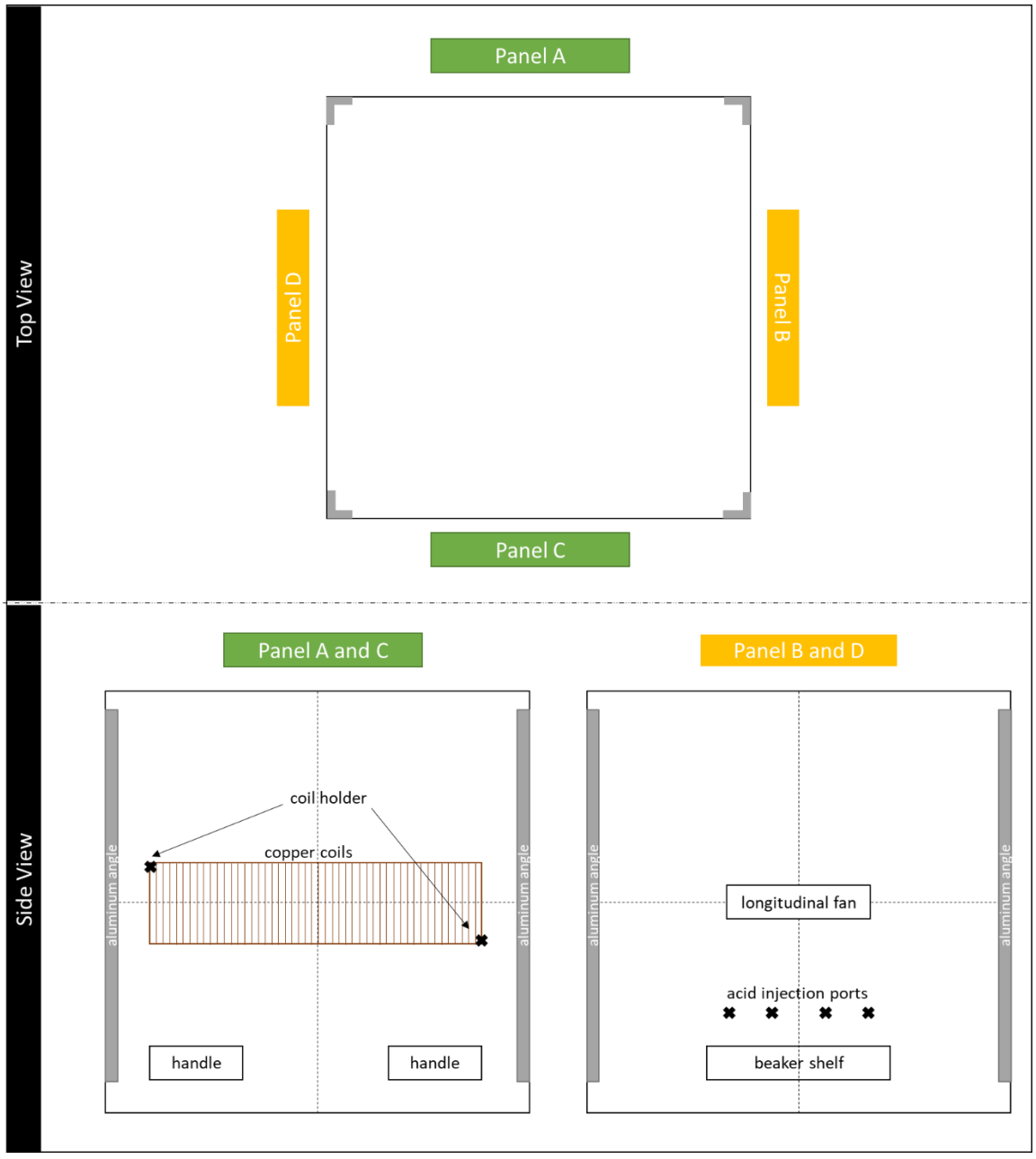

Supplemental figure 2.3 Schematic showing operation of dehumidification and air-cooling system.

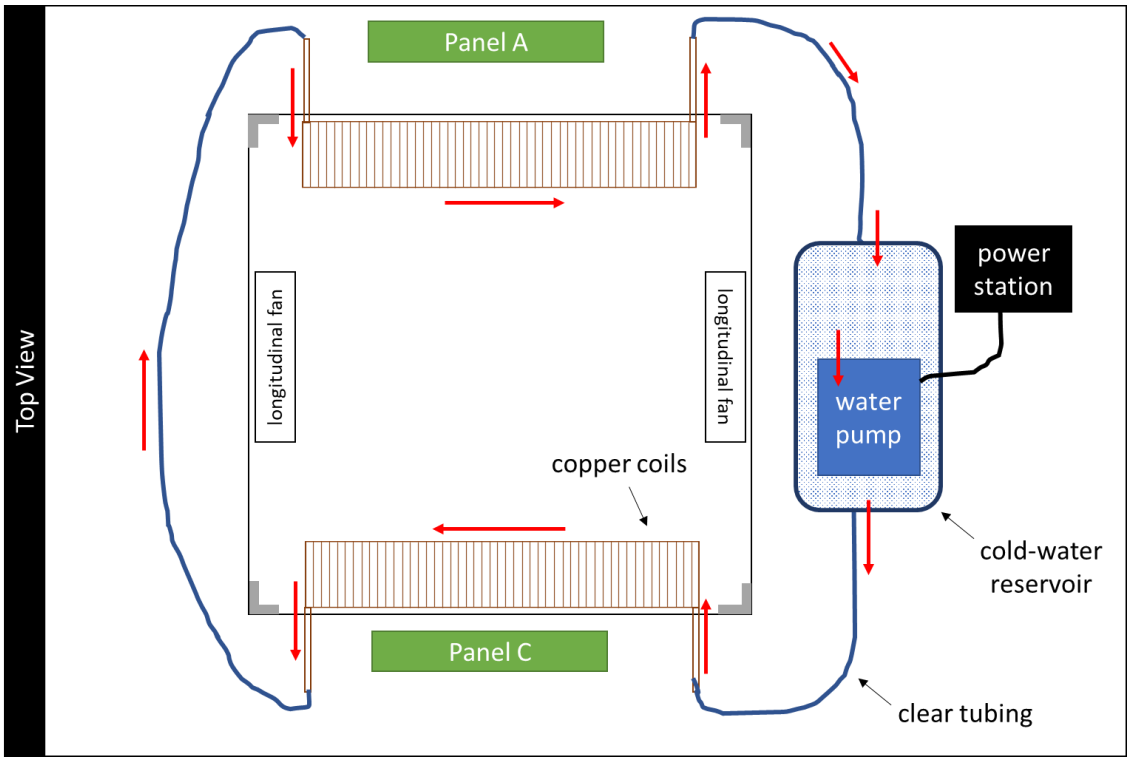

Supplemental figure 2.4 Wiring schematic for the chamber atmosphere sensor unit.

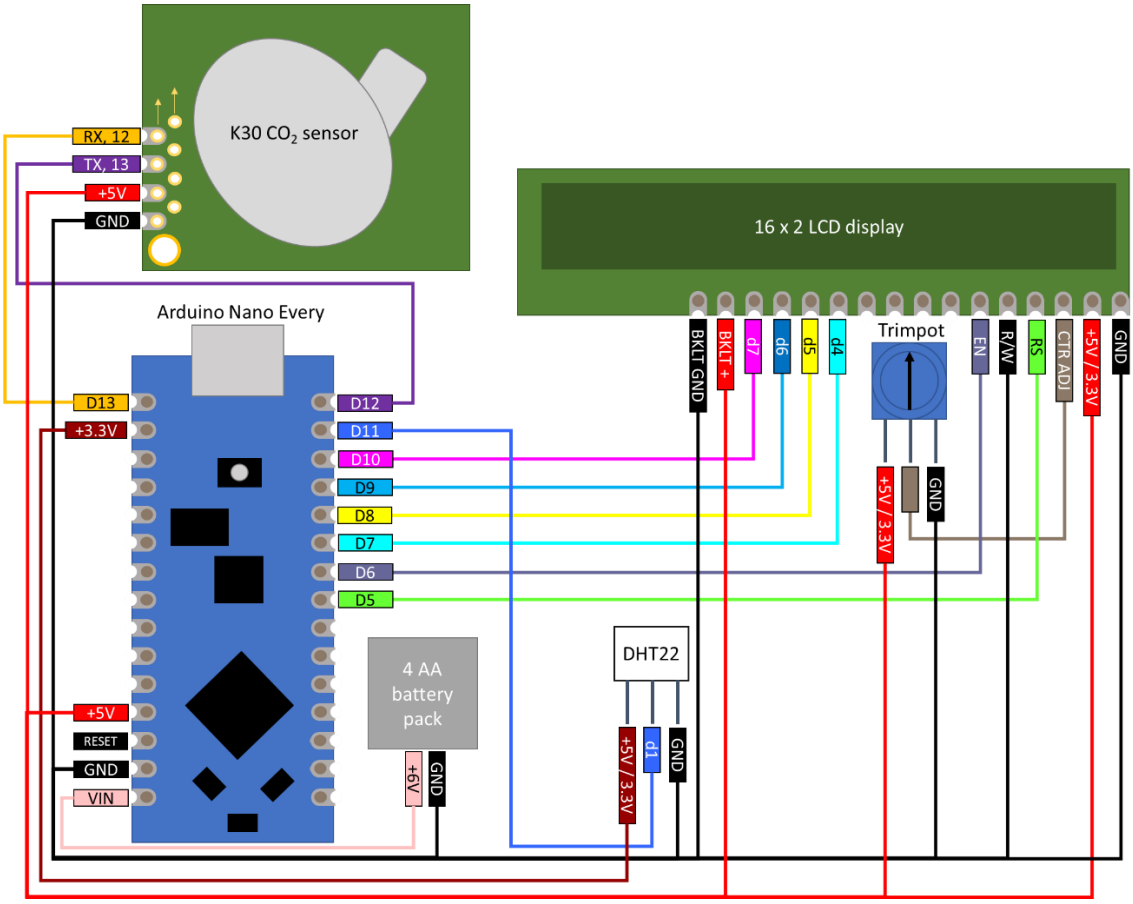

Additional Details on Shoot and Root Biomass Modeling

Model Used to Predict Shoot Biomass at Each Sampling Event

The Rosemount 2016 logistic presented in Jungers et al. (2018) was used to predict IWG aboveground biomass (g m^{-2}) at each of the sampling events in this study. This model predicts aboveground biomass as a function of growing degree days (GDD). There are three parameters in this model: β1 = asymptote, which is taken as the peak aboveground biomass achieved near physiological maturity; β2 = inflection point, which represents the point at which the growth rate begins to decline rather than increase; and β3 = a scaling factor. This model was adapted for this experiment by substituting the total aboveground biomass we measured at physiological maturity in each IWG field. The total aboveground biomass collected at maturity did not differ significantly between the first-year or second-year IWG stand. Since this trend has been seen in other studies where IWG was fertilized at 80 kg N ha^{-1} (Jungers et al. 2019, Pugliese et al. 2019), suggesting total aboveground biomass production does not differ as a function of stand age in IWG, we substituted β1 with the mean aboveground biomass when averaged across both IWG-1 and IWG-2. β2 and β3 were not modified from the original model published by Jungers et al. (2018). The final model parameters were: β1= 797.93 (g m^{-2}), β2 = 1734 (g m^{-2}), and β3 = 509.3. Using these parameters, the model predicted total aboveground biomass in these fields at maturity (8/3/2020) within 2% of measured value.

The exponential model presented in Bauer et al. (1987) was used to predict wheat shoot biomass as a function of wheat growth stage and GDD. The cumulative wheat GDD and corresponding Haun Growth Stage (HGS) were sourced from the North Dakota Agricultural Weather Network (NDAWN) database using Becker, MN as the location, which was the location in the database closest to our study sites. A planting and harvest date of 4/20/2020 and 7/24/2020, respectively, was input into the database. These dates were the actual planting and harvest dates of the spring wheat field in our study. The following model developed by Bauer et al. (1987) was used to link the spring wheat growth stage to accumulated dry matter: Y = 36.5(X)^2, where Y = accumulated dry matter (kg ha^{-1}) and X = Haun Growth Stage (1-16). The NDAWN database determines crop growth stage using the Haun Growth scale, which maxes out at 12, whereas the Bauer et al. (1987) model is based on a growth stage of 1-16. Thus, I manually added Feeke's growth stage which extend to 16 using info presented in Bauer et al. (1987). The original Bauer et al. model used a slope of 36.5 kg ha^{-1}. I modified the model based on measurements of total aboveground biomass from our spring wheat field at maturity on 7/24/2020. I set Y to equal 1026 g m^{-2} (the average total biomass yield at maturity) and X = 16 (growth stage indicating maturity), yielding a slope of 4.007 (which represents biomass in g m^{-2}).This model predicted spring wheat aboveground biomass at time of harvest (7/24/2020) would be 9344 kg ha^{-1}. The measured aboveground biomass at the

time of harvest was 9313 kg ha^{-1}, suggesting the model adequately estimates spring wheat aboveground biomass for this experiment.

Source for temperature data used to calculate IWG GDD in Rosemount for the 2020 season: https://www.dnr.state.mn.us/climate/historical/daily-data.html?sid=217107&sname=ROSEMOUNT%20RESEARCH%20AND%20OUTREACH%20CENTER&sdate=por&edate=por

Model Used to Predict Root Biomass at Each Sampling Event

Root biomass (g m^{-2}) at each sampling event was estimated using data from Woeltjen (2023, Chapter 1). Briefly, 5 cm soil cores were extracted to a depth of 15 cm on May 11, June 23, August 7, September 18, and October 20 of 2020. For each core, roots were separated from soil and used to determine root biomass at each sampling date. Following visual observation of root biomass trends over time, simple linear and quadratic models were fitted to the root biomass data within each field. Models with lower Akaike information criterion (AIC) and significant likelihood ratio test were selected for root biomass prediction. The temporal trend in root biomass in the IWG-1 and Wheat fields were best fit with the quadratic model, while the temporal root biomass trend in the IWG-2 field was best fit with a simple linear model. Since the modeled data was collected during the same growing season as the Chapter 2 study, all models predicted root biomass as a function of the day of year (DOY) on which the sampling event occurred.

Supplemental Data

Supplemental table 2.2 Analysis of variance and probability of significance for the proportion of ^{13}C recovered and mass of ^{13}C recovered when including cropping system, time, compartment and their interactions in linear mixed effects model.

Factor	Proportion of ^{13}C Recovered	Mass of ^{13}C Recovered
CS	NS	****
T	NS	****
C	****	***
CS x T	NS	****
CS x C	****	****
T x C	****	****
CS x T x C	**	****

* = P < 0.05, ** = P < 0.01, *** = P < 0.001, **** = P < 0.0001, NS = P > 0.05, – = factor not included in model

CS = cropping system, T = sampling time, C = compartment

Supplemental table 2.3 Total biomass and grain yield at maturity. Means not sharing any letters denote significantly different total biomass between fields ($p < 0.05$). No significant differences were detected in grain yield between fields ($p > 0.05$).

	Total biomass ($g\ m^{-2}$)	Grain ($g\ m^{-2}$)
IWG-1	862 ± 105 b	95 ± 28
IWG-2	765 ± 140 b	37 ± 10
Wheat	1026 ± 142 a	609 ± 130

Supplemental table 2.3 Measured shoot C content, model-predicted shoot compartment size and shoot carbon pool size at each sampling event.

	Sampling event	C content (%)	Model-predicted compartment Size (g m^{-2})	C pool size (g C m^{-2})
IWG -1	0 h	41.24 ± 0.08	121 ± 4	50 ± 2
	1.5 h	40.78 ± 0.33	121 ± 4	49 ± 1
	18 h	40.7 ± 0.15	127 ± 4	52 ± 2
	24 h	40.89 ± 0.13	127 ± 4	52 ± 2
	3 d	41.08 ± 0.19	140 ± 4	58 ± 2
	7 d	40.49 ± 0.08	175 ± 7	71 ± 3
	14 d	41.97 ± 0.17	246 ± 9	103 ± 4
	30 d	42.77 ± 0.18	540 ± 7	231 ± 3
	60 d	42.59 ± 0.11	761 ± 2	324 ± 1
	90 d	41.77 ± 0.32	9 ± 0	4 ± 0
IWG -2	0 h	41.19 ± 0.41	121 ± 4	50 ± 1
	1.5 h	41.11 ± 0.09	121 ± 4	50 ± 2
	18 h	40.86 ± 0.05	127 ± 4	52 ± 2
	24 h	40.79 ± 0.24	127 ± 4	52 ± 2
	3 d	40.96 ± 0.14	140 ± 4	58 ± 2
	7 d	40.63 ± 0.08	175 ± 7	71 ± 3
	14 d	41.9 ± 0.25	246 ± 9	103 ± 4
	30 d	42.81 ± 0.11	540 ± 7	231 ± 4
	60 d	42.55 ± 0.19	761 ± 2	324 ± 2
	90 d	42.16 ± 0.28	9 ± 0	4 ± 0
Wheat	0 h	38.49 ± 0.75	41 ± 3	16 ± 1
	1.5 h	39.08 ± 0.51	41 ± 3	16 ± 1
	18 h	37.76 ± 0.2	47 ± 4	18 ± 1
	24 h	38.46 ± 0.42	47 ± 4	18 ± 1
	3 d	38.85 ± 1.43	60 ± 5	23 ± 2
	7 d	38.07 ± 0.3	95 ± 6	36 ± 2
	14 d	40.42 ± 0.38	171 ± 9	69 ± 4
	30 d	41.78 ± 0.1	575 ± 9	240 ± 4
	60 d	40.59 ± 0.1	1026 ± 0	416 ± 1

Supplemental table 2.4 Measured root C content, model-predicted root compartment size and root carbon pool size at each sampling event.

	Sampling event	C content (%)	Model-predicted compartment Size (g m^{-2})	C pool size (g C m^{-2})
IWG -1	0 h	40.85 ± 1.79	51 ± 2	21 ± 2
	1.5 h	40.37 ± 1.97	51 ± 2	20 ± 1
	18 h	43.17 ± 0.26	54 ± 2	23 ± 1
	24 h	37.66 ± 2.02	54 ± 2	20 ± 2
	3 d	42.6 ± 0.45	61 ± 2	26 ± 1
	7 d	41.75 ± 0.27	73 ± 2	30 ± 1
	14 d	42 ± 0.4	93 ± 2	39 ± 1
	30 d	41.97 ± 0.44	142 ± 1	60 ± 0
	60 d	42.99 ± 0.56	179 ± 0	77 ± 1
	90 d	35.11 ± 0.15	179 ± 0	63 ± 0
IWG - 2	0 h	40.85 ± 1.98	325 ± 1	133 ± 6
	1.5 h	43.61 ± 0.41	325 ± 1	142 ± 1
	18 h	36.99 ± 1.59	323 ± 1	120 ± 5
	24 h	35.26 ± 0.17	323 ± 1	114 ± 1
	3 d	42.72 ± 0.48	321 ± 1	137 ± 2
	7 d	43.47 ± 0.39	317 ± 1	138 ± 1
	14 d	42.28 ± 0.42	309 ± 1	131 ± 2
	30 d	41.87 ± 0.11	285 ± 1	119 ± 0
	60 d	42.55 ± 0.2	254 ± 1	108 ± 1
	90 d	36.09 ± 0.48	212 ± 1	77 ± 1
Wheat	0 h	40.98 ± 0.63	17 ± 1	7 ± 0
	1.5 h	41.45 ± 0.54	17 ± 1	7 ± 0
	18 h	40.96 ± 0.61	18 ± 1	7 ± 0
	24 h	42.38 ± 0.34	18 ± 1	8 ± 0
	3 d	40.6 ± 0.91	21 ± 1	8 ± 0
	7 d	39 ± 0.85	25 ± 1	10 ± 0
	14 d	39.95 ± 0.63	33 ± 1	13 ± 0
	30 d	40.4 ± 0.29	47 ± 0	19 ± 0
	60 d	42.85 ± 0.17	50 ± 0	21 ± 0
	90 d	35.65 ± 0.59	22 ± 1	8 ± 0

Appendix 3

Additional Figures Depicting Tracer Application Methods Used in Chapter 3

Supplemental figure 3.1 The ^{15}N-enriched urea tracer was dissolved into deionized water, then sprayed onto microplots using a hand-sprayer. Wooden boards were set around the microplot to prevent the movement of ^{15}N outside of the enriched microplot area while spraying.

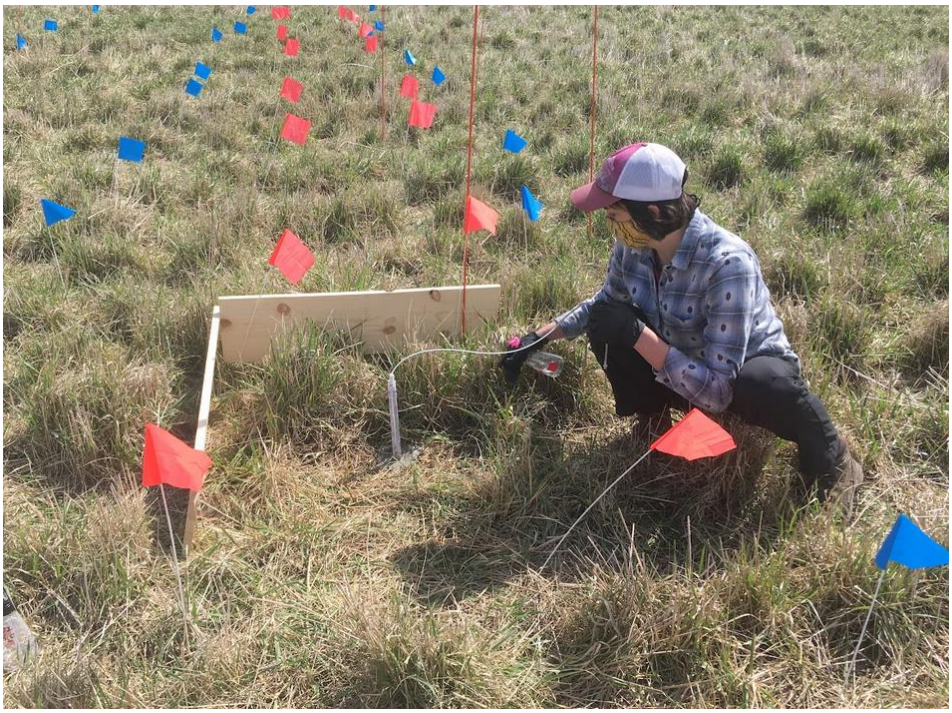

Supplemental figure 3.2 The IWG-1 field following fertilizer application and simulated irrigation.

Supplemental Data

Supplemental figure 3.3 Aboveground and belowground biomass yields (g m row^{-1}) across the study period. As there was a non-significant interaction between sampling time and stand age for root biomass, mean root biomass across stand age is presented.

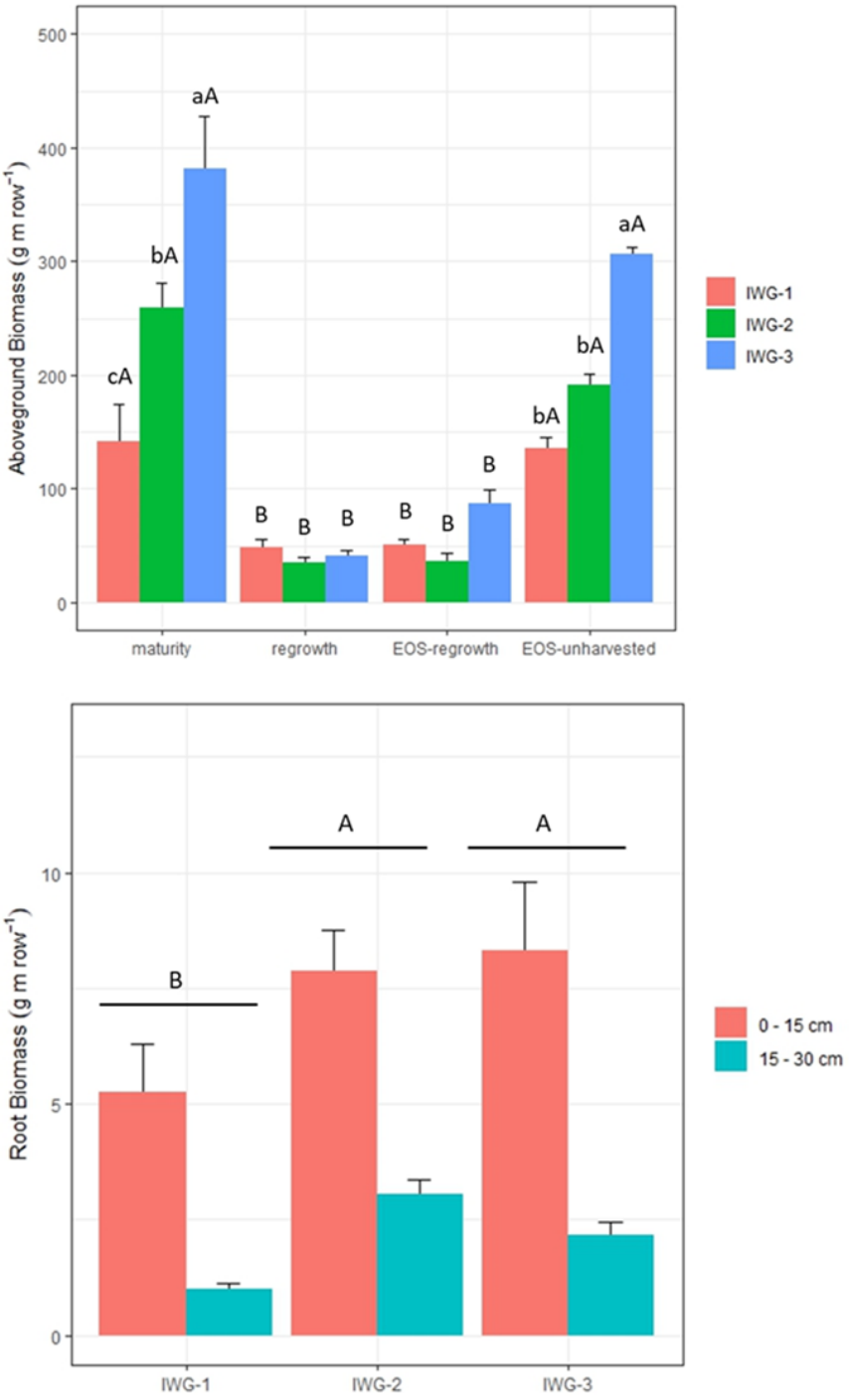

Supplemental figure 3.4 Lysimeter NO_3-N collected from each field over study period.